POLITECNICO DI MILANO

School of Industrial and Information Engineering

Master Degree in Energy Engineering

Axisymmetric Drop Shape Analysis: development of an in-house setup and application to fuel cell materials

Supervisor: Prof. Manfredo Gherardo Guilizzoni

Candidate:
Jessica Sapienza Matr. 920873

Academic Year 2019-2020

A mio nonno,
La forza interiore è la protezione più potente che hai.
Non aver paura di assumerti la responsabilità della tua felicità.

Acknowledgements

Prima di tutto vorrei ringraziare il mio relatore, Manfredo Gherardo Guilizzoni, non solo per la fiducia accordatami accettando il ruolo di mio relatore, ma soprattutto per l'aiuto attento e costante che ha saputo darmi nonostante il periodo così difficile, quale la situazione epidemiologica da Covid-19. Grazie anche per la pazienza e la competenza con cui mi ha indirizzato durante la stesura di questo lavoro di tesi.

Vorrei inoltre ringraziare il gruppo Mat4En2 del Dipartimento di Chimica, Materiali e Ingegneria Chimica "Giulio Natta" per la collaborazione, in particolare Saverio Latoratta e Andrea Stefano Basso per avermi permesso di assistere alla preparazione delle membrane e per avermele fornite permettendomi di testarle.

Un doveroso e sincero ringraziamento va ovviamente alla mia famiglia:

- a mia madre Barbara, pilastro fondamentale della mia esistenza. Grazie per essere stata una madre amorevole, per aver sempre creduto in me e per essermi stata accanto nei periodi di forte stress e sconforto. Mi fai sentire fiera di essere tua figlia.

- a mio fratello Marco, che ha ricoperto il ruolo di padre nella mia vita. Grazie per tutti i sacrifici che hai fatto per farci studiare e per essere stato sempre presente nonostante la distanza.

- alla mia gemella Amanda, che ha condiviso e supportato con me l'esperienza universitaria . Grazie per essermi accanto dal primo giorno e per tutto ciò che hai sempre fatto per me con amore e pazienza. Ti voglio bene.

- a mia nonna Maria, che nonostante le continue lamentale per il mio disordine mi ha accolta in casa sua e mi ha ospitato permettendomi di fare questa esperienza universitaria a Milano. Grazie per l'amore e il sostegno che solo una nonna sa dare.

- a mio Nonno Alfio, che ormai non c'è più ma so che da lassù mi ha protetta ogni giorno e mi ha dato forza.

- a tutti i miei zii: Vincenzo, Ornella, Teresa e Maurizio per essere stati delle seconde mamme e papà, per avermi aiutato nei momenti difficili e per avermi fatto sentire sempre a casa.

- ai miei cugini, per aver sempre fatto “il tifo” per me. Soprattutto grazie a te Leila per l’affetto che quotidianamente mi dimostri.

- a mio cognato Domenico per essere stato un secondo fratello. Grazie per tutte per tutte le volte che mi hai sostenuto e per tutte le critiche costruttive. Grazie soprattutto per le super cene che mi hai preparato chef!

Un caloroso ringraziamento va ovviamente anche ai miei più cari amici:

- a Giuliana, per avermi sopportato ogni giorno. Grazie per esserci sempre stata, per avermi saputo capire senza nemmeno parlare e per avermi sempre sostenuto dandomi forza. Grazie di cuore.

- a Manuela, Agnese, Giovanna, Jacqueline e Alessia per tutte le serate folli passate insieme e per tutti i momenti passati in spensieratezza. Grazie per il sostegno.

- alla mia compagna Roberta, con cui ho passato un fantastico anno. Ho trovato un amica! Grazie per tutte le mattine, giornate e nottate passate insieme a lezione e a studiare. Grazie soprattutto per tutte le volte che non potevo farcela e tu eri lì a incitarmi e darmi forza. Grazie per aver sempre risposto alle 2000 chiamate dove ti facevo domande su un esame e tu pazientemente rispondevi.

- a Jacopo e Lollo per essermi accanto da 10 anni. Per aver sostenuto insieme questo percorso universitario. A te “principe” che hai saputo sempre calmarmi e farmi ragionare quando ero disperata. Il tuo sostegno è stato prezioso.

- a Daniele e Marco per essere stati degli amici premurosi e affettuosi.

- al mio datore di lavoro Mirko che mi ha permesso di conciliare studio e lavoro e a tutto lo staff del “Immagine Bistrot” per essere stati una squadra tutti questi anni e per tutti i momenti passati insieme.

Extended Abstract

1. Introduction

Nowadays great attention is paid on the electric generation from renewable energy to reduce emission and to alleviate global dependence on hydrocarbons. One of the candidates is the Proton Exchange Membrane Fuel Cell (PEMFC), a technology that enables to produce electric energy with a high efficiency and friendly emission throughout a redox reaction between oxygen and hydrogen. A crucial component of a PEMFC is the ionomer membrane, which must be designed to achieve: high proton conductivity coupled to electrical insulation, low permeability to hydrogen and oxygen; chemical, mechanical and thermal stability. Generally Nafion was used, but in the last year many studies are conduced to replace this with other more efficient materials such as graphene membranes. Graphene, composed by one or more atomic carbon monolayers that can be arranged in different shapes, has acquired great importance thanks to his high conductivity.

The original scope of thesis should have been to test different sulfonated graphene oxide membranes (SGO-X) seen as future proton conductor for proton exchange membrane fuel cells. Membranes were produced by the Department of Chemistry, Materials and Chemical Engineering “Giulio Natta”.

Characterization of membranes comes from a wettability analysis of these by evaluating the static contact angle on “as placed” drops, with the Axisymmetric Drop Shape Analysis (ADSA) technique. Due to COVID-19 pandemy and the lockdown, a “in-house setup” was developed and tested.

1.1 Wettability Analysis

When a liquid comes in contact with a solid substrate, in a surrounding gaseous atmosphere, the possible mechanical and thermal interactions are manifold. The wettability of the surface results from such interactions and it is a sort of “summarizing outcome” of the close contact between the two [31]. To give a definition, wetting is “the tendency for a liquid to spread on a solid substrate” [32]. Young contact angle or static contact angle is the parameter that is used to evaluate the wettability of a solid surface. It is defined as the angle formed by the tangent to the drop profile with the tangent to the solid surface profile in a plane where the normal vectors to both the liquid-gas and the solid-gas interfaces are contained [39].

For a homogeneous, flat and smooth surface, in absence of external forces a sessile drop would have a spherical cap shape and the contact angle would be determined only by the three interfacial energies σ_{LV} (between liquid and vapor), σ_{SL} (between solid and liquid), σ_{SV} (between solid and vapor), according to the Young equation [40]:

$$cos\ \Theta_Y = \frac{\sigma_{SV} - \sigma_{SL}}{\sigma_{LV}}$$

where ΘY is the so called Young contact angle or static contact.

When a drop of liquid is placed on a solid surface we can observe different phenomena: the drop may spread continuously and wet the solid surface or the drop does not wet the surface. The first case shows the behavior of a wetting liquid or hydrophilic surface and the value of the static contact angle is $0° \leq \theta_Y \leq 90°$. The second case shows a non-wetting liquid or hydrophobic surface and the value of the contact angle is $90° \leq \theta_Y \leq 180°$. Surfaces with a value of contact angle of less than 10° are called superhydrophilic, while surfaces with a value of contact angle between 150° and 180° are called superhydrophobic, where there is a very reduced contact between the liquid drop and the surface (also known as "lotus effect").

The equilibrium contact angle described by the Young equation refers to a static state ,however, the phenomenon of wetting involves more than a static state, in fact many metastable states are present for a droplet on a solid substrate and contact angle can assume values within a range where the advancing contact is the maximum value and receding contact angle is the minimum [38]. We can measure the advancing and receding contact angles from dynamic experiments where droplets are in movement or easily tilting the surface where the drop is deposed. In these cases advancing contact angle θ_{adv} is where the drop becomes "larger", along the parts of the contact line (where the liquid advances or is in incipient advancement), while receding contact angle θ_{rec} is where it "becomes" smaller (where the liquid is receding or in incipient recession).
The difference between the maximum advancing and minimum receding contact angles is named contact angle hysteresis [39]:

$$H = \Theta_{adv} - \Theta_{rec}$$

The contact angle hysteresis can be seen as a result of substrate surface heterogeneity and roughness, impurities on to the surface, dilation of the surface (generally it may take place on polymer surfaces), consequence of the treatment of the surface by the solvent, etc [48,49,50].

Contact angle measurement on flat surface may be conducted by several techniques, ranging from the oldest and simplest ones to the most recent and accurate, such as ADSA that was used for these tests. ADSA is the only curve-fitting method with a physical basis, as it analyzes the drop shape based on the Young–Laplace equation: it finds the theoretical profile that best matches the drop profile exacted from the image of a real drop, from which the surface tension, contact angle, drop volume and surface area can be computed.

1.2 Scope and Structure of the Thesis

The main purpose of this work should have originally been to characterize the wettability of different materials for fuel cells, particularly focusing the attention on membranes made of graphene and graphene-carbon black composites.
All materials were produced by the Laboratory of Materials for Energy and Environment (Mat4En2) group of the "Politecnico di Milano, Department of Chemistry, Materials and Chemical Engineering "Giulio Natta" and should have been tested by measuring static contact angles on "as placed" drops method with the ADSA technique. All these tests and measurements had to be conducted in the Thermo-fluid Dynamics Laboratory at the Department of Energy, but due to the lockdown imposed by the COVID19 pandemy it was necessary to create a new in-house setup and to validate the measurements obtained by it. The opportunity was also got to perform an extensive sensitivity analysis on the technique itself. This thesis is structured into four chapters presenting the details and results of the work that was carried out. The first one is an introductive chapter which gives general information about contact angle history and application.
In the second chapter a sensitivity analysis of the software is described in details together with the description of the "in-house" setup and its optimization The third chapter describes the creation of some samples from everyday materials to test the setup, together with their contact angle calculation and the measurements for validation, done by re-testing fuel cell surfaces for which previous measurements (performed in the Thermo-fluid Dynamics Laboratory) were available. The fourth chapter concerns the characterization of the wetting behavior of the GO membranes.

2. Sensitivity Analysis and Validation “In-house” Setup

2.1 Sensitivity Analysis

Despite many attempts to improve the contact angle measurement, the technique remains to a certain degree subjective and depends on the experience and skillfulness of the operator. In this section the conducted sensitivity analysis and validation of the measurement technique are explained, to evidence and better understand possible causes of errors that affect the accuracy of contact angle measurement.
Practically the measurement of contact angle is made up of different steps:

1. Acquisition and preparation of the images (e.g. cropping if needed);
2. In case a separate image of the background is acquired, image registration and calculation of the difference from the image with the drop.
3. Image segmentation, extraction and smoothing of drop profile
4. Fitting of the Laplace-Young equation to the experimental boundary and determination of the contact angle.

In the following sub-sections the effect of the different investigated parameters will be described.

2.1.1 Number of iterations, smoothing, baseline value

Sensitivity analysis has been based on the evaluation of the effect of input values for number of iterations in the fitting step, smoothing value for contour smoothing, base line value and camera alignment, for computer-generated images at different images resolution (square images with 250, 500, 1000, 1250 and 1500 pixel along each direction), knowing the real contact angle and the Eotvos number of each drop. For each resolution the contact angle was calculated for two types of images: a first type in which the contour is directly traced and a second type when the starting point is a black-and-white image from which the contour must be calculated to estimate also the additional error due to this step). Each set of pictures at a given resolution includes drops with contact angle values from 10° to 170° with a step of 10° and per each contact angle value the Eotvos number varies from 0.2 to 5 with a step of 0.2. So per each contact angle there are 25 value corresponding to different Eotvos number for a total of 425 images for each resolution. For each assigned parameter value the relative error (namely MAPE - mean absolute percentage error) was calculated in order to understand the importance and weight of the parameters in the process.

The analysis was conducted by steps. First the best values of number of iteration was determined (keeping the smoothing and the baseline values at their reference values) throughout 100,500,1000 and 2500. Then the smoothing value between 0.01, 0.03, 0.05 and 0.07 was varied using for each resolution the optimum iteration value. Finally the contact angle errors caused by baseline displacement were calculated varying the value of ± 3 pixel. Given the large amount of data (more than 9000 value for each resolution) the results were summarized calculating the usual statistical parameters: arithmetic mean and median as "central" values, and standard deviation as an indicator of the dispersion of the distribution of values

What is observed is that the values are in general all very near to each other. No significant effect of the smoothing value can be identified, and concerning the number of iterations the only "strange" case is that at 250 resolution, for which a small number of iterations is the best choice. For all the other resolutions, the larger the number of iterations, the lower the MAPE, as it is reasonable; but the improvement is extremely slight so 500 iterations can be already considered adequate.

Rather than the other parameter for baseline value error is much more significant as show in the Table 2.1 - baseline value strongly affects the result - confirming the importance of trying to select the parameter as accurately as possible. A general observation is that at high image resolutions such difference becomes very small given that with high resolutions the relative importance of a single pixel is reduced, in relative term with respect to the drop dimensions. In general, both the MAPE and the standard deviation of the errors decrease with the increase of resolution. Contact angle values become more and more near to the real value. The resolution of the camera influence the error in the contact-angle measurement, as the fitting procedure is more precise with higher quality images and also accuracy of the placement of the baseline increases with resolution.

After the analysis of the images already depicting the drop contour, attention was focused on the images depicting full drop in black/white, from which the contour must be extracted – thus allowing to evaluate also the influence of this step on the errors. For B/W drop images present higher errors – as is was expected, considering that one more step is required to compute the contact angle value, so there is a propagation of error, more steps lead to bigger errors.

DROP CONTOUR PICTURE BASELINE VALUE								
RESOLUTION		**Y_STOP -3**	**Y_STOP -2**	**Y_STOP -1**	**Y_STOP**	**Y_STOP +1**	**Y_STOP +2**	**Y_STOP +3**
RESOL_0250	mean	4.62	3.29	**2.13**	2.39	3.32	4.36	5.38
	(st. deviation)	(3.40)	(3.34)	**(3.24)**	(2.68)	(2.78)	(3.09)	(3.42)
RESOL_0500	mean	1.57	0.87	**0.26**	0.64	1.38	2.20	3.07
	(st. deviation)	(0.75)	(0.53)	**(0.34)**	(0.45)	(0.75)	(1.25)	(1.94)
RESOL_0750	mean	1.49	1.01	0.53	**0.15**	0.45	0.96	1.47
	(st. deviation)	(0.66)	(0.49)	(0.32)	**(0.18)**	(0.24)	(0.42)	(0.66)
RESOL_1000	mean	0.76	0.41	**0.10**	0.34	0.71	1.09	1.48
	(st. deviation)	(0.34)	(0.24)	**(0.13)**	(0.21)	(0.33)	(0.49)	(0.69)
RESOL_1250	mean	0.89	0.60	0.30	**0.08**	0.29	0.59	0.89
	(st. deviation)	(0.37)	(0.27)	(0.17)	**(0.11)**	(0.17)	(0.28)	(0.40)
RESOL_1500	mean	0.73	0.49	0.26	**0.06**	0.25	0.49	0.74
	(st. deviation)	(0.36)	(0.28)	(0.21)	**(0.13)**	(0.14)	(0.20)	(0.29)
DROP B/W PICTURE BASELINE VALUE								
RESOLUTION		**Y_STOP -3**	**Y_STOP -2**	**Y_STOP -1**	**Y_STOP**	**Y_STOP +1**	**Y_STOP +2**	**Y_STOP +3**
RESOL_0250	mean	4.21	3.08	**2.42**	2.84	3.76	4.84	5.89
	(st. deviation)	(3.70)	(3.42)	**(3.01)**	(2.36)	(2.45)	(2.81)	(3.25)
RESOL_0500	mean	1.35	0.66	**0.37**	0.90	1.65	2.47	3.37
	(st. deviation)	(0.92)	(0.66)	**(0.35)**	(0.38)	(0.65)	(1.10)	(1.81)
RESOL_0750	mean	0.89	0.43	**0.26**	0.59	1.10	1.61	2.14
	(st. deviation)	(0.63)	(0.43)	**(0.23)**	(0.24)	(0.35)	(0.57)	(0.83)
RESOL_1000	mean	0.68	0.33	**0.17**	0.42	0.79	1.18	1.56
	(st. deviation)	(0.43)	(0.32)	**(0.15)**	(0.18)	(0.28)	(0.43)	(0.61)
RESOL_1250	mean	0.85	0.56	0.28	**0.13**	0.89	0.32	0.91
	(st. deviation)	(0.44)	(0.35)	(0.25)	**(0.13)**	(0.40)	(0.16)	(0.34)
RESOL_1500	mean	0.74	0.49	0.26	**0.10**	0.24	0.49	0.74
	(st. deviation)	(0.36)	(0.28)	(0.21)	**(0.13)**	(0.14)	(0.20)	(0.29)

Table 2.1 - MAPE of Contact Angle at different baseline value. For each cell the value is presented completed with the corresponding standard deviation in brackets. In orange are evidenced the cases with the minimum MAPE ("the winner").

2.1.2 Camera Alignment

To complete the analysis of the factors affecting contact angle measurement the alignment of the camera with the drop-sample system was evaluated.

In fact, the sample should be placed perfectly horizontal and the camera view should be on the same plane as the sample. A tilt in the camera view can be a source of relevant errors. If the stage is tilted some parts of the droplet will be covered by the stage, or vice versa the drop will be seen "from the top" altering its apparent shape, in both cases making the measurement inaccurate.

Two different sets of rendered images with contact angle values of 120° and 150° were considered. Each set was composed by a perfectly aligned image and other images with the camera too high or too low, with some degree misalignment. For each image it was also evaluated effect of the selection of the baseline. For all images the baseline was manually identified and then moved 1,2,3 px up and down. In all cases the error increases with the inclination. When the camera is put lower than the perfect sample alignment the contact angle decreases, that is reasonable because the bottom part of the drop is "cut", covered by the

sample. On the contrary with a higher position of the camera the contact angle value increases, because the projected, apparent cross section of the drop is flattened. Analyzing the variation of the baseline value for each inclination, the minimum error was obtained for the baseline value nearer to the correct baseline value of the perfect alignment picture.
It is found a linear trend is with respect to the baseline displacement (as it is reasonable given the minor amount of the latter), with significant effects on the measurement, confirming the importance of the parameter. Concerning the misalignment, the variations are not linear, and placing the camera too low causes larger errors - so it is better to risk an upwards misalignment. In any case this proves to be another major source of error, to which maximum attention should be given when acquiring the experimental images.

2.2 In-house Setup

Due to the lockdown imposed to contain the spreading of the Covid-19 virus, that also made impossible to access the Polimi laboratory, a new setup was studied, that could be built at home, trying to recreate the same basic fundamental characteristic of the setup (while being conscious of the limits). The new experimental setup consists of the following elements:

- A desk as a work bench where to conduct the experiments.
- A light source provided by a table lamp, that can be moved vertically, with the original yellow light substituted with a multi-LED white lamp.
- A medical syringe to depose the drop and partially calibrate its volume.
- One or two soft building blocks as the support of the sample.
- A Canon Power Shot SX520 HS as the camera.

Obviously pictures provided by the homemade laboratory have a lower quality with respect to those acquired at the Polimi laboratory where the setup is designed “ad hoc” with the use of a professional macro lens, a tripod, specific lighting, etc. Particularly the macro lens allows to focus at a very close distance, which is essential for photographing drops, while the tripod helps to keep the camera steady to better adjust the focus and to avoid vibrations. Moreover the drop photography technique requires mastery of two fundamental concepts: depth of field - it is essential to be able to have the whole image in focus and exposure times - to obtain still and sharp images.

Different picture tests showed that the best quality picture is provided with normal camera mode with low ISO (100-200), a medium diaphragm aperture (in the range of 7-8), relatively long exposure time (1/8’’) and low focus distance (11 mm).

All the found values are compatible with the ones used in Polimi laboratory, apart from the aperture, that using the macro lens must be much lower to have a suitable depth of field.

It was decided not to use the telephoto mode because it provides lower quality pictures and also because it requires long distance from the drop and, without a tripod, pictures are considerable affected by the operator ability to stay still.

Regarding alignment, that is an important factor because a not good position of the camera causes distortion in the contact angle measurement, camera was arranged as near as possible to the drop on a rigid support (as an example a book), aiming at the correct alignment with the drop base line. Obviously the precision granted by an anti-vibrating bench with height and inclination regulation could not be reached; nonetheless suitable alignments could be obtained.

A crucial factor to set was light. Generally pictures are taken with a back illumination where the drop is dark with the minimum reflection possible on a homogeneous and bright background. To be processed drops have to be dark on a bright background, so too much light makes the drop transparent on the contrary too low lighting makes all dark; in both case image binarization and extraction of the drop contour becomes impossible.

A desk lamp cannot provide a direct background illumination so as a solution a white background was created with simply a sheet of paper towards which light was headed in order to provide the diffuse light necessary to take a correct picture. Successively a long campaign with different source lights and different positions and intensities was carried out to find the best solution. Also light reflection was an issue to be considered; in fact in some picture the top part of the drop was too bright as a consequence of reflection and so during the segmentation processing it was wrongly assigned to the background.

The final choice was to cover the desk lamp with a sheet of paper (to mitigate light intensity), to point it toward the wall behind the drop, positioning in a central position and far from the drop (in order to give mainly diffuse light to reduce reflection).

3. Results for the Tested Samples

In this chapter we will illustrate the results of the measurements carried out on different surfaces using the technique and the details discussed in the previous chapters. More specifically, the characterization of the new graphene oxide membranes was the third of three steps, where the first two were the measurements of the contact angle on home-made samples and on samples already tested in previously works at the Thermo-fluid dynamics laboratory.
The first step permitted the optimization of the home-made setup and measurement technique. The second gave the validation of the technique and measurement thanks to the comparison of the contact angles obtained with the now previously found. After the validation of the home-made setup the contact angle measurements of new membranes produced at the Department of Chemistry, Materials and Chemical Engineering “Giulio Natta” were carried out.
In order to assess repeatability, for each sample 21 drop pictures were acquired:

- 9 pictures of a first drop: the camera was positioned in a first position for the first 3 pictures, in a second position for the second 3 pictures, and in a third position for the last 3 pictures;
- 3 pictures of a new drop: here, the camera was positioned in the first position for the first shot, in the second position for the second shot, and in the third position for the last shot. This procedure was repeated 4 times.

Contact angle was evaluated as the arithmetic mean of all the single measurements.

3.1 Home-Made Samples

A first set of samples was created with simple things that can be found in everyday life, like nail polish (a cosmetic product for coloring, protecting and fortifying nails) and ceramic polish (normally used to restore home parts), two aluminum covers and a common cleaning wet wipe.
Covers were cleaned and utilized both as samples and as bases for depositing layers of ceramic polish, normal and gel nail polish. One cover was used to test aluminum itself and the ceramic paste, while the second for normal and gel nail polish. The wet wipe was used as a third base on which a very thin layer of normal nail polish was settled on his fiber texture.
After the contact angle measurements on clean samples, limescale accretion on the same was also carried out by repeated wetting and drying with tap water for

10 days, to verify if limescale gives a hydrophobic behavior as often reported in the literature for other surfaces.

Aluminum, ceramic and normal nail polish was tested 3 times (for a total of 63 images) while gel nail polish only one time. As shows in Table 3.1 below all the samples present a hydrophilic behavior with a contact angle value in the range of 70°-80°, except the wipe which shows an high hydrophobicity with a mean contact angle value of 157°. Differences in contact angle value in the repeatability test can in part be due to the different drop volume deposed because it was placed with a common medical syringe unable to calibrate the volume as precisely as it would be possible with a precision syringe.

HOME-MADE SAMPLE										
SAMPLE	**DROP/TEST**	**1.1**	**1.2**	**1.3**	**2**	**3**	**4**	**5**	**MEAN**	**TOTAL MEAN**
ALUMINUM	1	69.4	68.3	67.4	68.5	71.1	72.7	69.4	69.5	**73.5**
	2	73.0	71.4	70.9	76.7	68.1	68.7	72.3	71.6	
	3	79.5	78.4	78.5	83.0	79.6	73.9	82.2	79.3	
CERAMIC POLISH	1	76.9	77.0	77.1	80.5	80.4	73.4	79.7	77.9	**77.1**
	2	75.1	74.3	73.4	69.8	79.1	72.4	78.0	74.6	
	3	79.0	78.8	78.3	78.3	80.0	80.0	78.1	78.9	
NORMAL NAIL POLISH	1	65.3	68.0	66.2	68.0	71.9	75.4	64.0	68.4	**72.2**
	2	67.0	68.8	66.7	72.9	72.1	73.4	62.1	69.0	
	3	81.8	83.5	80.1	75.5	76.4	77.6	79.8	79.2	
GEL NAIL POLISH	1	89.6	85.0	84.1	76.1	80.0	75.3	78.8	81.3	**81.3**
WET WIPES	1	162.4	164.9	168.7	141.4	133.7	164.5	165.3	157.3	**157.3**

Table 3.1 - Contact angle values on home-made samples.

About the limestone growth, it was evidenced that there is not an increase in contact angle values that remains practically the same so in these cases limestone did not give a hydrophobic characterization to the samples. This was surprising, but further studies should be performed to obtain more substantiated conclusions.

3.2 Polimi Samples

In order to validate the home-made setup, it was necessary to test it with samples for which the contact angle had already been calculated in the course of the other studies. By doing so, it was possible to compare the contact angle

values obtained by the home-made setup with the ones obtained by a professional laboratory.
Samples were selected among those that had been investigated in previous campaign at the Thermo-fluid dynamics laboratory and consists in:

1. aluminum sample;
2. brass sample;
3. three gas diffusion layers (GDL) for fuel cells, made by the Mat4En2 group using PTFE(polytetrafluoroethylene), FEP(fluorinated ethylene propylene), PFA (perfluoroalkoxy).

Table 3.2 shows the values of the contact angles measured on the Polimi samples, with an additional column reporting the old data. From the comparison it can be affirmed that the results obtained using the home-made setup are satisfactory, in particular with an excellent agreement for the GDL surfaces that are those on which the old data had been acquired with the better accuracy.

POLIMI SAMPLE											
SAMPLE	**TEST**	**1.1**	**1.2**	**1.3**	**2**	**3**	**4**	**5**	**TOTAL MEAN**	**MEDIAN**	**POLIMI MEDIAN**
ALUMINUM	1	64.8 (1.7)	63.0 (1.3)	62.7 (0.5)	73.7 (1.0)	64.1 (0.7)	67.0 (0.7)	73.8 (2.0)	66.2	**64.8**	**75±10**
BRASS	1	103.4 (0.4)	102.0 (0.7)	100.9 (1.3)	101.8 (2.6)	99.7 (0.4)	100.4 (1.0)	161.1 (0.4)	100.8	**100.3**	**80-82**
FEP	1	165.1 (1.4)	165.3 (1.0)	165.9 (3.3)	165.3 (0.4)	159.0 (1.5)	147.7 (3.1)	158.5 (1.9)	160.7	**160.9**	**158.8**
PFA	1	163.6 (0.8)	170.1 (1.9)	168.5 (0.4)	164.6 (1.6)	166.0 (5.8)	167.0 (0.4)	159.8 (0.7)	162.2	**164.2**	**161.5**
PTFE	1	161.7 (1.8)	164.8 (2.0)	161.0 (1.0)	156.8 (1.1)	164.7 (3.0)	157.4 (4.3)	158.5 (1.1)	165.7	**165.9**	**156.7**

Table 3.2- Contact angle values (MAPE and standard deviation) on Polimi samples.

3.3 Tadmor Model

Aluminum, brass, normal and gel nail polish, ceramic polish and FEP membrane were investigated to verify the presence of a Tadmor trend (meaning that the as-placed contact angle, θ_{AP}, of a sessile drop on a horizontal surface decreases with the increase of drop size due to the intensification of hydrostatic pressure). On each sample about 15 drops were placed with different volume size from the smallest one to the biggest. The volume raise was achieved adding a small quantity of water starting from a small drop.
Drop volume was calculated making the conversion from pixel to mm^3 (equivalent to microliters - that are a sort of standard unit for drop volumes) and the height of the drop thanks to the implementation of a specific code in MATLAB. Thus the contact angles evaluated were plotted along the y-

coordinate, with the volume or height along the x-coordinate. Results evidences a non-clear Tadmor trend. For FEP, brass, gel nail polish and ceramic polish we can notice that contact angle as a function of the volume respects Tadmor trend, even if there are some outliners. Concerning the dependence of contact angle on drop height, instead, we can clearly affirm there is no trend, only clouds of points.

3.3 Graphene Oxide Membranes

Table 3.3 shows the values of the contact angles measured on the graphene oxide membranes. These manifest degradation with water so it was possibly to acquire only 15 drop pictures to evaluate contact angles; furthermore it was not possible to depose consecutive drops on the same point because drops after the first are rapidly absorbed As it can be seen, all membranes show a hydrophilic behavior with contact angle values less of 90°, except the SGO-20 that shows hydrophobic contact angle values. With the exception of SGO-1, an increasing trend is evident in the contact angle with the increase of sulfuric acid-to-GO molar ratio.

GRAPHENE OXIDE MEMBRANES							
SAMPLE	**DROP/TEST**	**1.1**	**1.2**	**1.3**	**2**	**3**	**TOTAL MEAN**
GO	1	65.2 (0.7)	63.8 (0.5)	63.9 (1.2)	59.2 (0.6)	65.2 (2.5)	**61.8**
SGO-1	1	94.5 (3.1)	80.0 (2.9)	68.9 (1.3)	83.3 (2.1)	65.2 (5.3)	**76.6**
SGO-2.5	1	56.6 (1.5)	56.4 (0.8)	53.4 (0.5)	53.3 (2.1)	51.7 (0.8)	**53.5**
SGO-5	1	74.9 (0.5)	73.5 (1.0)	73.0 (1.5)	56.3 (0.6)	67.2 (0.2)	**65.7**
SGO-10	1	86.4 (1.9)	84.9 (88.6)	88.6 (7.0)	88.4 (0.8)	87.0 (1.0)	**87.3**
SGO-15	1	87.8 (0.6)	88.4 (0.9)	89.0 (2.5)	82.9 (2.0)	92.7 (1.3)	**88.0**
SGO-20	1	103.4 (1.5)	103.2 (1.4)	98.8 (5.6)	115.5 (0.2)	116.0 (4.9)	**111.1**

Table 3.3 - Contact angle values (MAPE and standard deviation) on graphene oxide membranes.

4. Conclusion

Concerning the sensitivity analysis of the ADSA procedure, it was showed that the variation of the number of iterations in the fitting process and the smoothing value for contour approximation lead to a really small variation in the contact angle measurement. What influenced significantly the measurement is the baseline value defined as the height at which the tracing of the drop profile is stopped and at which the contact angle is calculated. A non-correct evaluation of this, even in the order of ±1 pixel, can bring an incorrect contact angle valuation. Finally it was observed that with the increase of drop picture resolution errors decrease. So it is important to acquire high resolution images and to evaluate accurately the baseline value.

Concerning the in-house setup, it was built with everyday-use objects and tested first of all with a series of measurements on home-made samples (both clean and covered with limestone) and then with measurements for validation by re-testing fuel cell surfaces for which previous measurements in the Polimi laboratory had been done. Such tests evidenced that despite its obvious limitations, the in-house setup was able to grant an accuracy comparable with that of a common commercial contact angle meter.

From home-made samples we discovered that gel nail polish has an higher contact angle respect to common nail polish, so it can better resist to water and degradation for women happiness.
It was also surprising how limestone did not bring a hydrophobic behavior to samples, as often reported in the literature.

Finally, sulfonated graphene oxide (SGO-X) membranes produced by the Department of Chemistry, Materials and Chemical Engineering “Giulio Natta” were characterized. All membranes showed a hydrophilic behavior with contact angle values less of 90°, apart from the SGO-20 that reaches a contact angle of 110°. It was also observed an increasing trend of the angle with the increase of sulfuric acid-to-GO molar ratios. Generally membranes show a water uptake attitude till a molar ratio of 5.
These, also according to other evaluated properties, can therefore be attractive candidates for future fuel cells with the possibility to work at reduced humidification.

Sommario Esteso

Al giorno d'oggi grande attenzione viene data alla generazione di energia elettrica da fonti rinnovabili per ridurre le emissioni e alleviare la dipendenza globale dai combustibili comuni. Un valido candidato è la cella a combustibile a scambio protonico (PEMFC), una tecnologia che consente di produrre energia elettrica con un'elevata efficienza e zero emissioni attraverso una reazione di ossidoriduzione tra ossigeno e idrogeno. Componente cruciale di una PEMFC è la membrana ionomerica, che deve essere progettata per ottenere: elevata conducibilità protonica associata a isolamento elettrico, bassa permeabilità all'idrogeno e all'ossigeno, stabilità chimica, meccanica e termica. Generalmente viene utilizzato Nafion, ma negli ultimi anni sono stati condotti molti studi per sostituirlo con altri materiali più efficienti come le membrane di grafene.
Il grafene, composto da uno o più strati di carbonio atomico che possono essere disposti in diverse forme, ha acquisito grande importanza per la sua elevata conducibilità. L'obiettivo principale della tesi è di testare diverse membrane di ossido di grafene solfonato (SGO-X) viste come futuri conduttori di protoni per celle a combustibile a scambio protonico. Le membrane sono state prodotte dal Dipartimento di Chimica, Materiali e Ingegneria Chimica "Giulio Natta".
La caratterizzazione delle membrane deriva da un'analisi di bagnabilità di queste, che consiste nella valutazione dell'angolo di contatto statico su gocce d'acqua "gentilmente" deposte con la tecnica ADSA. In un primo momento le misurazioni avrebbero dovuto essere condotte nel Laboratorio di Termo-fluidodinamica bifase presso il Dipartimento di Energia, ma a causa del blocco imposto dalla pandemia COVID19 è stato necessario creare un setup sperimentale a casa e validare le misurazioni da esso ottenute. Per quanto riguarda la struttura della tesi, nel primo capitolo viene fornita una breve descrizione della storia e dell'applicazione dell'angolo di contatto. L'angolo di contatto di Young o angolo di contatto statico è il parametro utilizzato per valutare la bagnabilità di una superficie solida. È definito come l'angolo formato dalla tangente al profilo della goccia con la tangente al profilo di superficie solida in un piano in cui sono contenuti i vettori normali sia all'interfaccia liquido-gas che a quella solido-gas. Progressivamente, nel secondo capitolo, viene descritta l'analisi di sensitività del software utilizzato unitamente alla descrizione del setup "in casa" e della sua ottimizzazione. È stata eseguita un'analisi di sensitività sul numero di iterazioni, il valore di smooth e la linea base. Ciò che si osserva è che i valori sono in generale tutti molto vicini tra loro. Non è possibile identificare alcun effetto significativo del valore di smoothing, e per quanto riguarda il numero di iterazioni l'unico caso "strano" è quello a risoluzione 250, per il quale un piccolo numero di iterazioni è la scelta migliore. Per tutte le altre risoluzioni,

maggiore è il numero di iterazioni, minore è il MAPE, il che è del tutto ragionevole; ma il miglioramento è estremamente lieve, quindi 500 iterazioni possono essere già considerate adeguate.

Al contrario l'influenza della scelta della quota della linea di base è molto più significativa, il valore di base influenza fortemente il risultato - confermando l'importanza di cercare di selezionare tale parametro nel modo più accurato possibile. Quando la telecamera viene posizionata al di sotto del perfetto allineamento del campione, l'angolo di contatto diminuisce, ciò è ragionevole perché la parte inferiore della goccia è "tagliata", coperta dal campione. Al contrario con una posizione più alta della telecamera il valore dell'angolo di contatto aumenta, perché la sezione trasversale proiettata e apparente della goccia viene appiattita.

Per quanto riguarda il laboratorio "fatto in casa", è stato costruito con oggetti di uso quotidiano e testato prima con una serie di misurazioni su campioni fatti in casa (sia puliti che ricoperti di calcare) e poi con misurazioni per la validazione, fatte su superfici (specificamente gas diffusion layer fluorurati per celle a combustibile) per le quali erano state effettuate precedenti misurazioni nel laboratorio Polimi. Tali test hanno evidenziato che, nonostante i suoi ovvi limiti, il setup "domestico" è in grado di garantire una accuratezza paragonabile a quella di un comune misuratore di angolo di contatto commerciale.

La descrizione dei campioni fatti in casa e delle relative misure è descritta nel capitolo 3 della tesi. Da tali misure si è scoperto che lo smalto gel ha un angolo di contatto più elevato rispetto allo smalto comune, quindi può resistere meglio all'acqua e al degrado per la felicità delle donne. È stato anche sorprendente come il calcare non abbia portato un comportamento idrofobo ai campioni, contrariamente a quanto spesso riportato in letteratura.

Infine, il quarto capitolo riguarda la caratterizzazione delle membrane in ossido di grafene solfonato (SGO-X) prodotte dal Dipartimento di Chimica, Materiali e Ingegneria Chimica "Giulio Natta". Sono state esaminate un GO puro e sette diversi rapporti molari acido solforico/GO allo scopo di delineare il miglior rapporto di solfonazione che consente di ottenere un compromesso vincente tra composizione e proprietà funzionali. Tutte le membrane hanno mostrato un comportamento idrofilo con valori di angolo di contatto inferiori a 90 °, ad eccezione della SGO-20 che raggiunge un angolo di contatto di 110 °. È stata anche osservata una tendenza all'aumento dell'angolo con l'aumento dei rapporti molari acido solforico-GO. Generalmente le membrane mostrano un atteggiamento di assorbimento dell'acqua fino a una valore di frazione molare pari a 5. Queste, in unione ad altre proprietà valutate, le rendono un candidato interessante per future celle a combustibile con la possibilità di lavorare a umidificazione ridotta.

Contents

Sommario

Al giorno d'oggi grande attenzione viene data alla generazione di energia elettrica da fonti rinnovabili per ridurre le emissioni e alleviare la dipendenza globale dai combustibili comuni. Un valido candidato è la cella a combustibile a scambio protonico (PEMFC), una tecnologia che consente di produrre energia elettrica con un'elevata efficienza e zero emissioni attraverso una reazione di ossidoriduzione tra ossigeno e idrogeno. Componente cruciale di una PEMFC è la membrana ionomerica, che deve essere progettata per ottenere: elevata conducibilità protonica associata a isolamento elettrico, bassa permeabilità all'idrogeno e all'ossigeno, stabilità chimica, meccanica e termica. Generalmente viene utilizzato Nafion, ma nell'ultimo anno sono stati condotti molti studi per sostituirlo con altri materiali più efficienti come le membrane di grafene.

Il grafene, composto da uno o più strati di carbonio atomico che possono essere disposti in diverse forme, ha acquisito grande importanza per la sua elevata conducibilità. L'obiettivo principale della tesi è di testare diverse membrane di ossido di grafene solfonato (SGO-X) viste come futuri conduttori di protoni per celle a combustibile a scambio protonico. Le membrane sono state prodotte dal Dipartimento di Chimica, Materiali e Ingegneria Chimica "Giulio Natta".

La caratterizzazione delle membrane deriva da un'analisi di bagnabilità di queste, che consiste nella valutazione dell'angolo di contatto statico su gocce d'acqua "gentilmente" deposte con la tecnica ADSA. In un primo momento le misurazioni avrebbero dovuto essere condotte nel Laboratorio di Termo-fluidodinamica bifase presso il Dipartimento di Energia, ma a causa del blocco imposto dalla pandemia COVID19 è stato necessario creare un setup sperimentale a casa e validare le misurazioni da esso ottenute. Per quanto riguarda la struttura della tesi, nel primo capitolo viene fornita una breve descrizione della storia e dell'applicazione dell'angolo di contatto. Progressivamente, nel secondo capitolo, viene descritta l'analisi di sensitività del software utilizzato unitamente alla descrizione del setup "in casa" e della sua ottimizzazione. Il terzo capitolo descrive la creazione di alcuni campioni da materiali di uso quotidiano per testare il setup, insieme al calcolo del loro angolo di contatto e alle misurazioni per la validazione, fatto ri-testando alcune superfici per celle a combustibile (specificamente gas diffusion layer fluorurati) per le quali misurazioni precedenti eseguite nel Laboratorio di Termo-fluidodinamica erano disponibili. Il quarto capitolo riguarda la caratterizzazione delle membrane GO. Sono state esaminate un GO puro e sette diversi rapporti molari acido solforico/GO allo scopo di delineare il miglior rapporto di solfonazione che consente di ottenere un compromesso vincente tra composizione e proprietà funzionali.

Parole chiave: Cella a combustibile a scambio protonico (PEMFC); Bagnabilità delle superfici; Angolo di contatto ; ADSA (Axymmetric drop shape analysis) ; GDL (Gas diffusion layer) ; Membrane di ossido di grafene.

Abstract

Nowadays great attention is paid on the electric generation from renewable energy to reduce emission and to alleviate global dependence on hydrocarbons. One of the candidates is the Proton Exchange Membrane Fuel Cell (PEMFC), a technology that enables to produce electric energy with a high efficiency and friendly emission throughout a redox reaction between oxygen and hydrogen. A crucial component of a PEMFC is the ionomer membrane, which must be designed to achieve: high proton conductivity coupled to electrical insulation, low permeability to hydrogen and oxygen; chemical, mechanical and thermal stability. Generally Nafion was used, but in the last year many studies are conduced to replace this with other more efficient materials such as graphene membranes. Graphene, composed by one or more atomic carbon monolayers that can be arranged in different shapes, has acquired great importance thanks to his high conductivity.

The original scope of thesis should have been to test different sulfonated graphene oxide membranes (SGO-X) seen as future proton conductor for proton exchange membrane fuel cells. Membranes were produced by the Department of Chemistry, Materials and Chemical Engineering "Giulio Natta".

Characterization of membranes comes from a wettability analysis of these by evaluating the static contact angle on "as placed" drops, with the ADSA technique. At first measurements had to be conducted in the Thermo-fluid Dynamics Laboratory at the Department of Energy, but due to the lockdown imposed by the COVID19 pandemy it was necessary to create a new in-house setup and to validate the measurements obtained by it.

The thesis structure is as follows: a brief description of contact angle history and application is made in the first chapter. Progressively, in the second chapter, a sensitivity analysis of the used software is described together with the description of the "in-house" setup and its optimization. The third chapter describes the creation of some samples from everyday materials to test the setup, together with their contact angle calculation and the measurements for validation, done by re-testing some fuel cell surfaces (namely fluorurated gas diffusion layers) for which previous measurements (performed in the Thermo-fluid Dynamics Laboratory) were available. The fourth chapter concerns the characterization of the wetting behavior of the GO membranes.

A pure GO and seven different sulfuric acid-to-GO molar ratios membranes were examined with aim to delineate the best sulfonation ratio that enables to achieve a successful trade-off between composition and functional properties.

Key words: Proton Exchange Membrane Fuel Cell (PEMFC) ; Wettability ; Contact angle; ADSA (Axisymmetric drop shape analysis); GDL (gas diffusion layer) ; Graphene oxide membranes.

Introduction

Nowadays the global energy production is dominated by fossil fuels, which are an exhaustible energy sources. The increasing energy demand and the need to reduce environment pollution have led to greater interest in renewable energy sources and highly efficient energy conversion devices. Beside the common removable sources such as photovoltaic, wind and hydro systems there are the so called *fuel cells* which are electrochemical generators that convert chemical energy into electricity in a clean and efficient way, through the direct electrochemical oxidation of a fuel (usually hydrogen) and reduction of atmospheric oxygen. The crucial advantages given by fuel cells are no or reduced pollutant emissions because there isn't any combustion and air or oxygen is used as oxidant and no noise because moving mechanical parts are not present. Fuel cells are commercially available as stationary systems (e.g. the Japanese micro-combined heat and power system; Ene-Farm), or as portable systems (e.g. auxiliary power units or consumer electronics) [1].
Even if it is often considered a very recent technology, fuel cells started to be studied after the Second World War. The creator was Sir William Robert Grove, who discovered a current flow between the platinum electrodes with an extremity immersed into a solution of sulphuric acid while the others into hydrogen and oxygen [2]. Both containers were full of water and he discovered a decrease of water level in tubes during current flow. Improvements came with Francis Thomas Bacon, in 1939, who conducted his experiments with alkaline electrolytes, focusing his attention on potassium hydroxide. Bacon used porous electrodes, modifying electrode's morphology, which lead to a better gas diffusion and the increase of interaction areas between electrodes, electrolyte and the fuel.
The first application of fuel cells technology was in 1960, when were used in the USA space program of NASA (Gemini and Apollo missions) thanks to improvements made by General Electric Industry.
The most diffuse commercial type of fuel cells are the PEM fuel cells, i.e. Proton Exchange Membrane Fuel Cells. The central part of a PEM fuel cell is the membrane electrode assembly (MEA), which is made of a proton exchange membrane and two catalyst layers (i.e. anode and cathode). MEA is typically placed between bipolar plates (BP) which act as collectors. Between the BP and the MEA a gas diffusion layer (GDL) is introduced in order to manage water, in fact, an excess of water at the cathode side can have as consequence the flooding of the electrode and a decrease in cell performance because water hinders the transport of reactants.

GDLs must be hydrophobic to avoid flooding. They consist in a porous carbon paper or carbon cloth, wet-proofed with PTFE (Teflon) and coated with a thin microporous layer (MPL) consisting of a mixture of carbon powder and PTFE thanks to a dipping or spraying technique with heat treatment at 350 °C.

A crucial component of a PEMFC is the ionomer membrane, for which generally Nafion is used. It is a perfluorinated ionomer membrane, consisting of fluorinated carbon backbone chains with perfluoroside chains ending in sulfonic acid groups.

Nafion is the most used membrane for PEMFCs because, in typical operating conditions, it manifests high proton conductivity (>0.1 S cm^{-1}), good mechanical properties, effectiveness in gas separation. On the other hand, Nafion is also expensive and limits PEMFC operation to relatively low temperature (~80°C), due to the dependency on hydration for high proton conductivity. However the changing water content also leads to membrane shrinkage and swelling, which brings to degradation of the electrolyte electrocatalyst interface [3]. Finally, membrane degradation is caused by hydrogen peroxide radicals, inhibiting the use of non-precious catalysts in Nafion-based PEMFCs [4].

At higher operation temperatures Nafion reduces its mechanical stability due to its low glass transition temperature (~110°C) [5,6]. Fuel flow shows opposite trend, in fact, it increases with decreasing membrane thickness and increasing operation temperature, leading to lower efficiency and decreased fuel cell performance [7,8]. To reduce the cost and improve the performance of PEMFCs, new membrane materials are studied. An optimum material for use in PEMFCs as e.g. a catalyst support, or as a non-precious catalyst [9,10] is graphene. It acquired strong attention from researchers for its unique and special properties which cannot be replaced by other carbon based nanomaterials.

Graphene is a 2D structured allotrope of carbon. It differs from 3D structure of graphite, which is a crystal single-layer composed of sp^2 carbon atoms with hexagonal honey comb shaped carbon ring disposition [11,12]. It has three important qualities: firstly it presents a very strong electrical conductivity with a value of 10^6 S cm^{-1} [13], strong electrical mobility of 200 000 cm^2 $V^{-1}s^{-1}$ at a carrier density of ~10^{12} cm^{-2} [14]; secondly, it has a high specific area of 2630 m^{-2} g^{-1} [15], a Young's module value of 1 TPa with a breaking strength of 42 N m^{-1} [16], and excellent thermal conductivity (~5000 W $m^{-1}K^{-1}$) [17]; thirdly, graphene can absorb light with board wavelength (~2.3% opacity) which makes it transparent and appropiate for optoelectric applications [18].

Finally, another extremely important property it possesses is a special reactivity towards different materials. All these qualities make graphene an interesting material for different fields of applications like electrical, electronic, optoelectric, mechanical, environmental, and chemical engineering researches.

Due to its highly attractive properties explained above, various kinds of graphene based products were synthesized.

An attractive variation of graphene is graphene oxide (GO) [19,20,21]; an electronically insulating equivalent of the highly electrically conductive graphene [22]. GO is made up of aromatic areas containing unoxidized benzene rings and, regions with aliphatic six-membered rings influencing the extent of oxidation. Its basal plane is structured to contain mainly hydroxyl and epoxy oxygen groups, whilst the edges incorporate mainly hydroxyl and carboxyl groups [23,24]. GO membranes have been noted to be totally resistant to many liquids, vapors and gases, whilst permitting unimpeded permeation of water, thus indicating an affinity for hydration [25], whilst minimizing fuel crossover in PEMFCs.

Some studies were conducted in composite PEMFC membranes with known proton conductors such as Nafion, sulfonated poly ether ether ketone (SPEEK), polybenzimidazol (PBI), and poly vinyl alcohol (PVA). For example Kumar et al. showed improved PEMFC performance at 100°C for a 4 wt% GO/Nafion composite, compared to pure Nafion [26].

Jiang et al. discovered that the incorporation of sodium dodecylbenzene sulfonate-adsorbed GO in SPEEK leads to the increase of the ion-exchange capability, water uptake and proton conductivity, whilst reducing methanol permeability [27].

Also Xu et al. calculated for a PBI/ sulfonated GO composite membrane a maximum cell power density of 600 mW cm^{-2} at 175°C [28].

Tateishi et al. tested a fuel cell with a pure GO paper membrane, achieving a maximum power density of ~13 mW cm^{-2} at room temperature [29]. Scott and Ravikumar achieved a MEA power density of 113 mW cm^{-2} at 40°C testing a freestanding sulfonated GO paper membrane [30]. Such studies in the literature show the potential for GO to be used in fuel cells, however not many studies have investigated non-composite GO membranes at higher temperature where electrode kinetics and ionic transport are faster [9].

The main purpose of this work should have originally been to characterize the wettability of different materials for fuel cells, particularly focusing the attention on membranes made of graphene and graphene-carbon black composites.

All materials were produced by the Laboratory of Materials for Energy and Environment (Mat4En2) group of the "Politecnico di Milano, Department of Chemistry, Materials and Chemical Engineering "Giulio Natta" and should have been tested by measuring static contact angles on "as placed" drops method with the ADSA technique.

All these tests and measurements had to be conducted in the Thermo-fluid Dynamics Laboratory at the Department of Energy, but due to the lockdown imposed by the COVID19 pandemy it was necessary to create a new in-house setup and to validate the measurements obtained by it. The opportunity was also get to perform an extensive sensitivity analysis on the technique itself.

This thesis is structured into four chapters presenting the details and results of the work that was carried out. The first one is an introductive chapter which gives general information about contact angle history and application.
In the second chapter a sensitivity analysis of the software is described in details together with the description of the “in-home” setup and its optimization The third chapter describes the creation of some samples from everyday materials to test the setup, together with their contact angle calculation and the measurements for validation, done by re-testing fuel cell surfaces for which previous measurements (performed in the Thermo-fluid Dynamics Laboratory) were available. The fourth chapter concerns the characterization of the wetting behavior of the GO membranes.

Chapter 1

Theoretical Background

1.1 Wettability

When a liquid comes in contact with a solid substrate, in a surrounding gaseous atmosphere, the possible mechanical and thermal interactions are manifold. The wettability of the surface results from such interactions and it is a sort of "summarizing outcome" of the close contact between the two [31]. To give a definition, wetting is "the tendency for a liquid to spread on a solid substrate" [32] and is characterized by two important parameters [33,34]:

- Degree/extent of wetting
- Rate of wetting

The degree of wetting is commonly indicated by the contact angle formed at the interface between solid and liquid and it is mainly dependent on the surface and interfacial energies involved at the solid/liquid interface; while the rate of wetting indicates how fast the liquid wets the surface and spreads over the same and it is led by a number of factors such as the thermal conditions of the system, capillary forces, viscosity of the liquid, the chemical reactions occurring at the interface, etc. [35].

We can classify wetting in different ways: if we focus on the substrate we talk about reactive/no reactive wetting ,instead, if we focus on how the process is initiated and driven we talk about spontaneous/forced spreading [36]. We talk of non-reactive/inert wetting when there is no reaction between the spreading liquid on a solid substrate. A non-reactive wetting is that of polymeric liquids in contact with glass or metallic substrate; generally the contact on inert solids of most of non-metallic liquids is non-reactive type. On the other hand, we talk of reactive wetting when wettability is influenced by reactions that occur during the contact between the spreading liquid and the solid substrate, where there is alteration of the interface and formation of new (e.g. intermetallic) compounds. Two examples of reactive wetting are that of liquid metal on ceramic substrate and of spreading of solder on copper substrate.
Spontaneous spreading happens when a liquid drop spreads on the solid substrate without any external forces; forced spreading otherwise. An example of the first case is the spreading of solder paste during reflow soldering, while

the spreading of water drop after impacting from a finite distance is forced spreading since this is lead from the substantial kinetic energy acquired by the drop during its fall [35].

The wetting theory involves inter-atomic and intermolecular forces acting across a surface. These forces can be primary like ionic, covalent and metallic co-ordination bonds or secondary forces like van der Waals and hydrogen bonds and electrostatic forces. In a continuum model, when a system is heterogeneous (composed of different phases) the phases are divided by interfaces. In these "thin" regions there is concentration of impurities, electric currents etc. and they are described as having excess properties. One is the excess energy, that is usually expressed as energy per unit area [J/m^2] called "interface energy"- or force per unit length [N/m] called "interface tension".
When the interface is between a liquid or solid phase and a gaseous one, the latter are also named "surface energy" or "surface tension".

1.2 Surface Tension and Surface Free Energy

Surface energy is usually denoted by σ (or γ) and has the dimensions of energy per unit area, that is, in the SI system, J/m^2 . Thermodynamically, the concepts of surface free energy and surface tension are originally different [37]. Surface tension [N/m] stands for force needed to "stretch" an interface, or the energy/work (per unit area, [J/m2]) required to create new interface area. Surface free energy focuses on the breakage of intermolecular bonds that occurs when a surface is created. However, when temperature and pressure are supposed constant, the two concepts are equivalent to each other.

Surface tension is probably the easier concept to visualize, as it can be seen as if caused by the attraction between the molecules of the liquid by various intermolecular forces. In the bulk of the liquid each molecule is pulled equally in all directions by neighboring liquid molecules, resulting in a zero net force. At the surface of the liquid, the molecules are pulled inwards by other molecules deeper inside the liquid and are not attracted as intensely by the molecules in the neighboring medium (e.g., vacuum, air or another gas or liquid). Therefore the molecules at the surface are subject to an inward force of molecular attraction which can be balanced only by the resistance of the liquid to compression [38], resulting in an increase in the internal pressure. This inward pull tends to diminish the surface area, and in this respect a liquid surface resembles a stretched elastic membrane. Thus the liquid squeezes itself together until it has the locally lowest surface area. As an elastic membrane, an interface cannot resist to normal forces, but resist to tangential forces. This means that if an interface is curved, a pressure difference exists between the two sides of the interface. The equation that relates the pressure difference to the shape of the surface is the equation Young–Laplace equation:

$$P_{convex\ part} - P_{concave\ part} = \sigma K = \sigma(\frac{1}{R_I} + \frac{1}{R_{II}}) \qquad (1)$$

where K is the curvature and R_I and R_{II} are the two principal curvature radii of the surface.

Therefore, as already said the surface tension produces an additional pressure inside the liquid. As an example, for a sphere $\Delta P = 2\sigma / R$, or, so if we cross the curved interface moving along an inward direction, the pressure increases by $2\sigma/R$.

As the sphere is the solid having the lower external surface given the volume, in absence of other forces capillary interfaces, e.g. those of bubbles and drops, have a spherical shape.

In real conditions we than have to consider the presence of gravity so drops may lose their spherical shape under the influence of gravity. There exists a particular length, denoted λ, beyond which gravity becomes important. It is referred to as the capillary length :

$$\lambda = \sqrt{\frac{\sigma}{g\Delta\rho}} \qquad (2)$$

1.3 Young Contact Angle

Contact angle is the angle formed by the tangent to the drop profile with the tangent to the solid surface profile in a plane where the normal vectors to both the liquid-gas and the solid-gas interfaces are contained [39].
For a homogeneous, flat and smooth surface, in absence of external forces a sessile drop would have a spherical cap shape and the contact angle would be determined only by the three interfacial energies σ_{LV} (between liquid and vapor), σ_{SL} (between solid and liquid), σ_{SV} (between solid and vapor), according to the Young equation [40]:

$$\cos \theta_Y = \frac{\sigma_{SV} - \sigma_{SL}}{\sigma_{LV}} \tag{3}$$

where θ_Y is the so called Young contact angle or static contact angle and it is the parameter that is used to evaluate the wettability of a solid surface (Figure 1.1).

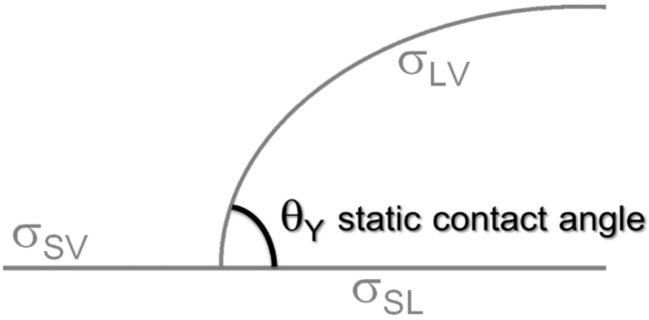

Figure 1.1 *- Young contact angle or static contact angle. Picture taken from [41].*

As show Figure 1.2 when a drop of liquid is placed on a solid surface we can observe different phenomena: the drop may spread continuously and wet the solid surface or the drop does not wet the surface. The first case shows the behavior of a wetting liquid or hydrophilic surface and the value of the static contact angle is 0°≤θ_Y≤90°. The second case shows a non-wetting liquid or hydrophobic surface and the value of the contact angle is 90°≤θ_Y≤180°. Surfaces with a value of contact angle of less than 10° are called superhydrophilic, while surfaces with a value of contact angle between 150° and 180° are called superhydrophobic, where there is a very reduced contact between the liquid drop and the surface (also known as “lotus effect”).

The term hydrophobic/philic was originally related only to water, nowadays it is often used to describe the contact with any liquid. The term “oleophobic/philic” is also used for oil and organic liquids. The term “amphiphobic/philic” is generally used to indicate surfaces that are both hydrophobic/philic and oleophobic/philic. Polar molecules leads surface to have a high energy and as a result to be hydrophilic, whereas non-polar molecules leads to have low energy and on the contrary to be hydrophobic [42].

θ_Y is theoretically the most rigorous contact angle but it is not common used experimentally [43,44] principally for contact angle value more than 10° [45] and in many cases it is not reached in itself, e.g., the drop is flattened by gravity and for rough surfaces the Wenzel or Cassie-Baxter wetting states are established.

Figure 1.2 *- Examples of contact angles formed by sessile liquid drops on an horizontal homogeneous solid surface: (a) hydrophilic surface/wetting drop with a* $\theta_Y < 90°$ *(b) threshold situation with* $\theta_Y = 90°$ *(c) hydrophobic surface/non-wetting drop with* $\theta_Y > 90°$ *(in this last case the surface is not smooth). Picture taken from [41].*

1.4 History of Contact Angle

Many researches in the past quested to explain the interaction between the two phases mainly a liquid and a solid surface, trying to understand acting forces by giving definitions with the help of mathematical modelling. Already in classical literature allusion to capillary phenomena appeared through the observation of insect behavior such as T. M. Plautus with “tippula”, an insect with the ability to run over water without sinking , or C. Aelianus with “ippouros”, an unknow Macedonian fly able to stay on the surface of water [46].

However, it was through the observation of thin solid body floating on water surface that what nowadays is known as surface tension came from. To explain this phenomena different theories was developed such as Aristotle's "theory of buoyancy" or Archimedes' "principle of hydrostatics" still Leonardo da Vinci in the Middle Ages, who introduced a detailed idea of the surface of things: "Tutti i termini delle cose non sono parte alcuna d'esse cose… Essi termini niente occupano". He understood the presence of a force that he called "tenacità" (tenacity) thanks to which he wanted to explain why a drop remained spherical and this lead the first qualitative idea of surface tension. During the years another interpretation of capillarity came thanks to Hauskbee who saw this in term of attractive force inside the fluid. He was followed by Jurin who in 1719 noticed that the rise or fall of a liquid inside a thin tube is inversely proportional to the diameter of the tube, and gave an equation known as Jurin law. However the studies and intuitions showed above did not bring a quantitative model for capillarity and also concepts such as surface tension or contact angle were not truly understand and explained.

A quantitative explanation of capillarity was given by Clairaut who described the capillary rise or fall of a liquid in a tube based on the existence of short-range forces that act on an arbitrary particle of the liquid due to the interaction with the liquid itself and the glass tube. He linked these forces only to geometrical parameters such as vertical distance from the free liquid surface, but he didn't describe the formation of the meniscus, neither the meniscus curvature and the forces used to explain capillary rise were not connected with the concept of "surface tension", and he didn't understand the existence of contact angle. So no proper theory was still developed for capillarity and surface tension till Segner, a Hungarian physicist and mathematician, who resumed the Da Vinci's "tenacitas" applying a primitive idea of a "surface tension" and ascribed it to forces of attraction. He approached the problem of the shape of a sessile liquid drop on a horizontal surface and on page 325 of his paper dated 1751 affirmed that, without gravity, the liquid drop would take the equilibrium shape of a sphere, but gravity flattens the constrained drop. Segner gave a useful, explicit mathematical formulation of the equilibrium conditions for the sessile drop, but his "tenacita" still did not fit accurately the modern concept of surface tension. The first correct description of surface tension was due to Monge ,a French mathematician in his paper published in 1787. From the observation of two small bodies floating on the water surface (including when both bodies are wetted by the liquid, both unwetted or one wetted and one not)he explained the attractive or repulsive forces that operated in the system. He concluded that forces acting near the liquid surface and the mutual adhesion of the liquid molecules were the cause of interactions. He stated that such forces are strongly only at the liquid surface and act tangentially to it, with the same value in all tangential directions.

Monge understood very deeply the concept of surface tension, but he didn’t provide a formalization of capillary equilibrium and also he did not recognize the fundamental role of the contact angle [46].

Thomas Young with his famous works on cohesion and adhesion of fluids published in 1805 was the first who stated and described the existence of contact angle between a liquid and solid. When he analyzed the adhesion of a liquid to a solid he considered the relationship between the contact angle and the surface tension for a solid in equilibrium with liquid and vapor, at the solid–liquid interface. He described, in words, the relation between the cosine of the contact angle and the forces that interfacial tensions exert on a liquid droplet deposited onto a solid surface, a relationship that is now known as the Young equation [40].

1.5 Work of Adhesion and Capillary Action

As we explained in the previous sections, molecules in the liquid state are involved in strong intermolecular attractive forces and a primary understanding of the contact angle requires the knowledge of their balance . When such forces are between like molecules as inside the drop itself, they are referred to as cohesive forces, while when the attractive forces are between unlike molecules as those in the liquid and in the solid, they are said to be adhesive forces and are responsible of capillary action.

The work of adhesion can be seen as the work that must be performed per unit area of the interface to separate the two phases [35].
Dupré defined the work of adhesion between solid and liquid as follow [47]:

$$W_{SL} = \sigma_{SV} + \sigma_{LV} - \sigma_{SL} \tag{3}$$

That combining with Young equation leads to the Young–Dupré equation:

$$W_{SL} = \sigma_{LV}(1 + cos\theta_{Y}) \tag{4}$$

This means that knowing the values of droplet surface tension and contact angle we are able to calculate directly the work of adhesion under the assumptions of spreading of non-reactive liquid on an ideal (physically and chemically inert,

smooth, homogeneous and rigid) solid. It shows the intensity of the bounds between the phases: lower is the contact angle better is the adhesion. Equation 4 gives also the condition for perfect wetting (ϴ=0°) as $Wa \geq 2\sigma_{lv}$ [35].
When ϴ=0° the surface free energy balance is given by S, spreading coefficient, because of Young equation halt in this condition. S is linked to the surface energies as follow:

$$S = \sigma_{SV} - (\sigma_{SL} + \sigma_{LV}) \tag{5}$$

When S>0 the liquid spreads completely whereas S<0 the liquid drop does not spread completely.

The capillary rise is the result of cohesion of water molecules and adhesion of those molecules to a solid material. When a narrow tube is brought in contact with a wetting liquid, some of the liquid rises inside the tube because capillary pressure jump induces a disequilibrium that is balanced by the rise and consequent increase in the gravitational pressure contribution. The height h of a liquid column is given by Jurin law:

$$h = \frac{2\, \gamma_{lv}\, cos\Theta}{\Delta\rho\, g\, r} \tag{6}$$

where h is the height of the capillary rise with respect to the reference level, g is the gravity acceleration (9.8 m/s^2), ρ is the density of the liquid, r is the radius of the tube, σ is the surface tension, θ is the contact angle of the liquid on the tube surface.

1.6 Contact Angle Hysteresis

The equilibrium contact angle described by the Young equation refers to a static state ,however, the phenomenon of wetting involves more than a static state, in fact many metastable states are present for a droplet on a solid substrate and contact angle can assume values within a range where the advancing contact is the maximum value and receding contact angle is the minimum [38].

We can measure the advancing and receding contact angles from dynamic experiments where droplets are in movement or easily tilting the surface where the drop is deposed. In these cases advancing contact angle θ_{adv} is where the drop becomes “larger”, along the parts of the contact line (where the liquid advances or is in incipient advancement), while receding contact angle θ_{rec} is where it “becomes” smaller (where the liquid is receding or in incipient recession) as show in Figure 1.3. The difference between the maximum advancing and minimum receding contact angles is named contact angle hysteresis [39].

$$H = \theta_{adv} - \theta_{rec} \tag{8}$$

The contact angle hysteresis can be seen as a result of substrate surface heterogeneity and roughness, impurities on to the surface, dilation of the surface (generally it may take place on polymer surfaces), consequence of the treatment of the surface by the solvent, etc [48,49,50]. Generally for the same substance, the cleaner is the surface, the smaller is the contact angle hysteresis[35].

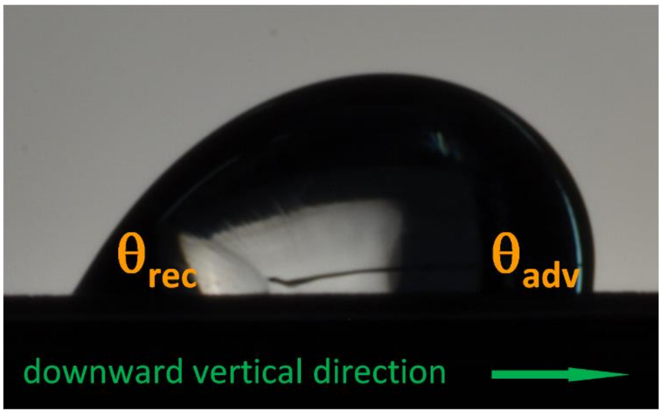

Figure 1.3 *- Illustration of the advancing and receding contact angles. Picture taken from [41].*

Contact angle hysteresis can be affected by the barrier effect, that increases it with growing roughness, and the capillary attraction/depression [50]. Due to the barrier effect it is observed that growing roughness of the surface may lead to an increase of the advancing contact angle (θ_{adv}) while the receding contact angle (θ_{rec}) decreases of the same amount. Hence, a contact angle θ_e that stands for pure barrier effect equilibrium contact angle can be calculated by the following relation: $\theta_e=0.5(\theta_{adv}+\theta_{rec})$. Due to capillary effects caused by the grooves present on the surface we can observe an increase in both advancing and receding contact angles with growing roughness for $\theta_e<90°$ (wettability improves) and an opposite effect is observed if θ_e>90° (wettability will be worsened on a rough surface rather than on a smooth one) [35].

Many studies on the advanced and receiving contact angles were performed to find what are the factors affecting hysteresis. Gaydos and Newman demonstrated that also texturing of a solid modifies the contact angle hysteresis [51] through an experiment where they evaluated the minimum patch size necessary to cause contact angle hysteresis based on the alteration of surface energy and reported a large value of about 1 µm [52].
Krasovitski and Marmur [53] pointed out that θ_A and θ_R in a tilted surface are different from a flat surface and they are functions of the tilt angle. On the other hand, different studies (e.g., [54,55,56,57]) showed that for a drop on horizontal surface θ_A and θ_R are functions of the drop size [45].
Tadmor and Yadav offered a partial solution by obtaining a unique value of θ_A which is independent of drop size with their experiment in which “Muscovite mica” was used as a substrate. They built a model for a drop that is placed gently on a surface. The model describes the deviation of θ_{AP} (“as-placed” drop) from θ_A due to the hydrostatic pressure that the finite size drop exerts on the three phase contact line; it is thus possible predict θ_A from measurement on drops of different sizes. The model is restricted to non-volatile drops with no vapor available for condensation [45].

1.7 Factors Affecting Wetting

As already said, wetting is a complex phenomenon that can be affected by a large number of factors. In non-reactive wetting some factors are in a non-exhaustive list the chemical nature spreading liquid and of the substrate, heterogeneity and roughness of the surface, intrinsic physical properties of the spreading liquid or external factor such as atmospheric conditions, while for reactive wetting some addition factors are flux usage, trace impurity addition, etc [45].
The important factors that affect wetting are briefly discussed in the next sub-sections.

1.7.1 Substrate Surface Roughness and Heterogeneity-Wenzel and Cassie-Baxter Models

Young equation cannot explain the behavior of real surfaces, which exhibit roughness. A rough surface , in fact, provides an additional interfacial area for the spreading liquid and the true contact angle would be different than the nominal contact angle. On surfaces with a morphology/texture/roughness the wetting state may be described by two models:

- the Wenzel model
- the Cassie-Baxter model

Wenzel proposed the following equation to describe the equilibrium contact angle for a liquid on a rough surface when the liquid completely penetrates the cavities of the superficial structure ('homogeneous wetting' regime)[35]:

$$\cos \Theta^{W} = r \cos \Theta^{Y} \tag{9}$$

where r is the roughness parameter and it is defined as the ratio of the true surface area and it's nominal area ($r = A_T/A_N$) [46], θ^Y is the equilibrium contact angle, θ^w is the apparent contact angle on the rough surface (Wenzel angle).
The apparent contact angle is the angle between the apparent solid surface and the tangent to the liquid-fluid interface. For two-dimensional or axisymmetric systems, there exists a unique correspondence between this definition and experimentally measured contact angles. However, for three-dimensional systems with no special symmetry, the apparent contact angle may vary from point to point [58] .

An increase of r in Wenzel model brings an improvement in hydrophobicity for hydrophobic surface ($\Theta > 90°$) and an improvement in hydrophilicity for a hydrophilic surface ($\Theta < 90$) [59,60] ,so surface roughness can be used to enhance the behavior of the corresponding smooth surface.

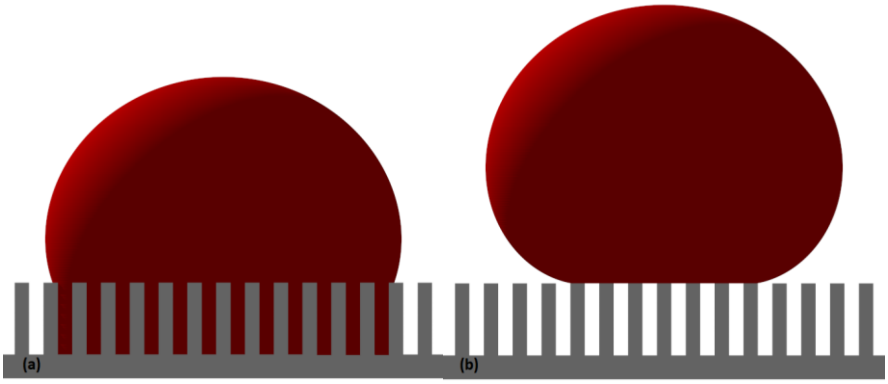

Figure 1.4 *- Representation of the Wenzel and Cassie-Baxter models for drops on rough surfaces. (a) Wenzel model: the drop penetrates completely the surface cavities so that the wetted area is greater than that projected; (b) Cassie-Baxter model: the drop remains only touching the top ends of the surface, so that the wetted area is less than the apparent one.*
Picture taken from [41].

Wenzel equation serves as a good approximation only when the roughness state is sufficiently small relative to the drop size.

Roughness has a different role and effect in non-reactive and reactive systems. In the first case it can be observed an alteration of interfacial area and the value of surface free energy associated with interface changing. In the second case, additional effects can be observed, in fact, asperities and grooves can be favored sites for reaction, diffusion, adsorption, nucleation, etc [35].

The Cassie equation for a chemically heterogeneous (two component) surfaces is:

$$\cos \Theta^{C} = f_1 \cos\Theta_1^{Y} + f_2 \cos\Theta_2^{Y} \tag{10}$$

where Θ_1^Y and Θ_2^Y are Young's contact angles respectively of the two components of heterogeneous surface; f generally is the fractional area of a component of the solid surface ($f_1 + f_2 = 1$) but with the last interpretation of this model f can be interpreted as the fraction of the three-phase contact line that crosses heterogeneous patches. Again, the Cassie equation serves as a good approximation only when the heterogeneity size is sufficiently small relative to the drop size [46].

The Cassie–Baxter equation is then used to predict contact angle when the liquid is unable to fill the gap between surface protrusions and consequently air is trapped below the droplet. In this case the equation becomes:

$$\cos \Theta^{CB} = f_1 \cos \Theta^{Y} - f_2 \tag{11}$$

where f_1 and f_2 are the total areas of the solid–liquid interface and liquid–air interface, respectively, per unit area under the drop. To take into account roughness the Cassie–Baxter equation can be further modified as follow:

$$\cos\Theta^{CB} = r_1 f_S \cos\Theta - (1 - f_s) \tag{12}$$

where f_s is the fraction of the liquid base in contact with the solid surface ($f_s < 1$); $(1 - f_s)$ is the fraction of the liquid base in contact with air pockets; r_1 is the roughness ratio of the wetted solid and it changes in relation with the amount of liquid that penetrates the surface structure; typically it is different from the Wenzel roughness factor r. Both Cassie and Cassie–Baxter equations are approximate equations for the equilibrium condition of the drop. With the increase of the drop dimension the approximation becomes better as compared with the largest wavelength of the surface heterogeneity [46].

1.7.2 Liquid Properties

Spreading of a liquid drop over a solid substrate is affected by viscosity, surface tension and density. We know that wettability of a surface for a liquid can be improved by reducing the liquid surface tension, for this scope surfactants are generally used. It is well known that viscosity will resist any spreading activity by the liquid. Viscosity has an important role in wettability, it is reasonable to expect that a droplet of an higher viscosity liquid spreads little compared to that of lower viscosity, this is because, higher viscous dissipation reduces the rate of spread.

1.7.3 Gravity

The effect of gravity is generally not taken into account in wetting studies since the liquid drops involved in the experiments are small enough to affect the drop shape. It is accepted that if the drop radius is less than the already cited capillary length, the gravity force does not affect the spreading process [35].

1.7.4 Atmosphere

As wettability is a function of the triplet solid, liquid, surrounding gaseous atmosphere, the latter obviously influences both reactive and non-reactive wetting and has a prominent role in the spreading of metallic liquids like solders. It was observed that with the reduction in residual oxygen level in the atmosphere spreading starts at lower temperatures. In reactive system oxided surface causes a deterioration in wettability so the use of flux is necessary and inert atmosphere is helpful in improving efficiency/function of fluxes [61,62]. Nitrogen is a good element to remove oxygen, because it is an inert and chemically non-reactive element with most of the metals. This acts as a protection of the metal surfaces from oxidation during heat-up and proper flux action. An improvement in wetting is also observed in N_2 atmosphere with respect to especially for soldering [63].Good wetting or solderability is generally attributed to low surface tension of the spreading liquid.

1.7.5 Temperature

Temperature is a factor affecting wetting both non-reactive and reactive systems. Properties of liquid as well as substrate like viscosity, surface tension, oxidation behavior, reaction rate are affected by temperature. An increase of wettability in non-reactive system can be obtained by an increase in temperature thanks to the decrease in viscosity and surface tension of the liquid [64]or, in reactive systems, with the increase of the diffusion rate, resulting in severe oxidation in most of metals.

1.7.6 Fluxes

Fluxes are used in reactive wetting to overcome the barrier effects of oxide film [65] and have two major functions [66] [67] [68]: their chemical function is to provide a tarnish-free surface and to keep the surface clean, while the physical function is to remove the reaction products from the surfaces to allow the solder to come into direct contact with the base metal surfaces.

Fluxes can be classified into two categories: inorganic and organic. The first category includes inorganic acids, salts and gases that has corrosive action, for this reason cleaning is necessary after their use. Those in the second category are milder than inorganic ones and include rosin base or resin base fluxes and generally contain small quantity of activators. There is good agreement in the literature about that fluxes improve the wetting force by increasing the solid/vapor interfacial energy or by lowering the solid/liquid interfacial energy, in fact many experiments were made by different researchers such as Takao, Lopez or Plas [35].

Therefore, oxide layers present on the surface alter the interfacial properties and cause inferior wetting (that is why fluxes are used to remove the oxides and other contaminants from the surface). Temperature also affects fluxes that being generally composed of organic solvents or halides are active at temperatures about 10–20° below the melting/liquidus temperatures of solders. The increase in the temperature beyond their activation temperature may cause evaporation of the flux and this might be the reason for poorer wettability reported by some researchers at higher temperatures.

1.7.7 Trace elements

Trace elements are used to improved wettability in reactive system. It has been observed that wettability is increased by the branzing and soldering with binary and ternary lead free soldering which helps increase mechanical properties too. Improvements in wettability can be seen compared to the original substrate when mixtures with alloy metals and other chemical species mixture are sprayed over [69].

Chen et al. examined the action on wettability of addition of gallium on Sn–Zn–Ag and Sn–Zn–Ag–Al lead-free solder alloys [70]. As a result of their experiment they observed a significant reduction in wetting time and increase in wetting force.

To reduce the contact angle, rare earth elements (“RE”) increases the effective grain size and reduce the surface tension, so that the substrate and the solder show a reduced contact angle. On the contrary, an higher proportion will increase viscosity and cause a reduction in wettability because of oxidation of RE over solder. One experiment was conduct by Wang et al. discovering the effect of Zn addition to lead-free Sn–0.7Cu solder alloy on wetting behavior of the alloy with Cu substrate [71]. The Zn was added in the range of 0-1 wt% . They measured an increase in contact angle values from 42° at 0% Zn to 50° at 1% addition of Zn so the addition leads to a decrease of wettability [35].

1.8 Measurement of Contact Angle

Given the importance of the quantity, many techniques have been developed to measure the contact angle. Most of such techniques can be classified into two main groups: the direct optical method and the indirect force method. The next sections will be devoted to brief descriptions of the most used techniques, from the conventional telescope-goniometer method to, the Wilhelmy balance method and to the developed drop shape analysis.

1.8.1 Direct Measurement by Telescope-Goniometer

For flat surfaces, the wetting property was initially determined by direct measurement of contact angle by viewing the drop profile. Bigelow et al. demonstrated that a telescope goniometer was capable to view the liquid drop profile placed over the smooth surface making it possible to measure the angle formed due to the three interfacial tensions [72]. Using bubbles, an image of the adhering bubble can be projected onto a screen and the outlines traced, there after the angle is measured. Most importantly, a photographic image can be captured for better understanding as proposed by Leja and Poling in 1960.

The first commercial telescope goniometer was manufactured by Rame-Hart instrument company and designed by Zisman. It is one of the most widely used techniques for contact angle measurement, where a horizontal telescope is used to directly measure the tangent angle of the liquid droplet on the solid surface. The equipment is made up of a horizontal stage for holding the substrate, a micrometer pipette to form a liquid drop, an illumination source and a telescope equipped with a protractor eyepiece. The measurement is achieved by simply aligning the tangent of the sessile drop profile at the contact point with the surface and reading the protractor through the eyepiece[38]. During the years, to improve the accuracy and precision of measurement some equipment modifications have been made such as the integration of a camera to take photographs of the drop profile, high magnifications for a detailed examination of the intersection profile [73],a motor-driven syringe to add or remove amount of liquid to study advancing, receding, or dynamic contact angles [74].

The points of strength and of weakness of this technique are:

- PROS: simplicity of operation; request of small amounts of liquid (a few microliters) and small surface substrates (a few square millimeters).

- CONS: presence of impurities due to the small size of the liquid and substrate; error in the measurement because relies on the accuracy and consistency of the operator in determining the tangent line; no accuracy for low contact angle (below 20°) due to the flatness of droplet that make difficult the assignment of the tangent line; imaging device only focuses on the largest meridian section of the sessile drop, which means the profile image reflects only the contact angle at the point in which the meridian plane intersects the three-phase line; problems due to the dependence of contact angle on the drop [75,76] ; variation in contact angle measurement due to surface heterogeneity or roughness.

It is demonstrated that the accuracy that can be obtain with the direct measurement of sessile drop contact angles is approximately ±2° [77,78].

McDougall and Ockrent [79] was able to calculate both advancing and receding contact by tilting the solid surface till the drop moves. This method is recognized as “tilted plate” method where the contact angle at the lowest and highest point in an incipient moving drop are respectively assigned as advancing and receding contact angles. Thanks to this method Extrand and Kumagai [80,81] was capable to evaluate contact angle hysteresis (difference between advancing and receding contact angle) of liquid on different polymer surfaces such as silicon wafers and elastomeric surfaces.

Zisman and his co-workers [82] were the first who replace the micrometer pipette with a fine platinum wire to create sessile drops. In their experiments a cleaned and heated wire (8 cm long and 0.05-0.10 mm in diameter) was put into the liquid and fixed to produce a pendant drop. This at first hanged from the tip of the wire and after was slowly brought in contact with the solid sample in order to form a sessile drop. Their studies was based on the evaluation of the kinetic energy acquired from the drop when flew off the wire and about its deformation when it leaves the wire which can lead to metastable angles.

Another instrument used to evaluate a drop profile photograph was the “tangentometer”. Used by Phillips and Riddiford [83], as well as McIntyre [84] consisted in a mirror set at the drop baseline. The mirror at the drop tip was put normal to the photograph, and it is rotate still a continuous curve is obtained by the drop shape with its reflection image in the mirror.
In this method the tangent line is the straight edge and protractor attached to the mirror indicated the contact angle. This method still suffer low accuracy.

1.8.2 Captive Bubble Method

The technique was introduced by Taggart et al. [85] and consist in the injection of a small amount of air (about 0.05 ml) into the liquid of interest to form an air bubble below the solid sample. This is a direct measurement of contact angle and is characterized by:

- PROS: solid surface in contact with a saturated atmosphere; minimum contamination of the solid-vapor interface (less than in the sessile drop method); easy control of the temperature of the liquid; possibility to study the temperature-dependence of contact angles.

- CONS: more amount of liquid required than in the sessile drop method; swelling of the solid sample after immersion into the liquid; dissolution of the solid film by the liquid.

1.8.3 Wilhelmy Balance Method

To improve the methods for contact angle analysis, another simple technique was introduced in 1863: the Wilhelmy plate method [86].
It is an indirect method, often used to determine the wetting properties of biomaterials. When a thin, smooth, vertical plate is brought in contact with a testing liquid, the change in its weight is detected by a balance. The forces acting on the plate are a combination of buoyancy and the force of wetting (the force of gravity remains the same). The total force F exerted on the plate is given by:

$$F = \gamma_{lv}\, p\, cos\Theta - \, V\, \Delta\rho\, g \tag{13}$$

where V is the volume of the displaced liquid, $\Delta\rho$ is the difference in density between the liquid and air, g is the acceleration of gravity. So the value of contact angle can be easily calculated knowing the liquid surface tension and the solid perimeter.
Advancing or receding contact angle can be measured respectively pushed into or pulled out the solid sample from the liquid.

- PROS: high accuracy because the measure of contact angle is reduced to the measurements of weight and length; the measured force at any given depth of immersion is already an averaged value; more accurate contact angle value that reflects the property of the entire sample; useful for studying dynamic contact angles and contact angle hysteresis at different wetting speeds.

- CONS: solid sample must have uniform cross section and regular geometry; difficulties in measurement of the perimeter and the wetted length of samples; sample must have the same composition and topography at all sides, which can be difficult to obtain especially to investigate films or anisotropic systems; large amount of liquid, which might cause the solid sample to swell and/or absorb vapor unintentionally.

1.8.4 Capillary Rise along Vertical Plate

When a liquid comes in contact with a vertical plate, it will rise due to the capillary effect and the height at which it reaches can easily be calculated by the Laplace equation [87]:

$$sin\,\Theta = 1 - \frac{\Delta\rho\, g\, h^2}{2\gamma_{LV}} \tag{14}$$

where $\Delta\rho$ is the difference in density between liquid and vapor, g is the acceleration of gravity, and γ_{lv} is the liquid surface tension. Thus the contact angle measurement has been brought down to a measurement of a capillary rise, with the theoretical requirement of being “infinitely” wide can be satisfied by plates that are about 2 cm in width. Dynamic contact angles are achieved by moving the plate up or down.

- PRO: particularly suitable for measuring the temperature-dependence of contact angles [88].
- CONS: surface tension of the liquid must be known; uncertainty in the valuation of surface tension in case of solutions that comprise surface active materials; adsorption of the surface active agents so that different interfaces can change the surface tension and alter the contact angle measurement.

With this method the accuracy that can be reached for a specially, good prepared surface that forms a practically straight meniscus line, is ± 0.1°.

1.8.5 Capillary Tube

The Wilhelmy balance method can also be used to measure the contact angle by means of a capillary tube when both the inside and outside surfaces of the latter are made of the same substance. The sum of the inner and outer perimeters should be designed as the perimeter p of tube. For a vertical capillary with a sufficiently narrow circular cross section, the meniscus might be considered as spherical, and the capillary rise is given by:

$$h = \frac{2\,\gamma_{lv}\, cos\Theta}{\Delta\rho\, g\, r} \tag{15}$$

where r is the capillary radius, g is the gravity acceleration, and $\Delta\rho$ is the difference in density between the liquid and vapor. From the experimental measurement of h and r the contact angle can be calculated. Equation 15 is known as the Jurin rule, named after James Jurin, who studied this phenomenon in 1718.

1.8.6 Axisymmetric Drop Shape Analysis (ADSA)

ADSA methods are based on the numerical fit between the shape of experimental drops and the mathematical model given by the classical Laplace equation of capillarity. Under the assumption that the experimental drop is Laplacian and axisymmetric, and the only external force is gravity, in the numerical scheme, some Laplacian curves with known surface tension are fitted to the experimental profile. The correct value of liquid-fluid interfacial tension is identified by the best fit. In ADSA, an image processing algorithm (including edge detection and optical correction) provides the coordinates of the experimental profile. The experimental profile and physical properties such as density difference are inputs to the following numerical scheme.

ADSA-P (perimeter) is the first generation of the axisymmetric drop shape analysis profile method developed by Rotenberg et al. [89]. According to this method an objective function is defined as the sum of the squares of the normal distances between experimental profile points and corresponding theoretical profile points, and its minimization is the match. The numerical integration of the theoretical drop profile is usually done in the peculiar coordinate system arc length – turning angle (Fig. 1.5), that makes it very simple. ADSA-P was improved by Cheng et al. [90] implementing a computer-based edge detection operator (Sobel [91]) in order to automate the extraction of the drop interface profiles. To improve the accuracy an optical distortion correction technique was also introduced. The method failed in analyzing large and flat sessile drop, for which in fact no accurate results are achieved due to the flatness of the apex of the drop. ADSA-P was extended by Rio and Neumann [92] who integrated a more efficient algorithm.

To analyze non-ideal surfaces and very low contact angle (less than 20°) another branch of the ADSA method was created —the axisymmetric drop shape analysis diameter (ADSA-D) [93,94]. ADSA-D is based on the analysis of a top view image of the drop and on the measure of the contact diameter. By measuring different contact angle with these two methods it was proven that the values obtained are closely the same, varying no more than ±0.4°, with ADSA-D that gives a higher precision for low contact angles.

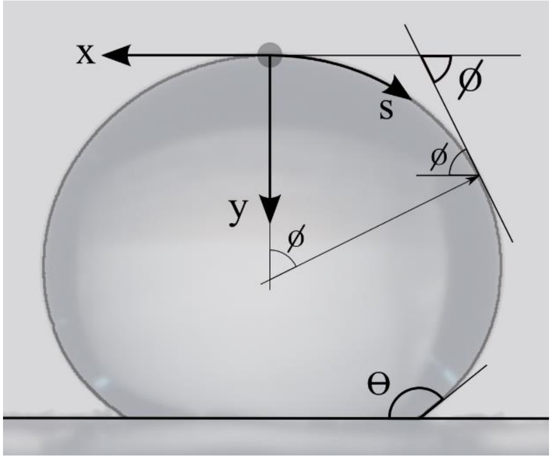

Figure 1.5 *- Coordinate system used in the numerical integration of the Laplace equation for axisymmetric liquid-fluid interfaces. S is the path length from top (arc length from the drop apex), θ is the angle from the vertical axis.*

1.9 New Challenge: Superhydrophobic Surfaces

As already said, superhydrophobicity is the tendency of a surface to very strongly repel water drops. A surface is classified as superhydrophobic if it exhibits a high apparent contact angle (>150°), low contact angle hysteresis (<10°), low sliding angle (<5°) and high stability of Cassie state. In the 1990s, biologists and materials scientists started to study natural superhydrophobic surfaces and particular interest was pointed on leaves of water-repellent plants such as Nelumbo nucifera (Lotus). Their hierarchical structures, responsible for superhydrophobicity, were studied by Burton and Bhushan [95] and Bhushan and Jung [96]. The SEM study reveals that the Lotus leaf surface is very rough and covered by papillose epidermal cells , which are in their turn covered by an additional layer of epicuticular waxes [97]. The wax is present in crystalline tubules, composed of a mixture of long-chain aliphatic compounds, principally nonacosanol and nonacosanediols. The water droplets on these surfaces readily sit on the apex of the nanostructures because air bubbles fill in the valleys of the structure under the droplet, so the surface exhibits considerable superhydrophobicity with a value of static contact angle and contact angle hysteresis respectively of 164° and 3° respectively [98,99] .The water droplets on the leaves remove any contaminant particles from their surfaces when they roll off, leading to self-cleaning [100].

The interest in self-cleaning surfaces is driven by the desire to fabricate such surfaces for satellite dishes, solar energy panels, photovoltaics, exterior architectural glass and green houses, and heat transfer surfaces in air conditioning equipment. Also in biomedical applications the non-wettable character has been claimed in ranging from blood vessel replacement to wound management. Fabrication of superhydrophobic surfaces has been an area of active research since the mid-1990s. Techniques to make superhydrophobic surfaces can be simply divided into two categories: first, it is possible to make a rough surface from an initially hydrophobic material and, second, to modify a rough hydrophilic surface by modifying surface chemistry or applying a hydrophobic material upon it.

1.9.1 Roughening a low surface energy material

1. Fluorocarbons

Fluorinated polymers has low surface energies so roughening these polymers in certain ways directly leads to superhydrophobicity [101,102,103].
Zhang et al. [65] in their work presented how to achieve superhydrophobic film in a clear and efficient way by stretching a poly(tetrafluoroethylene) (Teflon®) film. Superhydrophobicity is assumed to be due to the void spaces presents through the fibrous crystals that the film is composed.
Shiu et al. [66] treated a Teflon® film with oxygen plasma and obtained a rough surface with a WCA of 168°. Many fluorinated materials have low solubility, for this reason they can not be directly used but they are generally linked [104]or blended [105] with other materials (which are often easy to roughen) to achieve superhydrophobic surfaces.

2. Silicones

Polydimethylsiloxane (PDMS) is another material with low surface energy, intrinsic deformability and hydrophobic property, for that it can be quickly turned into superhydrophobic surfaces using various methods thanks of its [106,107,108].

For example, Khorasani et al. [106] treated PDMS using a CO_2-pulsed laser as an excitation source. Another way to exploit the low surface energy of PDMS is to use a block copolymer such as poly(styrene-b-dimethylsiloxane) (PS-PDMS). For instance, Ma et al. [109] made a superhydrophobic membrane in the form of a nonwoven fiber mat by electrospinning a PS-PDMS block copolymer blended with PS homopolymer.

3. Organic and inorganic materials

It was observed that nature achieves non-wetting and self-cleaning properties using paraffinic hydrocarbons so several groups studied and created superhydrophobic surfaces made from organic materials.

For example, a cheap and simple method to produce a highly porous superhydrophobic surface of polyethylene (PE) was suggested by Lu et al. [110] by controlling its crystallization process. An improvement of non-wettability (CA up to 173°) was also obtained by adding nonsolvent (cyclohexanone) to the PE/xylene solution to form nanostructured floral-like crystal structures. Jiang et al. [111] obtained a superhydrophobic film made of porous microparticles and nanofibers by using electrostatic spinning and spraying a PS solution in dimethylformamide (DMF). In the last few years other organic materials were turned into superhydrophobic surfaces such as polyamide [112], polycarbonate [113] and alkylketene dimer [114].

Yan et al. [115] synthesized a poly(alkylpyrrole) film by electrochemical polymerization the needle-like poly(alkylpyrrole) structures grown perpendicularly to the surface of the electrode yielded an environmentally stable superhydrophobicity.

Also from some inorganic materials superhydrophobic surfaces have been produced for example, from ZnO [116,117] and TiO_2 synthesized through two-step solution method.

1.9.2 Making a rough substrate and modifying it with low surface energy materials

1. Lithography

Lithography (e.g. photolithography, electron beam lithography, X-ray lithography, soft lithography, nanosphere lithography and so on) is a useful and common technique that alloys the creation of a large area periodic micro-/nanopattern [118,119]. The effects of the pore size and shape on wetting was studied by Abdelsalam et al. [120] by conducting systematic observation and study of the wetting of structured gold surfaces combined by electrodeposition through a template of submicrometer spheres.
Fabrication of ordered arrays of nanopits and nanopillars by using electron beam lithography and plasma etching was made by Martines et al. [121]. They obtained a superhydrophobic surface made of tall pillars with cusped tops with CA of 164° and hysteresis of 1° after a hydrophobization with octadecyltricholorosilane.

2. Sol–gel processing

Sol–gel processes permits to fabricate superhydrophobic surfaces from a variety of materials [116,122,123,124,125].The sol–gel process causes the decrease of the surface energy of materials and so no post-process hydrophobization is required for the achievement of superhydrophobicity. For example, for organo-triethoxysilanes which exhibited binary switching between superhydrophobicity and superhydrophilicity when exposed to different temperatures, Shirtcliffe et al.[124] used a porous sol–gel foams. Hikita et al. [126] created a sol–gel film with super liquid repellency by hydrolysis and condensation of alkoxysilane compounds using colloidal silica particles and fluoroalkylsilane as the starting materials. Instead of blending low surface energy materials in the sol.-gels, Shang et al. [127] described a procedure to make transparent superhydrophobic surface by modifying silica based gel films with a fluorinated silane.

3. Layer-by-layer (LBL) and colloidal assembly

To create a pH-sensitive PHH/PAA multilayer which formed a honeycomb-like structure on the surface after an appropriate combination of acidic treatment, LBL techniques is used by Zhai et al. [128]. Once the structure is cross-linked, silica nanoparticles are deposited on the surface via alternating dipping of the substrates into an aqueous solution of the negatively charged nanoparticles and an aqueous PAH solution, followed by a final dipping into the nanoparticle suspension. Once the surface is modified by the chemical vapour deposition of (tridecafluoro-1,1,2,2- tetrahydrooctyl)-1-trichlorosilane superhydrophobicity is obtained follow by a 2 h thermal annealing. LBL self-assembly could also be combined to prepare superhydrophobic surfaces with electrochemical deposition as shown by Zhang et al. [129,130,131]. Correct surface roughness for superhydrophobicity is demonstrated by assembly from colloidal systems [132,133,134].

4. Electrochemical reaction and deposition

Another method used to create superhydrophobic surfaces is electrochemical reaction and deposition. A validation of the technique came from Zhang et al. [131] who evidenced that a surface with dendritic gold clusters layer, which was formed by electrochemical deposition onto an indium tin oxide (ITO) electrode modified with a polyelectrolyte multilayer, showed superhydrophobic properties after deposition of a n-dodecanethiol monolayer.

Shirtcliffe et al. [135] arranged a resembled “chocolate chip cookies”, a double-roughened copper surface, by electrodeposition and patterning technique. Further hydrophobization with fluorocarbons yielded superhydrophobicity with CA of 160°. Recently Cho’s group [136] presented a lotus leaf-like superhydrophobic metal surface created by using electrochemical reaction of Cu or Cu–Sn alloy coated on steel sheets with sulfur gas, and followed by perfluorosilane treatment.

Chapter 2

Experimental Setup and Sensitivity Analysis

2.1 Introduction

As already said, the aim of this work is three-fold: first of all, the contact angle measurement procedure will be analyzed to assess its accuracy; then the home-made setup will be tested; finally it will be used to measure the contact angle for water in air on various surfaces and particularly on those of interest for fuel cells. This chapter will describe the first two aspects.

Starting from the analysis of the measurement technique, it mainly consist in a sensitivity analysis conducted over a series of artificial, computer-generated, drop images. The result of the first analysis is the optimization of the used software parameters. The process is based on the calculation of the relative error that affects measurements when processing images at different resolution. The "best" parameters are obviously the ones giving lower error and leading to the best drop fitting.

The second part of the chapter describe the creation of the "home-made" laboratory (due to the closure of Polimi Laboratories for the Covid-19 global emergency period), also evidencing the problems of a direct drop measurement and the difficulties to create a valid experimental setup in order to achieve a suitable drop image to process. This is even more true when considering that the setup was built with domestic objects and also the samples were created with simple things that can be found in the daily life, like nail polish and ceramic polish normally used to restore home parts.

To make the description of the sensitivity analysis more clear and easier to follow, the experimental setup and measurement procedure will be described first.

2.2 Experimental Setup

Experiments involve the study of the shape of sessile drops (drops sitting on a surface after a gentle deposition) on various surfaces, in order to measure the contact angle and characterize their surface properties.

Drop-surface pictures are analyzed using dedicated software, which effectively employs image processing and numerical techniques to fit the theoretical expression of the Laplace-Young equation to the experimental shape of the drop, from which the contact angle can be extracted. A home-made system is built to place the drops on the surface and for the subsequent image capture, made possible using a reflex camera.

The contact angle measurement requires pictures in back-illumination, with precise characteristics, that can be taken following four simple rules:

1. The background have to be homogeneous and well discernible from the drop.

2. The surface have to be flat and perfectly still during the deposition of the sessile drop (and also during drop removal if a picture of the background is also taken).

3. If a second image is used to help in background subtraction, the two images (with and without the drop) must be perfectly aligned.

4. Each image must contain only one drop.

So having a suitable setup is fundamental to provide high quality pictures.

2.2.1 Polimi Laboratory

Different studies on wettability were conducted at the Energy Department, Politecnico di Milano, such as the influence of temperature on wettability, tests involving materials for HVAC system and studies involving the effect of different hydrophobic agents onto the surface of gas diffusion layers and microporous layers for PEM-FC.

For such campaigns, the experimental tests were conducted using the setup available at the Multiphase Thermo- Fluid Dynamics Laboratory. The measurement of static contact angles or the dynamic advancing angles, as well as the measurement of surface tension is carried out with the video supported contact angle measurement setup. The system (Figure2.1) is composed by an anti-vibrating optical bench (Newport, SA Series, 1.2 0.80 m) with a carrying structure in aluminum alloy. A high precision metering pump (Cole-Parmer Instrument Company, model AD74900) completed by suitable syringes (Hamilton) is used to generate microliter drops of controlled volume. Moreover there is a ‘‘surface analyzer’’ (SM Sistemi di Misura s.r.l., model RT80) to characterized the surface under investigation in terms both of profile and of roughness. A 800 W lamp equipped with a diffuser provides the lighting necessary to the photographic acquisitions, which are taken using a SLR digital camera Nikon D90 with a AFS 60 mm F2.8 Macro lens. Side shots of the deposed drop are acquired and transferred to a personal computer. Ad hoc software, developed, within the MATLAB programming environment [137], is used to implement the procedures

Figure 1.1 *- Experimental setup at the Multiphase Thermo- Fluid Dynamics Laboratory. (Picture taken from C. Santoro et al. CARBON 67 (2014) 128 –139).*

2.2.2 In-house experimental setup

Due to the lockdown imposed to contain the spreading of the Covid-19 virus, that also made impossible to access the Polimi laboratory, a new setup was studied, that could be built at home, trying to recreate the same basic fundamental characteristic of the setup (while being conscious of the limits). The new experimental setup (Figure2.2) consists of the following elements:

- A desk as a work bench where to conduct the experiments.
- A light source provided by a table lamp, that can be moved vertically, with the original yellow light substituted with a multi-LED white lamp.
- A medical syringe to depose the drop and partially calibrate its volume.
- One or two soft building blocks as the support of the sample.
- A Canon Power Shot SX520 HS as the camera.

Figure 2.2 *- In-house experimental setup.*

Obviously pictures provided by the homemade laboratory have a lower quality with respect to those acquired at the Polimi laboratory where the setup is designed "ad hoc" with the use of a professional macro lens, a tripod, specific lighting, etc. Particularly the macro lens allows to focus at a very close distance,

which is essential for photographing drops, while the tripod helps to keep the camera steady to better adjust the focus and to avoid vibrations.
Moreover the drop photography technique requires mastery of two fundamental concepts: depth of field - It is essential to be able to have the whole image in focus and exposure times - to obtain still and sharp images.

So the camera was first of all put in manual focus mode. Different examinations were conducted in order to understand the best camera parameter to set, best position of light and correct camera alignment to reduce the noise and disturbances.
Comparison was performed between pictures obtained placing the camera near the drop in two different mode, normal and macro, and far from the drop using all the camera zoom extension. For each position it was also varied the ISO (Sensor Sensitivity), time of exposition and diaphragm aperture in order to set the best values.
Different picture tests showed that the best quality picture is provided with normal camera mode with low ISO (100-200), a medium diaphragm aperture (in the range of 7-8), relatively long exposure time (1/8’’) and low focus distance (11 mm).
All the found values are compatible with the ones used in Polimi laboratory , apart from the aperture, that using the macro lens must be much lower to have a suitable depth of field.
It was decided not to use the telephoto mode because it provides lower quality pictures and also because it requires long distance from the drop and, without a tripod, pictures are considerable affected by the operator ability to stay still.
Regarding alignment, that is an important factor because a not good position of the camera causes distortion in the contact angle measurement, camera was arranged as near as possible to the drop on a rigid support (as an example a book), aiming at the correct alignment with the drop base line. Obviously the precision granted by an anti-vibrating bench with height and inclination regulation could not be reached; nonetheless suitable alignments could be obtained.
A crucial factor to set was light. Generally pictures are taken with a back illumination where the drop is dark with the minimum reflection possible on a homogeneous and bright background. To be processed drops have to be dark on a bright background, so too much light makes the drop transparent on the contrary too low lighting makes all dark; in both case image binarization and extraction of the drop contour becomes impossible.
A desk lamp cannot provide a direct background illumination so as a solution a white background was created with simply a sheet of paper towards which light

was headed in order to provide the diffuse light necessary to take a correct picture. Successively a long campaign with different source lights and different positions and intensities was carried out to find the best solution. Also light reflection was an issue to be considered; in fact in some picture the top part of the drop was too bright as a consequence of reflection and so during the segmentation processing it was wrongly assigned to the background.
The final choice was to cover the desk lamp with a sheet of paper (to mitigate light intensity), to point it toward the wall behind the drop, positioning in a central position and far from the drop (in order to give mainly diffuse light to reduce reflection).

2.3 Description of the technique

Contact angle is calculated on “as placed drops”, i.e. gently deposed drops on a static surface with no vibration or other disturbances. As explained in the previous chapter , contact angle measurement on flat surface may be conducted by several techniques, ranging from the oldest and simplest ones to the most recent and accurate, such as ADSA that was used for these tests. ADSA is the only curve-fitting method with a physical basis, as it analyzes the drop shape based on the Young–Laplace equation: it finds the theoretical profile that best matches the drop profile exacted from the image of a real drop, from which the surface tension, contact angle, drop volume and surface area can be computed. The strategy employed is to fit the shape of an experimental drop to a theoretical drop profile according to the Young-Laplace equation of capillarity, using the Eotvos number (Eo) or surface / interfacial tension plus apex curvature as the adjustable parameters. For the best fit the contact angle can be determined. So ADSA is based on the fitting of theoretical equation to an experimental contour. In its dimensionless version based on the Eo number – the one used in this work - the only input is a side photograph of the drop surface system.
Practically the measurement of contact angle is made up of different steps (Figure 2.3):

1. Acquisition and preparation of the images (e.g. cropping if needed);
2. In case a separate image of the background is acquired, image registration and calculation of the difference from the image with the drop.
3. Image segmentation, extraction and smoothing of drop profile
4. Fitting of the Laplace-Young equation to the experimental boundary and determination of the contact angle.

The first steps consists in taking a picture of the drop on an homogeneous background and cropping it to reduce the weight of calculation. In fact, the drop occupies only a part of the image and for this reason it is reasonable to consider only the part containing it.

The second step was not necessary for the analyses in this thesis because drop extraction from the background could be performed directly on the images including the drop, with no need to “help” background subtraction using a second image with the background alone.

After the image acquisition, the drop is processed to extract it from the background; then it extracts the drop profile, interpolates the points acquired through a polynomial curve and finally calculates the contact point and the corresponding value of the turning angle.
To separate the drop from its background a standard technique of image processing is used, consisting in the image conversion in gray tones and its segmentation on two level (binarization). The process is implemented using different built-in MATLAB functions:
rgb2gray converts RGB image or colormap to grayscale by eliminating the hue and saturation information while retaining the luminance;

graythresh calculates a global threshold for image binarization, using Otsu's method, which chooses the threshold to minimize the intraclass variance of the thresholded black and white pixels [138].

im2bw produces binary images from indexed, intensity, or RGB images. To do this, it converts the input image to grayscale format (if it is not already an intensity image), and then converts this grayscale image to binary by thresholding. The output binary image has values of 1 (white) for all pixels in the input image with luminance greater than a certain level (here the output of the graythresh function is used) and 0 (black) for all the other pixels.

Once the binary image is obtained, the boundary between the regions (which represents the drop contour) is obtained by another built-in MATLAB function, **bwtraceboundary.**

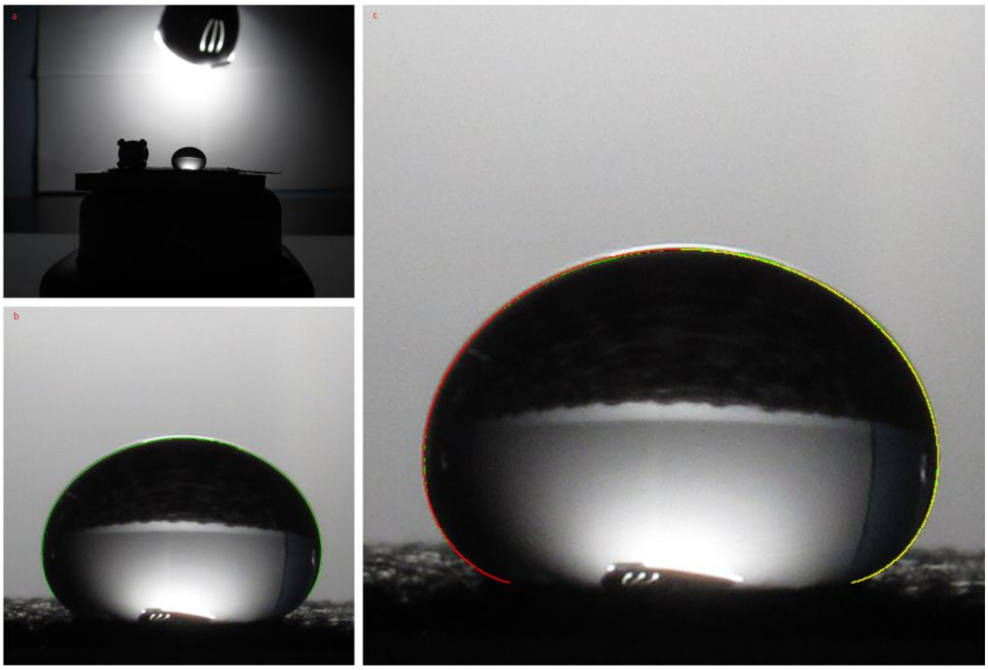

__Figure 2.3__ - Extraction of the drop contour and contact angle measurement (a) Drop picture (b) Contour extraction (c) Contour fitting.

The theoretical drop profile is calculated by basic finite difference (centered form) integration of the axisymmetric Laplace–Young equation in its dimensionless arc-length expression, that was implemented in a new MATLAB function.

Then fitting of the different possible Laplacian curves at the experimental contour is made by minimizing total mean-square error between the theoretical and experimental profiles. In this case the MATLAB built-in function **fminsearch**. The Young-Laplace fit gives the best correspondence between the theoretical drop shape and the real drop shape.
Further details about the used functions can be found in Appendix A.

All the steps defined in the description of process have some parameters whose values must be chosen by the operator.
When the image is processed the image region to be processed must be chosen, by setting an height under which the image is not considered. Generally it is set to a value that is just above the minimum height at which the drop appears. This is particularly useful for the case of fabrics, etc. to avoid disturbances due to fibers protruding from the surface and when performing the difference between

the drop and background images, because despite the attention when the sample are "complex" there is no way to avoid non-zero differences between image with and without drop (even only due to the shadow of the drop or reflections).

Other important parameters are set during the extraction and fitting of the contour, like threshold and smoothing values, number of iterations and finally the base line value at which the angle is calculated.

The threshold value is used to binarize the difference image by passing it from tones of gray to white / black. If the experimental images are very well contrasted setting this value is easier, otherwise some “fine tuning” may be necessary.

Attention must also be paid in choosing the value of smoothing because an approximating cubic spline is used. Generally the larger the smooth value the more the contour becomes smooth but it also loses accurate following of the pixels in the original contour.

The procedure also have a maximum number of iteration after which the process is stopped.

Finally, the base line value, in terms of the height at which the tracing of the drop profile is stopped and contact angle is estimated, must be selected. It is the quota of the base segment, side projection of the triple line. A not correct value of the base line can lead to significant errors, especially for conditions of high hydrophobicity and hydrophilicity, because a single pixel of difference can vary the contact angle measurement of various degree. Despite many test for automatic selection, based on sample extraction by image processing or techniques to identify straight lines (e.g. Hough transform), no satisfactory results were obtained, so this is still a step entrusted to the operator.

2.4 Sensitivity Analysis

Sensitivity analysis can be defined as “ a method to determine the stability of an evaluation by understanding how much results can be influenced by change in method, models, differences in values and assumptions” with the aim to identify “results that depends on wrong value” [139]. It is the study of how the uncertainty in the output of a mathematical model or system (numerical or otherwise) can be split off and assigned to different sources of uncertainty in its inputs. [140,141]. In fact, beside some experimental influencing quantities such as drop displacement, drop volume, horizontal or inclined set-up, etc., contact

angle determination also depends on the image analysis and the used fitting procedure to extract the contact angle from the experimental.
In this section the conducted sensitivity analysis and validation of the measurement technique are explained, to evidence and better understand possible causes of errors that affect the accuracy of contact angle measurement.

As already said, despite many attempts to improve the contact angle measurement, the technique remains to a certain degree subjective and depends on the experience and skillfulness of the operator. During the process the operator have to choose the value of some important parameters. These values are relevant for the contact angle measurement and if not chosen appropriately the validity of measurement can be heavily affected.

Sensitivity analysis has been based in this work on the evaluation of the effect of input values for number of iterations in the fitting step, smoothing value for contour smoothing, base line value and camera alignment, for images at different images resolution (square images with 250, 500, 1000, 1250 and 1500 pixel along each direction), knowing the real contact angle and the Eotvos number of each drop.

For each assigned parameter value the relative error (namely MAPE - mean absolute percentage error:

$$M = \frac{1}{n}\sum_{t=1}^{n}\left|\frac{F_t - A_t}{A_t}\right| \tag{16}$$

where F_t is the forecast value and A_t is the actual value)

was calculated in order to understand the importance and weight of the parameters in the process. This procedure leads to the software optimization, discovering the best value for fitting, that are the values that minimized the relative errors.

In the following sections the effect of the single parameters will be described.

2.4.1 Number of iterations, smoothing, base line value

The effect of the dimensions of the droplet in pixel was investigated using artificial drop images, created by MATLAB implementing the numerical integration of the Young-Laplace profile. In this way focus can be on the software part of the procedure alone, without the effects of all the experimental aspects (e.g. camera, lighting, etc.); moreover, the correct value of the contact angle is known (as it is an input in the creation of the images) and calculation of the errors can be done against a certain reference.

Different resolutions of image were analyzed (as already said square images with side 250, 500, 750, 1000, 1250, 1500 pixel respectively), to simulate situations from low resolution cameras to high resolution with best quality. For each resolution the contact angle was calculated for two types of images: a first type in which the contour is directly traced as in the Figure 2.4.1(a) and a second type when the starting point is a black-and-white image from which the contour must be calculated as in the Figure 2.4.1(b), to estimate also the additional error due to this step).

Each set of pictures at a given resolution includes drops with contact angle values from 10° to 170° with a step of 10° (17 values), and per each contact angle value the Eotvos number varies from 0.2 to 5 with a step of 0.2 (25 values). So per each contact angle there are 25 value corresponding to different Eotvos number for a total of 425 images for each resolution.

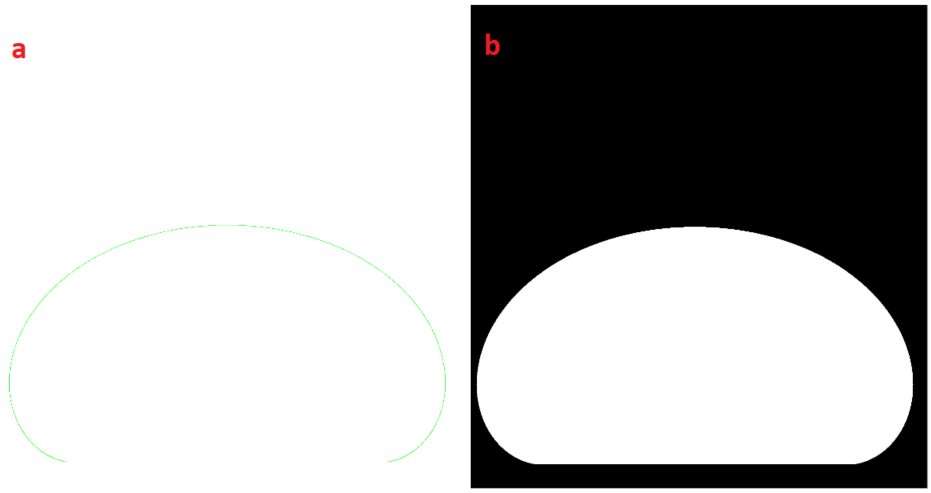

Figure 2.4 *- (a) picture with contour drop traced (b) picture in which contour must be calculated (B/W picture).*

As an example, figure 2.5 shows some of the analyzed images for resolution 750, when varying contact angle and Eo.

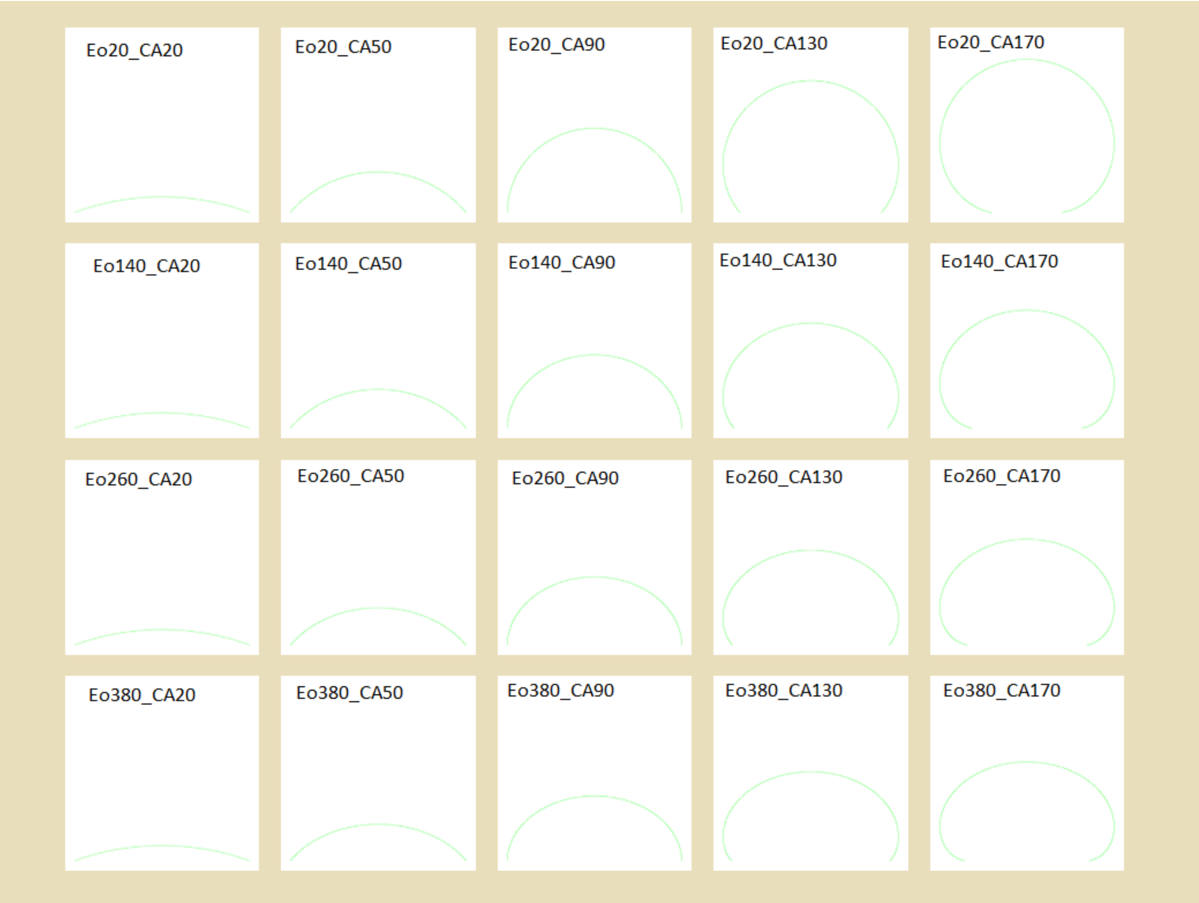

Figure 2.5 *- Examples of drop pictures with contour traced with different Eötvös number (here in % value) and different contact angles. Each picture contains the respective Eötvös (Eo) and contact angle (CA) value above.*

Due to the large number of resulting images (4250 considering the two image types and all resolutions), to keep everything ordered and suitable for automatic processing, the Eotvos number and contact angle value of each drop and the image resolution are memorized in the file name of each image.

Given the many parameters whose influence should be evaluated, the analysis was conducted by steps. First the best values of number of iteration was determined (keeping the smoothing and the baseline values at their reference values), then the smoothing value was varied using for each resolution the optimum iteration value; finally the contact angle errors caused by baseline displacement were calculated. A more rigorous possibility would have been to perform a simultaneous optimization on all the parameters, but the first, simpler approach was preferred here. Given the results, that will be presented in the following, practically no difference was observed for the smoothing value so the approach was *a posteriori* confirmed as valid.

The reference value of the baseline was manually identified (using Microsoft Paint); different values for the number of iterations were tested and the best one selected; successively the smoothing value was varied and fixed and finally the baseline value was tested. For the latter analysis, the baseline was moved up or down 1, 2, 3 pixel from the reference value (i.e. the best estimate of the correct position according to the operator's choice), examining the change in the measured contact angle. As MATLAB identifies heights in images from top to bottom (consistently with the rows in a matrix) an increase in the baseline value means moving towards the bottom and thus considering a larger height for the drop.

Values used for the different parameters are respectively:

- *Smooth* = 0.01, 0.03, 0.05, 0.07;
- *Number of iteration* = 100, 500, 1000, 2500;
- *Base-line value* = reference value (named y_stop in the following tables) -3 , -2, -1 , +0, +1 , +2, +3;

For each value tested it was calculated the relative error between the contact angle value obtained from the procedure and the theoretical value (used to create the picture).

Given the large amount of data (more than 9000 value for each resolution) the results were summarized calculating the usual statistical parameters: arithmetic mean and median (that unlike the arithmetic mean is not affected by the presence of a few anomalous data) as "central" values, and standard deviation as an indicator of the dispersion of the distribution of values

To show results, to avoid a large amount of data, only some parameters value are selected: one for number of iteration, one for smooth and base-line value with one more and less pixel.

2.4.2 Summary of the Obtained Results

In the following tables, results of the sensitivity analysis are presented.

The first issue that emerged from the analysis is that very small and very high values of the contact angle are a problem for the software: in the majority of the 10° cases and in about one half of the 170° case it gave 180° as an answer, which is the value returned when the fitting completely fails.
Therefore, the 10° and 170° sets of images were excluded from the analysis.

For all the other cases, Table 2.1 shows the results in terms of MAPE when varying the number of iterations (while keeping smoothing and baseline at their reference values); Table 2.2 shows the results when varying the smoothing value (while keeping number of iterations and baseline at their reference values). In both tables the results at different image resolutions are reported separately.

As it can be observed, the values are in general all very near to each other. No significant effect of the smoothing value can be identified, and concerning the number of iterations the only "strange" case is that at 250 resolution, for which a small number of iterations is the best choice. For all the other resolutions, the larger the number of iterations, the lower the MAPE, as it is reasonable; but the improvement is extremely slight so 500 iterations can be already considered adequate.

Table 2.3 shows the results when varying the baseline value (called y_stop in the table), while keeping the number of iterations and the smoothing value at their optimum values determined at the previous steps. In this case the effect is much more significant - baseline value strongly affects the result - confirming the importance of trying to select the parameter as accurately as possible.

As it can be seen, the best results are obtained or with the manually identified value or the same minus 1 (i.e. taking the baseline one pixel up the reference value); with no overall "winner" between these two. So in this case the "take home message" should be to calculate the contact angle using both and consider the difference as an unavoidable uncertainty. Luckily, at high image resolutions such difference becomes very small - as obvious, given that with high resolutions the relative importance of a single pixel is reduced, in relative term with respect to the drop dimensions. In general, both the MAPE and the standard deviation of the errors (that will be presented in the following sections) decrease with the increase of resolution. Contact angle values become more and more near to the real value. The resolution of the camera influence the error in the contact-angle measurement, as the fitting procedure is more precise with higher quality images and also accuracy of the placement of the baseline increases with resolution. Considering the standard deviation, in fact, at low resolution values are quite scattered while when this increases value become closer to the average. So, even if this obviously cannot eliminate the error completely, it can be said that acquiring high resolution and high quality pictures is one of the most important aspects of the procedure.

NUMBER OF ITERATION VALUE					
RESOLUTION		**ITER_100**	**ITER_500**	**ITER_1000**	**ITER_2500**
RESOL_0250	mean (st. deviation)	**2.39** **(2.68)**	3.29 (29.49)	6.00 (54.90)	6.00 (54.90)
RESOL_0500	mean (st. deviation)	2.19 (3.07)	0.66 (0.44)	0.65 (0.43)	**0.65** **(0.43)**
RESOL_0750	mean (st. deviation)	2.07 (3.30)	0.15 (0.19)	0.15 (0.19)	**0.15** **(0.19)**
RESOL_1000	mean (st. deviation)	1.98 (2.98)	0.43 (0.41)	0.43 (0.41)	**0.43** **(0.41)**
RESOL_1250	mean (st. deviation)	1.86 (3.01)	0.09 (0.12)	0.09 (0.12)	**0.09** **(0.12)**
RESOL_1500	mean (st. deviation)	1.90 (3.22)	0.07 (0.11)	0.07 (0.11)	**0.07** **(0.11)**

Table 2.1 *- MAPE of Contact Angle at different number of iterations. For each cell the value is presented completed with the corresponding standard deviation in brackets. In orange are evidenced the cases with the minimum MAPE ("the winner").*

SMOOTH VALUE					
RESOLUTION		**SM_0.01**	**SM_0.03**	**SM_0.05**	**SM_0.07**
RESOL_0250	mean (st. deviation)	**2.43** **(2.79)**	2.44 (2.80)	2.44 (2.76)	4.13 (32.90)
RESOL_0500	mean (st. deviation)	0.68 (0.42)	0.66 (0.43)	0.65 (0.43)	**0.64** **(0.45)**
RESOL_0750	mean (st. deviation)	0.15 (0.22)	0.15 (0.18)	**0.15** **(0.17)**	0.15 (0.19)
RESOL_1000	mean (st. deviation)	0.43 (0.41)	0.43 (0.41)	0.43 (0.41)	**0.42** **(0.41)**
RESOL_1250	mean (st. deviation)	0.08 (0.11)	**0.08** **(0.11)**	0.09 (0.12)	0.09 (0.12)
RESOL_1500	mean (st. deviation)	0.07 (0.11)	0.07 (0.12)	**0.07** **(0.11)**	0.07 (0.11)

Table 2.2 *- MAPE of Contact Angle at different smoothing values. For each cell the value is presented completed with the corresponding standard deviation in brackets. In orange are evidenced the cases with the minimum MAPE ("the winner").*

DROP CONTOUR PICTURE BASELINE VALUE								
RESOLUTION		**Y_STOP -3**	**Y_STOP -2**	**Y_STOP -1**	**Y_STOP**	**Y_STOP +1**	**Y_STOP +2**	**Y_STOP +3**
RESOL_0250	mean (st. deviation)	4.62 (3.40)	3.29 (3.34)	**2.13** **(3.24)**	2.39 (2.68)	3.32 (2.78)	4.36 (3.09)	5.38 (3.42)
RESOL_0500	mean (st. deviation)	1.57 (0.75)	0.87 (0.53)	**0.26** **(0.34)**	0.64 (0.45)	1.38 (0.75)	2.20 (1.25)	3.07 (1.94)
RESOL_0750	mean (st. deviation)	1.49 (0.66)	1.01 (0.49)	0.53 (0.32)	**0.15** **(0.18)**	0.45 (0.24)	0.96 (0.42)	1.47 (0.66)
RESOL_1000	mean (st. deviation)	0.76 (0.34)	0.41 (0.24)	**0.10** **(0.13)**	0.34 (0.21)	0.71 (0.33)	1.09 (0.49)	1.48 (0.69)
RESOL_1250	mean (st. deviation)	0.89 (0.37)	0.60 (0.27)	0.30 (0.17)	**0.08** **(0.11)**	0.29 (0.17)	0.59 (0.28)	0.89 (0.40)
RESOL_1500	mean (st. deviation)	0.73 (0.36)	0.49 (0.28)	0.26 (0.21)	**0.06** **(0.13)**	0.25 (0.14)	0.49 (0.20)	0.74 (0.29)
DROP B/W PICTURE BASELINE VALUE								
RESOLUTION		**Y_STOP -3**	**Y_STOP -2**	**Y_STOP -1**	**Y_STOP**	**Y_STOP +1**	**Y_STOP +2**	**Y_STOP +3**
RESOL_0250	mean (st. deviation)	4.21 (3.70)	3.08 (3.42)	**2.42** **(3.01)**	2.84 (2.36)	3.76 (2.45)	4.84 (2.81)	5.89 (3.25)
RESOL_0500	mean (st. deviation)	1.35 (0.92)	0.66 (0.66)	**0.37** **(0.35)**	0.90 (0.38)	1.65 (0.65)	2.47 (1.10)	3.37 (1.81)
RESOL_0750	mean (st. deviation)	0.89 (0.63)	0.43 (0.43)	**0.26** **(0.23)**	0.59 (0.24)	1.10 (0.35)	1.61 (0.57)	2.14 (0.83)
RESOL_1000	mean (st. deviation)	0.68 (0.43)	0.33 (0.32)	**0.17** **(0.15)**	0.42 (0.18)	0.79 (0.28)	1.18 (0.43)	1.56 (0.61)
RESOL_1250	mean (st. deviation)	0.85 (0.44)	0.56 (0.35)	0.28 (0.25)	**0.13** **(0.13)**	0.89 (0.40)	0.32 (0.16)	0.91 (0.34)
RESOL_1500	mean (st. deviation)	0.74 (0.36)	0.49 (0.28)	0.26 (0.21)	**0.10** **(0.13)**	0.24 (0.14)	0.49 (0.20)	0.74 (0.29)

Table 2.3 *- MAPE of Contact Angle at different baseline value. For each cell the value is presented completed with the corresponding standard deviation in brackets. In orange are evidenced the cases with the minimum MAPE ("the winner").*

After the analysis of the images already depicting the drop contour, attention was focused on the images depicting full drop in black/white, from which the contour must be extracted – thus allowing to evaluate also the influence of this step on the errors.
As it can be observed from the previous tables, B/W drop images, for which the contour was to be calculated, present higher errors – as is was expected, considering that one more step is required to compute the contact angle value, so there is a propagation of error, more steps lead to bigger errors.
Nonetheless, such additional error is in general extremely small.

To try to understand the cause of the discrepancies images (with the same contact angle and Eotvos number) where the contour was extracted and with the contour directly drawn were superposed. This showed that on the extremities of the drop the fitting may differ of one pixel between the two images, due to the behavior of the MATLAB *bwtraceboundary* function.

In the following sub-sections, further details about the results at the different resolutions will be shown.

2.4.3 Detailed analysis at the different resolutions

2.4.3.1 Resolution_0250

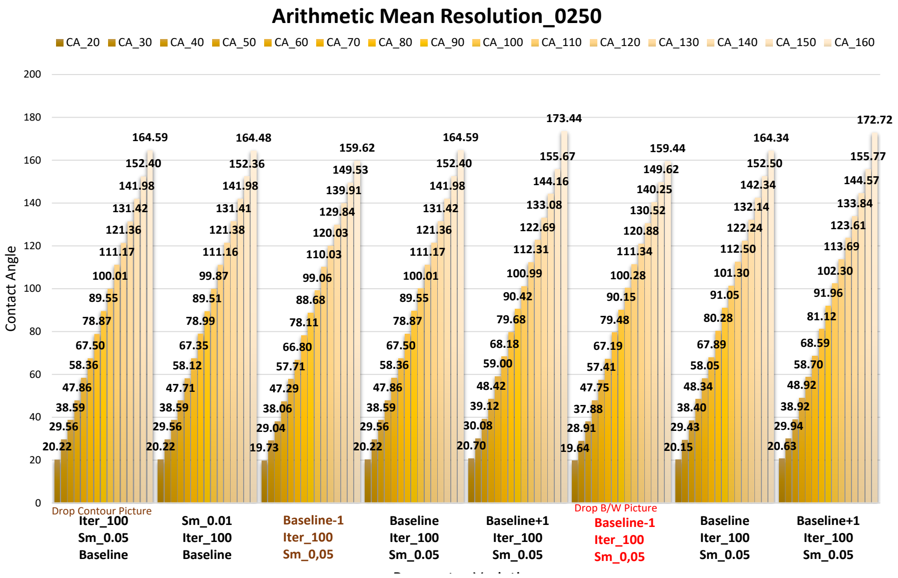

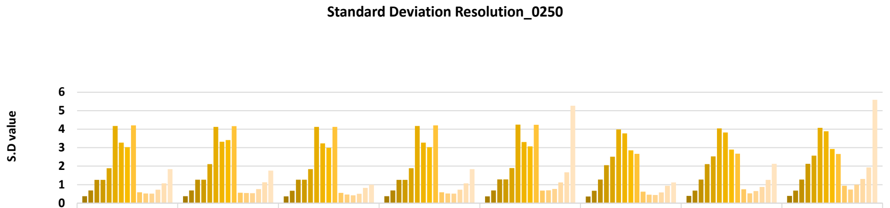

	Iter_100 Sm_0.05 Baseline	Sm_0.01 Iter_100 Baseline	Baseline-1 Iter_100 Sm_0,05	Baseline Iter_100 Sm_0.05	Baseline+1 Iter_100 Sm_0.05	Baseline-1 Iter_100 Sm_0,05	Baseline Iter_100 Sm_0.05	Baseline+1 Iter_100 Sm_0.05
S.D_20	0.38	0.37	0.37	0.38	0.37	0.36	0.39	0.39
S.D_30	0.69	0.69	0.67	0.69	0.68	0.67	0.68	0.68
S.D_40	1.26	1.27	1.27	1.26	1.28	1.27	1.27	1.28
S.D_50	1.26	1.27	1.27	1.26	1.28	2.06	2.11	2.13
S.D_60	1.89	2.11	1.84	1.89	1.90	2.51	2.52	2.57
S.D_70	4.18	4.12	4.12	4.18	4.24	3.98	4.04	4.08
S.D_80	3.27	3.32	3.23	3.27	3.30	3.77	3.82	3.88
S.D_90	3.03	3.41	2.99	3.03	3.06	2.86	2.89	2.93
S.D_100	4.20	4.16	4.13	4.20	4.24	2.66	2.67	2.66
S.D_110	0.59	0.56	0.56	0.59	0.68	0.62	0.75	0.94
S.D_120	0.52	0.55	0.47	0.52	0.70	0.46	0.53	0.74
S.D_130	0.51	0.54	0.42	0.51	0.77	0.44	0.65	0.99
S.D_140	0.73	0.76	0.51	0.73	1.12	0.58	0.88	1.30
S.D_150	1.07	1.13	0.83	1.07	1.67	0.94	1.26	1.93
S.D_160	1.84	1.75	0.99	1.84	5.27	1.12	2.13	5.59

Table 2.4 *- Resolution_0250: Contact angle arithmetic mean and standard deviation for pictures with contour drop traced and B/W pictures. In the first two columns are present values coming for choosing different smoothing value rather than "the winner". In the other columns are presented contact angle value varying the baseline ±1 pixel from the one choosing by the operator. In brown it is evidenced the best fitting value for picture with contour drop traced, in red the best fitting for B/W picture.*

2.4.3.2 Resolution_0500

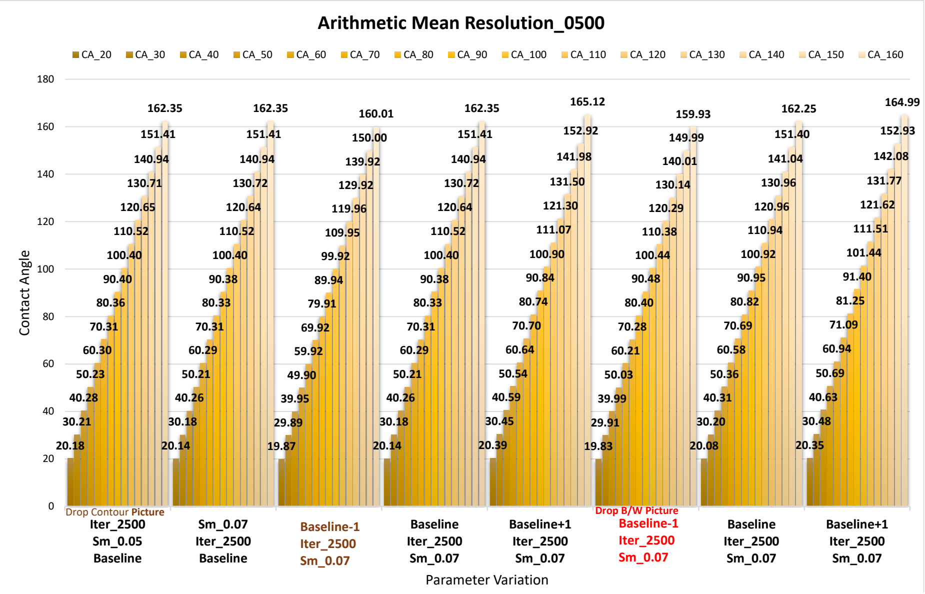

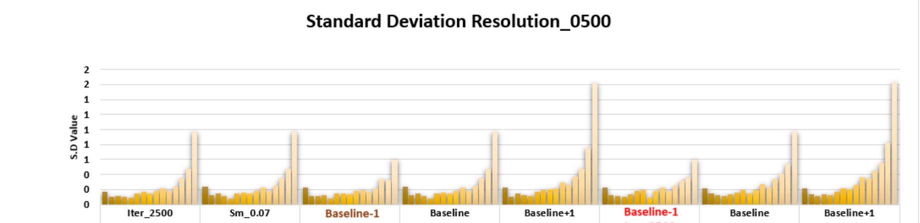

	Iter_2500 Sm_0.05 Baseline	Sm_0.07 Iter_2500 Baseline	Baseline-1 Iter_2500 Sm_0.07	Baseline Iter_2500 Sm_0.07	Baseline+1 Iter_2500 Sm_0.07	Baseline-1 Iter_2500 Sm_0.07	Baseline Iter_2500 Sm_0.07	Baseline+1 Iter_2500 Sm_0.07
S.D_20	0.17	0.24	0.23	0.24	0.23	0.22	0.21	0.21
S.D_30	0.10	0.12	0.11	0.12	0.10	0.13	0.15	0.14
S.D_40	0.12	0.15	0.11	0.15	0.15	0.12	0.12	0.12
S.D_50	0.10	0.11	0.12	0.11	0.12	0.11	0.11	0.13
S.D_60	0.09	0.08	0.08	0.08	0.12	0.14	0.14	0.13
S.D_70	0.15	0.15	0.14	0.15	0.17	0.18	0.16	0.17
S.D_80	0.17	0.16	0.15	0.16	0.20	0.19	0.19	0.21
S.D_90	0.15	0.15	0.14	0.15	0.21	0.09	0.15	0.21
S.D_100	0.18	0.18	0.18	0.18	0.22	0.18	0.19	0.26
S.D_110	0.21	0.22	0.19	0.22	0.30	0.22	0.27	0.36
S.D_120	0.19	0.18	0.17	0.18	0.26	0.18	0.23	0.35
S.D_130	0.24	0.25	0.22	0.25	0.37	0.25	0.35	0.45
S.D_140	0.35	0.35	0.34	0.35	0.48	0.32	0.41	0.56
S.D_150	0.48	0.48	0.33	0.48	0.76	0.36	0.54	0.83
S.D_160	0.97	0.97	0.60	0.97	1.62	0.60	0.97	1.62

Table 2.5 *- Resolution_0500: Contact angle arithmetic mean and standard deviation for pictures with contour drop traced and B/W pictures. In the first two columns are present values coming for choosing different smoothing value rather than “the winner”. In the other columns are presented contact angle value varying the baseline ±1 pixel from the one choosing by the operator. In brown it is evidenced the best fitting value for picture with contour drop traced, in red the best fitting for B/W picture.*

2.4.3.3 Resolution_0750

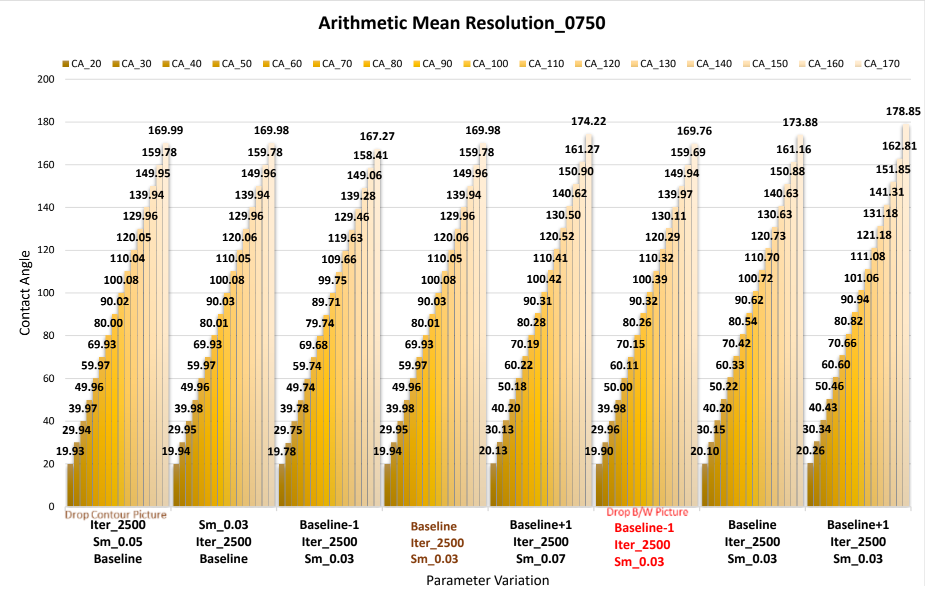

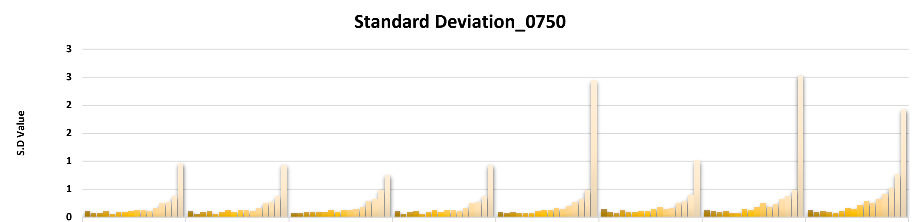

	Iter_2500 Sm_0.05 Baseline	Sm_0.03 Iter_2500 Baseline	Baseline-1 Iter_2500 Sm_0.03	Baseline Iter_2500 Sm_0.03	Baseline+1 Iter_2500 Sm_0.07	Baseline-1 Iter_2500 Sm_0.03	Baseline Iter_2500 Sm_0.03	Baseline+1 Iter_2500 Sm_0.03
■ S.D_20	0.11	0.11	0.07	0.11	0.09	0.14	0.12	0.13
■ S.D_30	0.07	0.06	0.07	0.06	0.07	0.09	0.10	0.10
■ S.D_40	0.08	0.08	0.08	0.08	0.09	0.07	0.08	0.10
■ S.D_50	0.10	0.10	0.10	0.10	0.06	0.12	0.11	0.09
■ S.D_60	0.06	0.06	0.09	0.06	0.07	0.09	0.07	0.08
■ S.D_70	0.09	0.09	0.08	0.09	0.07	0.09	0.08	0.10
■ S.D_80	0.10	0.12	0.12	0.12	0.11	0.10	0.14	0.16
■ S.D_90	0.10	0.09	0.10	0.09	0.12	0.10	0.12	0.15
■ S.D_100	0.12	0.12	0.13	0.12	0.12	0.14	0.17	0.21
■ S.D_110	0.13	0.12	0.12	0.12	0.16	0.18	0.24	0.28
■ S.D_120	0.10	0.10	0.13	0.10	0.15	0.14	0.18	0.25
■ S.D_130	0.16	0.16	0.17	0.16	0.20	0.17	0.23	0.33
■ S.D_140	0.24	0.24	0.29	0.24	0.27	0.26	0.32	0.42
■ S.D_150	0.27	0.27	0.32	0.27	0.33	0.29	0.37	0.52
■ S.D_160	0.37	0.37	0.48	0.37	0.48	0.40	0.48	0.77
■ S.D_170	0.96	0.93	0.76	0.93	2.44	1.01	2.52	1.92

Table 2.6 *- Resolution_0750: Contact angle arithmetic mean and standard deviation for pictures with contour drop traced and B/W pictures. In the first two columns are present values coming for choosing different smoothing value rather than “the winner”. In the other columns are presented contact angle value varying the baseline ±1 pixel from the one choosing by the operator. In brown it is evidenced the best fitting value for picture with contour drop traced, in red the best fitting for B/W picture.*

2.4.3.4 Resolution_1000

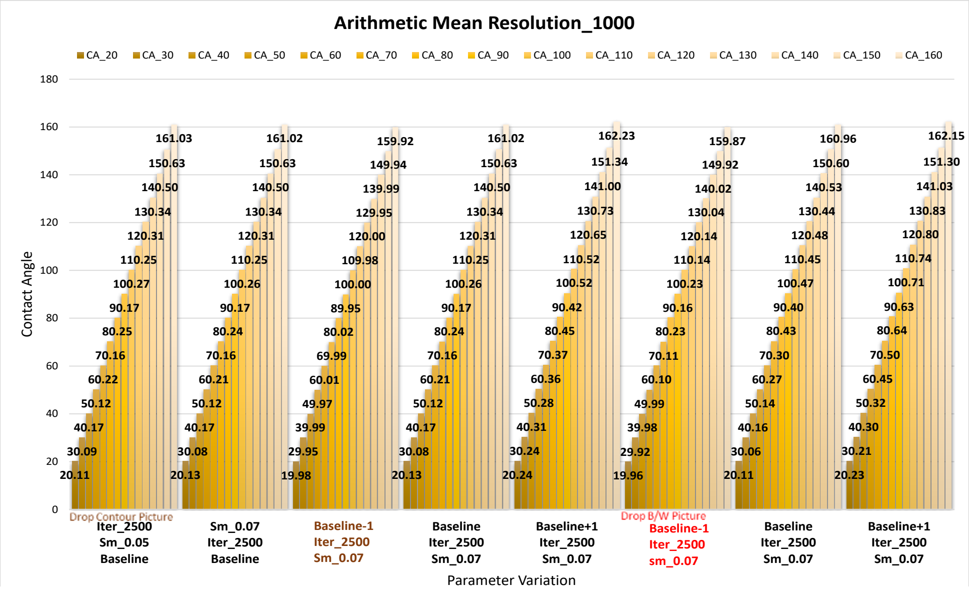

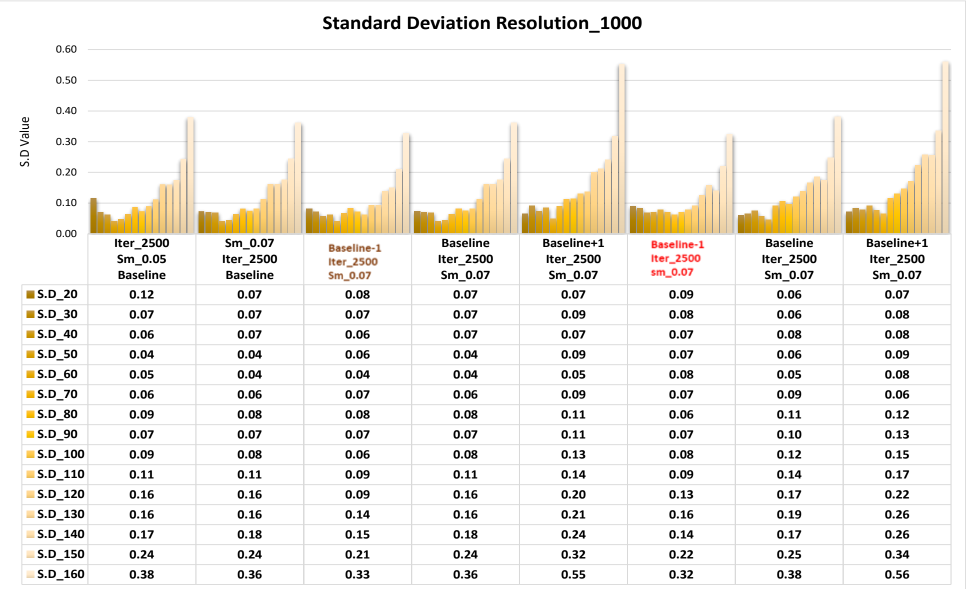

	Iter_2500 Sm_0.05 Baseline	Sm_0.07 Iter_2500 Baseline	Baseline-1 Iter_2500 Sm_0.07	Baseline Iter_2500 Sm_0.07	Baseline+1 Iter_2500 Sm_0.07	Baseline-1 Iter_2500 sm_0.07	Baseline Iter_2500 Sm_0.07	Baseline+1 Iter_2500 Sm_0.07
S.D_20	0.12	0.07	0.08	0.07	0.07	0.09	0.06	0.07
S.D_30	0.07	0.07	0.07	0.07	0.09	0.08	0.06	0.08
S.D_40	0.06	0.07	0.06	0.07	0.07	0.07	0.08	0.08
S.D_50	0.04	0.04	0.06	0.04	0.09	0.07	0.06	0.09
S.D_60	0.05	0.04	0.04	0.04	0.05	0.08	0.05	0.08
S.D_70	0.06	0.06	0.07	0.06	0.09	0.07	0.09	0.06
S.D_80	0.09	0.08	0.08	0.08	0.11	0.06	0.11	0.12
S.D_90	0.07	0.07	0.07	0.07	0.11	0.07	0.10	0.13
S.D_100	0.09	0.08	0.06	0.08	0.13	0.08	0.12	0.15
S.D_110	0.11	0.11	0.09	0.11	0.14	0.09	0.14	0.17
S.D_120	0.16	0.16	0.09	0.16	0.20	0.13	0.17	0.22
S.D_130	0.16	0.16	0.14	0.16	0.21	0.16	0.19	0.26
S.D_140	0.17	0.18	0.15	0.18	0.24	0.14	0.17	0.26
S.D_150	0.24	0.24	0.21	0.24	0.32	0.22	0.25	0.34
S.D_160	0.38	0.36	0.33	0.36	0.55	0.32	0.38	0.56

Table 2.7 *- Resolution_1000: Contact angle arithmetic mean and standard deviation for pictures with contour drop traced and B/W pictures. In the first two columns are present values coming for choosing different smoothing value rather than “the winner”. In the other columns are presented contact angle value varying the baseline ±1 pixel from the one choosing by the operator. In brown it is evidenced the best fitting value for picture with contour drop traced, in red the best fitting for B/W picture.*

2.4.3.5 Resolution_1250

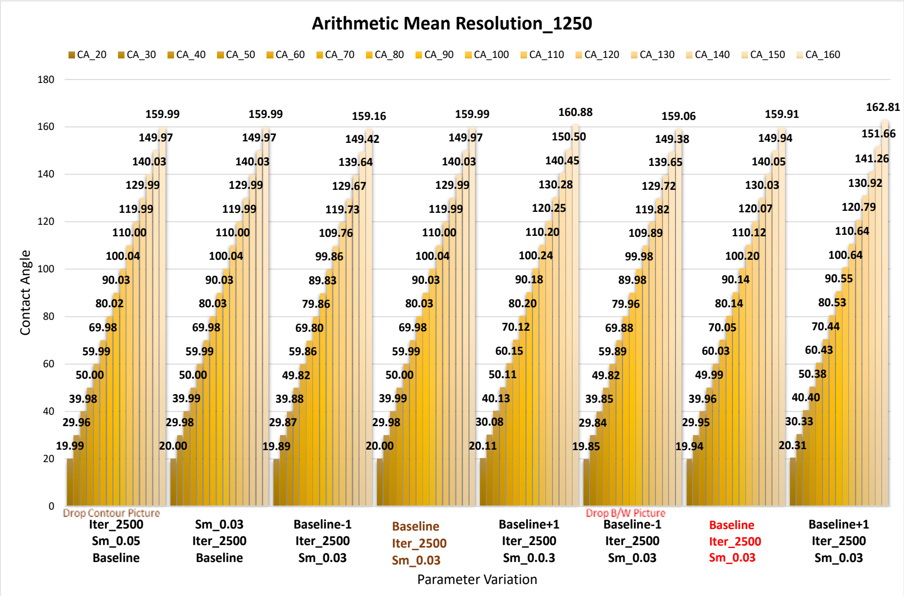

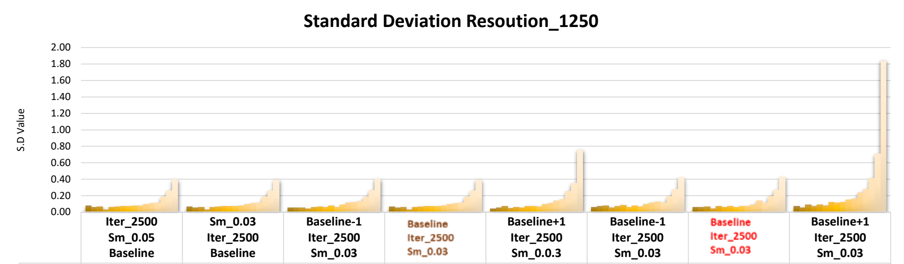

	Iter_2500 Sm_0.05 Baseline	Sm_0.03 Iter_2500 Baseline	Baseline-1 Iter_2500 Sm_0.03	Baseline Iter_2500 Sm_0.03	Baseline+1 Iter_2500 Sm_0.0.3	Baseline-1 Iter_2500 Sm_0.03	Baseline Iter_2500 Sm_0.03	Baseline+1 Iter_2500 Sm_0.03
S.D_20	0.08	0.06	0.05	0.06	0.04	0.06	0.06	0.07
S.D_30	0.06	0.05	0.05	0.05	0.05	0.07	0.06	0.06
S.D_40	0.06	0.06	0.05	0.06	0.07	0.08	0.06	0.09
S.D_50	0.03	0.03	0.04	0.03	0.04	0.05	0.04	0.07
S.D_60	0.06	0.06	0.06	0.06	0.06	0.07	0.07	0.09
S.D_70	0.06	0.06	0.06	0.06	0.05	0.09	0.06	0.08
S.D_80	0.07	0.07	0.06	0.07	0.07	0.06	0.07	0.12
S.D_90	0.07	0.07	0.08	0.07	0.07	0.08	0.06	0.11
S.D_100	0.08	0.07	0.06	0.07	0.07	0.07	0.07	0.12
S.D_110	0.08	0.08	0.09	0.08	0.09	0.10	0.07	0.15
S.D_120	0.09	0.09	0.11	0.09	0.11	0.12	0.09	0.16
S.D_130	0.11	0.11	0.12	0.11	0.13	0.13	0.13	0.23
S.D_140	0.11	0.11	0.13	0.11	0.16	0.12	0.11	0.28
S.D_150	0.18	0.18	0.18	0.18	0.25	0.19	0.19	0.41
S.D_160	0.26	0.26	0.26	0.26	0.35	0.28	0.27	0.71
S.D_170	0.40	0.39	0.40	0.39	0.76	0.42	0.43	1.84

Table 2.8 *- Resolution_1250: Contact angle arithmetic mean and standard deviation for pictures with contour drop traced and B/W pictures. In the first two columns are present values coming for choosing different smoothing value rather than "the winner". In the other columns are presented contact angle value varying the baseline ±1 pixel from the one choosing by the operator. In brown it is evidenced the best fitting value for picture with contour drop traced, in red the best fitting for B/W picture.*

2.4.3.6 Resolution_1500

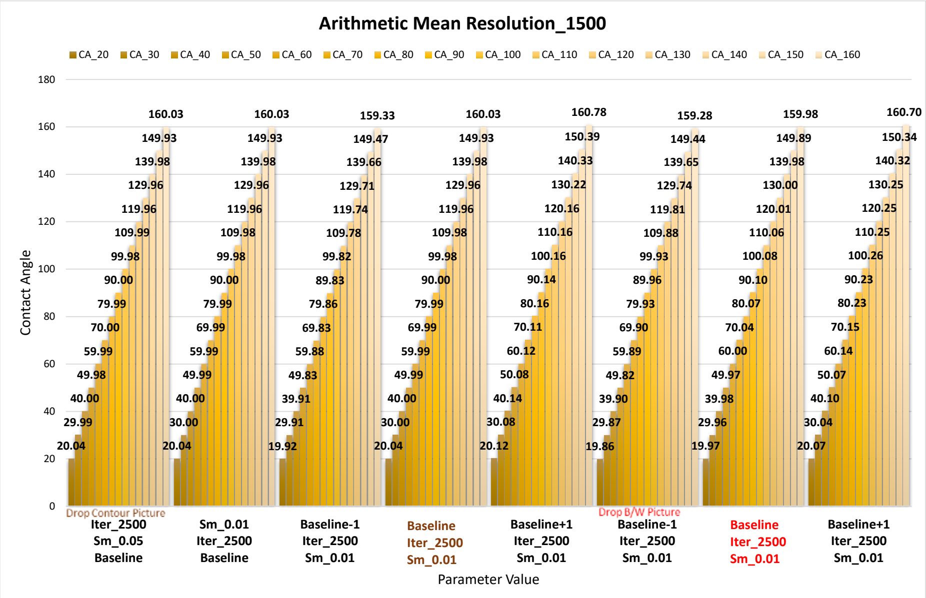

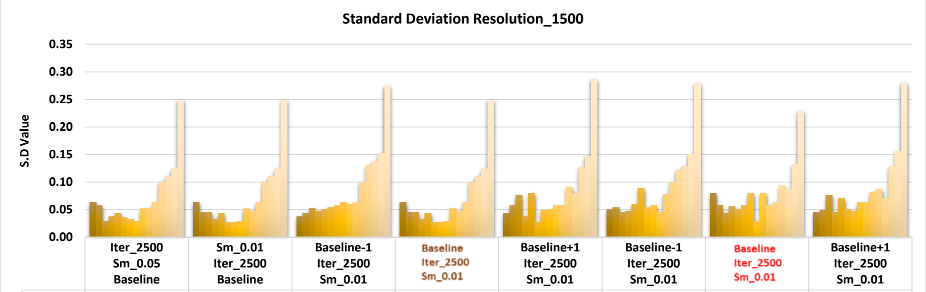

	Iter_2500 Sm_0.05 Baseline	Sm_0.01 Iter_2500 Baseline	Baseline-1 Iter_2500 Sm_0.01	Baseline Iter_2500 Sm_0.01	Baseline+1 Iter_2500 Sm_0.01	Baseline-1 Iter_2500 Sm_0.01	Baseline Iter_2500 Sm_0.01	Baseline+1 Iter_2500 Sm_0.01
S.D_20	0.06	0.06	0.04	0.06	0.04	0.05	0.08	0.05
S.D_30	0.06	0.05	0.04	0.05	0.06	0.05	0.06	0.05
S.D_40	0.03	0.05	0.05	0.05	0.08	0.05	0.04	0.08
S.D_50	0.04	0.03	0.05	0.03	0.04	0.05	0.06	0.05
S.D_60	0.04	0.04	0.05	0.04	0.08	0.06	0.05	0.07
S.D_70	0.04	0.03	0.05	0.03	0.03	0.09	0.06	0.05
S.D_80	0.03	0.03	0.06	0.03	0.05	0.05	0.08	0.05
S.D_90	0.03	0.03	0.06	0.03	0.05	0.06	0.03	0.06
S.D_100	0.05	0.05	0.06	0.05	0.06	0.05	0.08	0.06
S.D_110	0.05	0.05	0.06	0.05	0.06	0.08	0.06	0.08
S.D_120	0.06	0.06	0.10	0.06	0.09	0.10	0.06	0.09
S.D_130	0.10	0.10	0.13	0.10	0.08	0.12	0.09	0.07
S.D_140	0.11	0.11	0.14	0.11	0.13	0.13	0.09	0.13
S.D_150	0.12	0.12	0.15	0.12	0.15	0.15	0.13	0.16
S.D_160	0.25	0.25	0.27	0.25	0.29	0.28	0.23	0.28

Table 2.9 *- Resolution_1500: Contact angle arithmetic mean and standard deviation for pictures with contour drop traced and B/W pictures. In the first two columns are present values coming for choosing different smoothing value rather than "the winner". In the other columns are presented contact angle value varying the baseline ±1 pixel from the one choosing by the operator. In brown it is evidenced the best fitting value for picture with contour drop traced, in red the best fitting for B/W picture.*

2.4.4 Camera Alignment

To complete the analysis of the factors affecting contact angle measurement the alignment of the camera with the drop-sample system was evaluated.

In fact, the sample should be placed perfectly horizontal and the camera view should be on the same plane as the sample. A tilt in the camera view can be a source of relevant errors. If the stage is tilted some parts of the droplet will be covered by the stage, or vice versa the drop will be seen “from the top” altering its apparent shape, in both cases making the measurement inaccurate.

Even if the qualitative effect of this motion can be easily foreseen, verifying and quantifying it given the complex shape of real drops is not viable analytically; therefore also this analysis was performed using computer-generated drop pictures – so that their contact angle and Eotvos numbers were exactly known – with a camera positioned respectively higher and lower with respect to the perfect alignment. In this case 3D drops were generated in MATLAB, then exported in OBJ format (a format widely used for computer graphics) and imported in a software for rendering (namely Appleseed https://appleseedhq.net/) to obtain realistic images of the drops. Appleseed is a physically-based rendering engine, but strict photorealism was not of interest here. Figure 2.6 shows two examples of the used pictures.

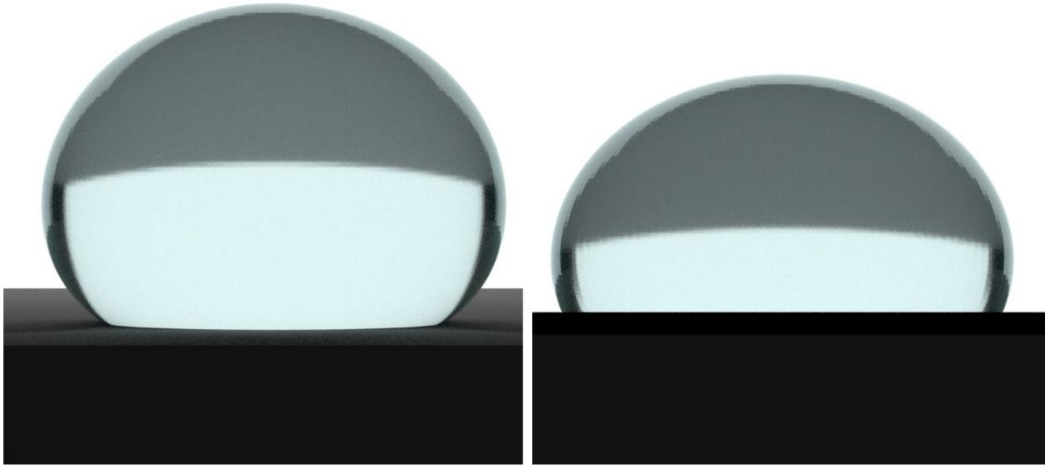

Figure 2.6 *- Two examples of computer-generated drops. On the left a drop picture taken with a positive camera inclination (lens center higher than the baseline). On the right picture takem with a negative camera inclination (lens center lower that the baseline).*

Two different sets of rendered images with contact angle values of 120° and 150° were considered. Each set was composed by a perfectly aligned image and other images with the camera too high or too low, with a misalignment in degrees as in Table 2.10. For each image it was also evaluated effect of the selection of the baseline. For all images the baseline was manually identified and then moved 1,2,3 px up and down. In all cases the error increases with the inclination. When the camera is put lower than the perfect sample alignment the contact angle decreases, that is reasonable because the bottom part of the drop is "cut", covered by the sample. On the contrary with a higher position of the camera the contact angle value increases, because the projected, apparent cross section of the drop is flattened.

Camera position	**Inclination [deg]**
Low	1.00
	0.50
Perfect Alignement	0
High	0.5
	1
	1.4
	2.4

Table 2.10 *- Degree inclination of camera.*

Analyzing the variation of the baseline value for each inclination, the minimum error was obtained for the baseline value nearer to the correct baseline value of the perfect alignment picture.

As it can be seen from the following figures trend is practically linear with respect to the baseline displacement (as it is reasonable given the minor amount of the latter), with significant effects on the measurement, confirming the importance of the parameter. Concerning the misalignment, the variations are not linear, and placing the camera too low causes larger errors - so it is better to risk an upwards misalignment. In any case this proves to be another major source of error, to which maximum attention should be given when acquiring the experimental images.

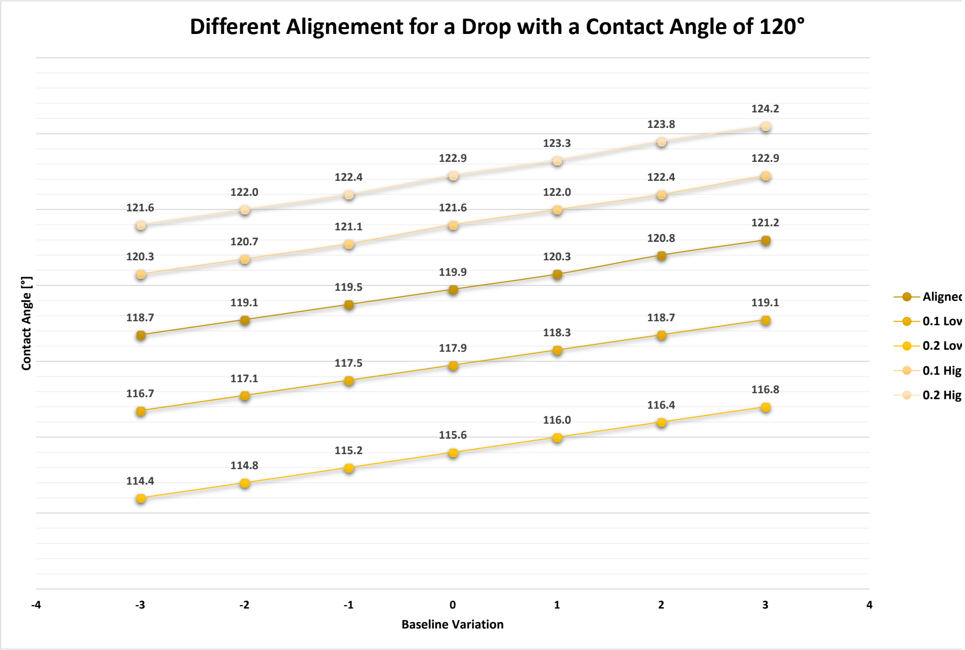

__Figure 2.7__ - Contact angle distortion due to a not correct alignment of camera for a drop with a contact angle value of 120°. Each line corresponds to different inclination with the respective contact angle value varying the baseline value of ± 3 pixel.

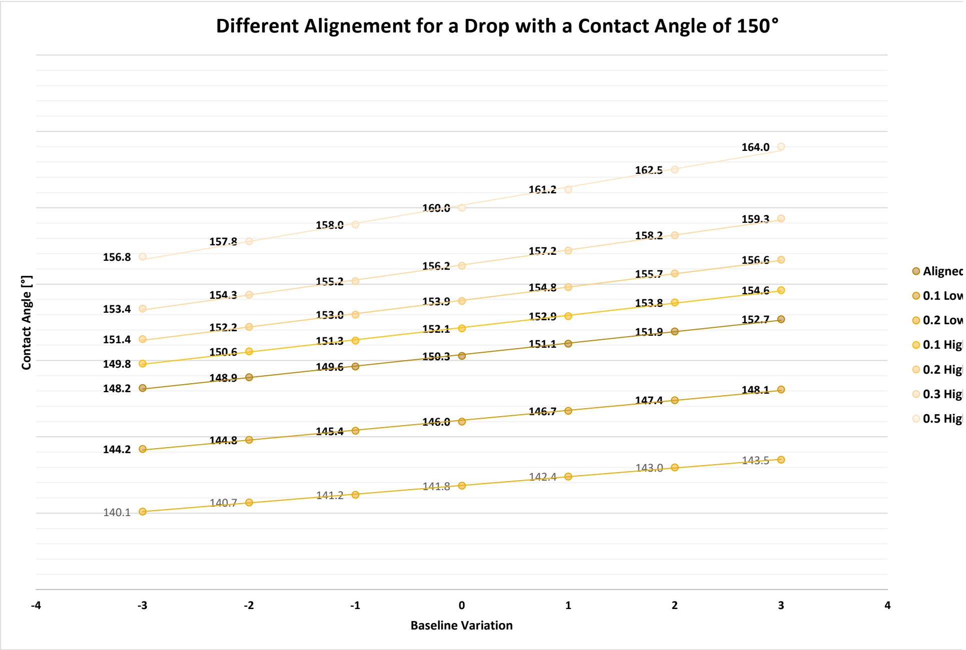

__Figure 2.8__ - Contact angle distortion due to a not correct alignment of camera for a drop with a contact angle value of 150°. Each line corresponds to different inclination with the respective contact angle value varying the baseline value of ± 3 pixel.

Chapter 3

Experimental results for home-made samples and fluorinated gas diffusion layers

3.1 Introduction

In this chapter we will illustrate the results of the measurements carried out on different surfaces using the technique and the details discussed in the previous chapters. More specifically, the characterization of the new graphene oxide membranes (described in the following chapter) was the third of three steps, where the first two (described here) were the measurements of the contact angle on home-made samples and on samples already tested in previously works at the Thermo-fluid dynamics laboratory.

The first step permitted the optimization of the home-made setup and measurement technique. The second gave the validation of the technique and measurement thanks to the comparison of the contact angles obtained with the now previously found.

After the validation of the home-made setup the contact angle measurements of new membranes produced at the Department of Chemistry, Materials and Chemical Engineering “Giulio Natta” were carried out.
In order to assess repeatability, for each sample 21 drop pictures were acquired:
- 9 pictures of a first drop: the camera was positioned in a first position for the first 3 pictures, in a second position for the second 3 pictures, and in a third position for the last 3 pictures;
- 3 pictures of a new drop: here, the camera was positioned in the first position for the first shot, in the second position for the second shot, and in the third position for the last shot. This procedure was repeated 4 times.

Contact angle was evaluated as the arithmetic mean of all the single measurements.

3.2 Home-made samples

As explained before, a first set of samples was created with simple things that can be found in everyday life, like nail polish (a cosmetic product for coloring, protecting and fortifying nails) and ceramic polish (normally used to restore home parts), two aluminum covers and a common cleaning wet wipe (Figures 3.1 and 3.2).
Covers were cleaned and utilized both as samples and as bases for depositing layers of ceramic polish, normal and gel nail polish. One cover was used to test aluminum itself and the ceramic paste, while the second for normal and gel nail polish. The wet wipe was used as a third base on which a very thin layer of normal nail polish was settled on his fibre texture.
After the contact angle measurements on clean samples, limescale accretion on the same was also carried out by repeated wetting and drying with tap water for 10 days, to verify if limescale gives a hydrophobic behavior as often reported in the literature for other surfaces.

Chemical composition of the solutions and materials used are briefly described below:

- normal nail polish and gel nail polish: conventional nail polish consists of a polymer, most commonly nitrocellulose, dissolved in a solvent, usually ethyl acetate or butyl acetate. When it is applied the solvent evaporates, leaving the polymer to form a film on the nail. Adhesive polymer resins that are also contained within the formulation help the polymer film to stick to the nail. These so-called film modifiers also impart a glossiness to the polymer finish. This conventional nail polish is not the only option, however. Gel nail polish is an alternative formulation which consists of methacrylate compounds and photoinitiating compounds such as benzoyl peroxide. In both conventional and gel nail polishes, plasticisers are also used. These are compounds added to stop the polish from easily cracking or chipping. They remain behind when the solvents evaporate or when the polish is cured with UV light; in fact they are used in a wide range of plastics, not just polishes, and help to add flexibility.

- ceramic polish : it is a two-component epoxy nail to restore ceramic surfaces, most commonly in the bathroom. It is quick to dry and resistant to hot water, detergents and high temperature.

- wet wipe: a common commercial wet wipe that was let dry-off in order to depose the nail polish over it.

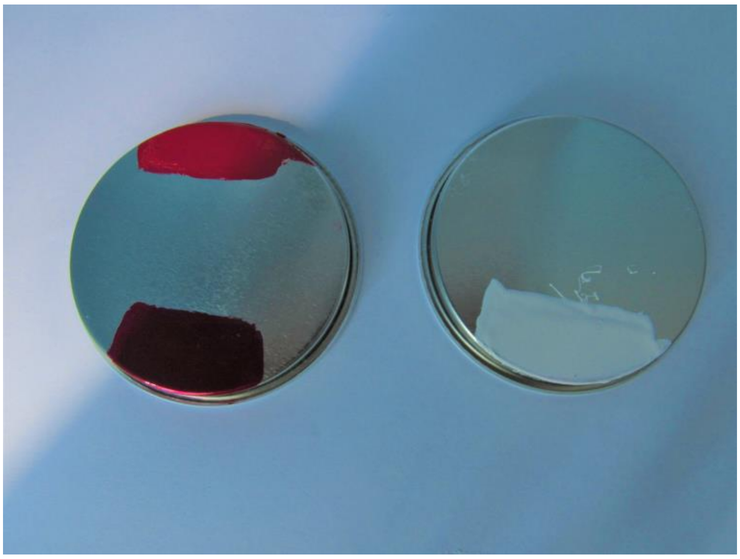

Figure 3.1- *Covers used to create experimental samples, , with normal and gel nail polish (left) and ceramic polish (right).*

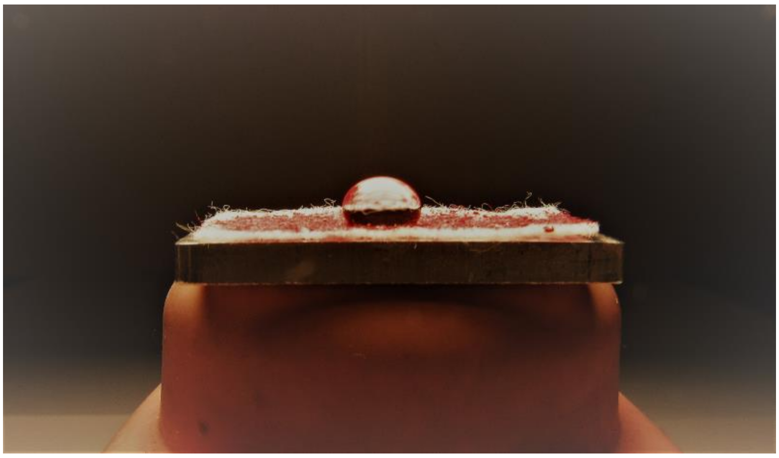

Figure 3.2 - *Picture of a drop deposited on the wipe coated with a thin layer of nail polish. Sample showed an hydrophobic behavior.*

3.2.1 Results for the home-made samples

Aluminum, ceramic and normal nail polish was tested 3 times (for a total of 63 images) while gel nail polish only one time. As shows in Table 3.1 below all the samples present a hydrophilic behavior with a contact angle value in the range of 70°-80°, except the wipe which shows an high hydrophobicity with a mean contact angle value of 157°. Differences in contact angle value in the repeatability test can in part be due to the different drop volume deposed because it was placed with a common medical syringe unable to calibrate the volume as precisely as it would be possible with a precision syringe.

HOME-MADE SAMPLE										
SAMPLE	**DROP/TEST**	**1.1**	**1.2**	**1.3**	**2**	**3**	**4**	**5**	**MEAN**	**TOTAL MEAN**
ALUMINUM	1	69.4	68.3	67.4	68.5	71.1	72.7	69.4	69.5	**73.5**
	2	73.0	71.4	70.9	76.7	68.1	68.7	72.3	71.6	
	3	79.5	78.4	78.5	83.0	79.6	73.9	82.2	79.3	
CERAMIC POLISH	1	76.9	77.0	77.1	80.5	80.4	73.4	79.7	77.9	**77.1**
	2	75.1	74.3	73.4	69.8	79.1	72.4	78.0	74.6	
	3	79.0	78.8	78.3	78.3	80.0	80.0	78.1	78.9	
NORMAL NAIL POLISH	1	65.3	68.0	66.2	68.0	71.9	75.4	64.0	68.4	**72.2**
	2	67.0	68.8	66.7	72.9	72.1	73.4	62.1	69.0	
	3	81.8	83.5	80.1	75.5	76.4	77.6	79.8	79.2	
GEL NAIL POLISH	1	89.6	85.0	84.1	76.1	80.0	75.3	78.8	81.3	**81.3**
WET WIPES	1	162.4	164.9	168.7	141.4	133.7	164.5	165.3	157.3	**157.3**

Table 3.1 *- Contact angle values on home-made samples.*

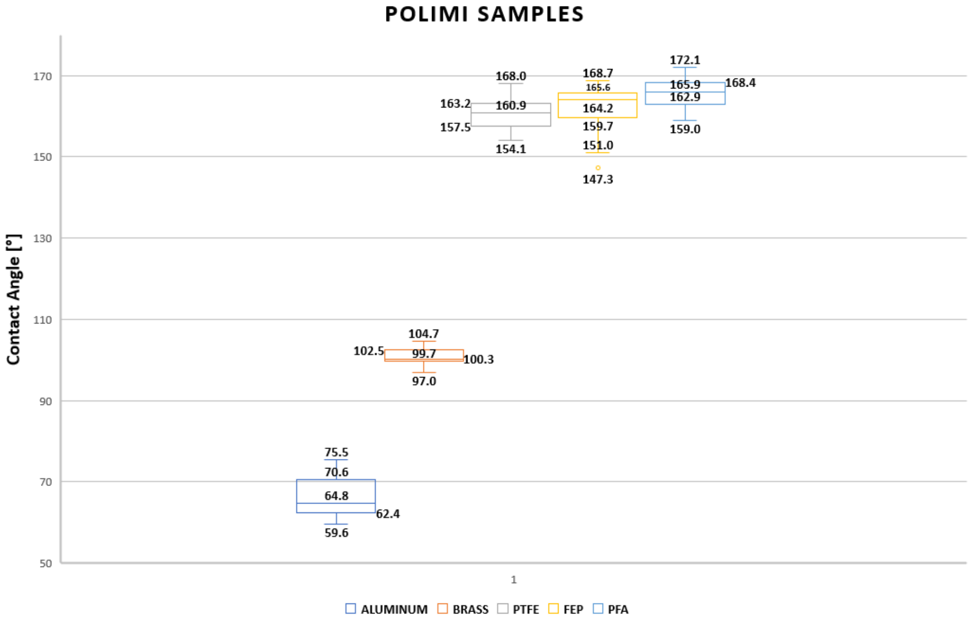

Figure 3.3 *- Box plot of the contact angle values on the home-made samples. In each box plot are respectively represented the minimum, first quartile, median, third quartile and maximum value for each distribution.*

About the limestone growth, it was evidenced that there is not an increase in contact angle values that remains practically the same as shown in Table 3.2. So in these cases limestone did not give a hydrophobic characterization to the samples. This was surprising, but further studies should be performed to obtain more substantiated conclusions.

LIMESTONE									
SAMPLE	**DROP/TEST**	**1.1**	**1.2**	**1.3**	**2**	**3**	**4**	**5**	**TOTAL MEAN**
ALUMINUM	1.0	65.5	64.4	64.3	76.4	78.9	81.5	80.9	**73.1**
CERAMIC POLISH	1.0	77.5	81.3	76.4	80.9	80.2	79.3	77.2	**79.0**
NORMAL NAIL POLISH	1.0	73.8	74.3	69.2	75.5	76.7	75.2	76.0	**74.4**

Table 3.2*- Contact angle values after ten days of limestone growth on home-made samples.*

3.3 Polimi samples:

In order to validate the home-made setup, it was necessary to test it with samples for which the contact angle had already been calculated in the course of the other studies. By doing so, it was possible to compare the contact angle values obtained by the home-made setup with the ones obtained by a professional laboratory.

Samples were selected among those that had been investigated in previous campaign at the Thermo-fluid dynamics laboratory and consists in:

5. aluminum sample;
6. brass sample;
7. three gas diffusion layers (GDL) for fuel cells, made by the Mat4En2 group using PTFE(polytetrafluoroethylene), FEP(fluorinated ethylene propylene), PFA (perfluoroalkoxy).

Brass and Aluminum were cleaned with common alcohol solution before testing. GDLs were tested as they were, after fixing them with double side scotch tape on an aluminum support (Figure 3.4).

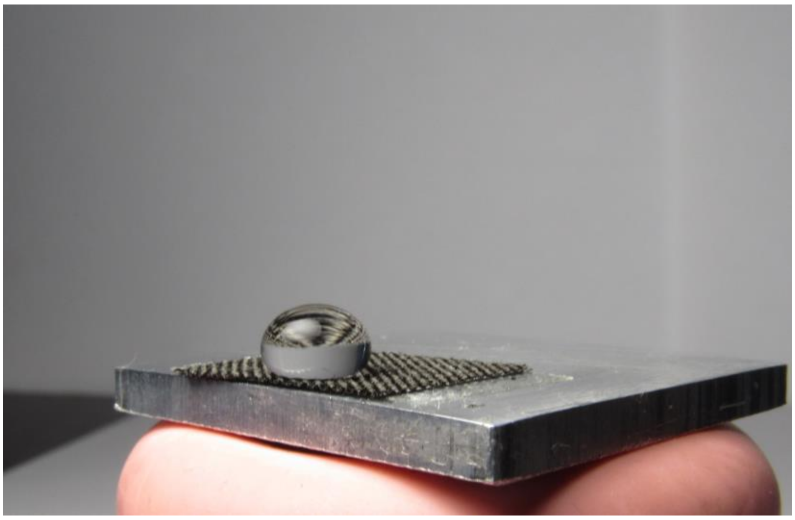

Figure 3.4- *Picture of a drop on a FEP GDL.*

3.3.1 Results on Polimi samples

Table 3.3 shows the values of the contact angles measured on the Polimi samples, with an additional column reporting the old data.

From the comparison it can be affirmed that the results obtained using the home-made setup are satisfactory, in particular with an excellent agreement for the GDL surfaces that are those on which the old data had been acquired with the better accuracy.

POLIMI SAMPLE											
SAMPLE	**TEST**	**1.1**	**1.2**	**1.3**	**2**	**3**	**4**	**5**	**TOTAL MEAN**	**MEDIAN**	**POLIMI MEDIAN**
ALUMINUM	1	64.8 (1.7)	63.0 (1.3)	62.7 (0.5)	73.7 (1.0)	64.1 (0.7)	67.0 (0.7)	73.8 (2.0)	66.2	**64.8**	**75±10**
BRASS	1	103.4 (0.4)	102.0 (0.7)	100.9 (1.3)	101.8 (2.6)	99.7 (0.4)	100.4 (1.0)	161.1 (0.4)	100.8	**100.3**	**80-82**
FEP	1	165.1 (1.4)	165.3 (1.0)	165.9 (3.3)	165.3 (0.4)	159.0 (1.5)	147.7 (3.1)	158.5 (1.9)	160.7	**160.9**	**158.8**
PFA	1	163.6 (0.8)	170.1 (1.9)	168.5 (0.4)	164.6 (1.6)	166.0 (5.8)	167.0 (0.4)	159.8 (0.7)	162.2	**164.2**	**161.5**
PTFE	1	161.7 (1.8)	164.8 (2.0)	161.0 (1.0)	156.8 (1.1)	164.7 (3.0)	157.4 (4.3)	158.5 (1.1)	165.7	**165.9**	**156.7**

Table 3.3 *- Contact angle values (MAPE and standard deviation) on Polimi samples.*

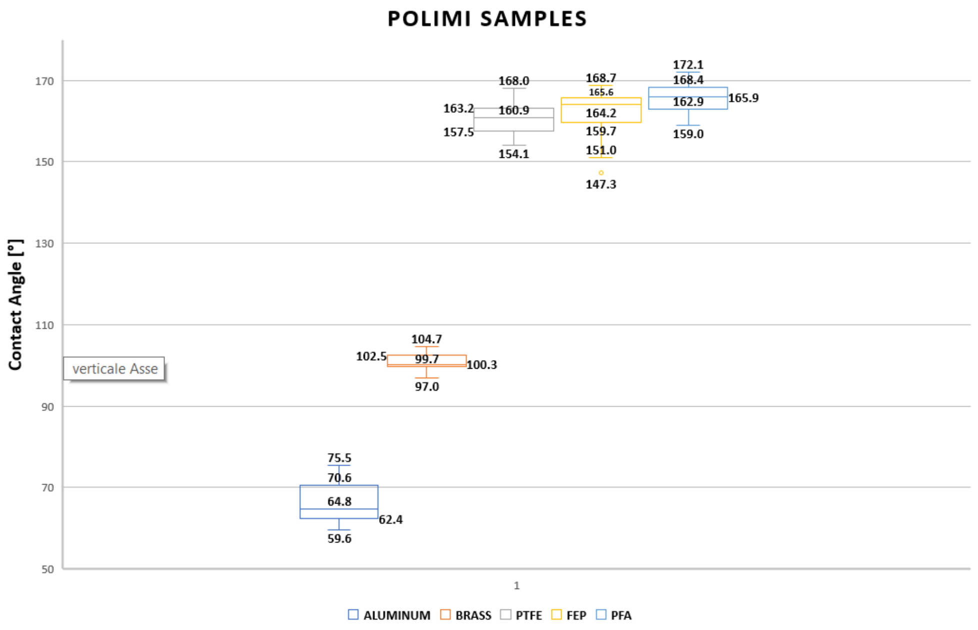

Figure 3.5 *- Box plot of the contact angle values on the Polimi samples. In each box plot are respectively represented the minimum, first quartile, median, third quartile and maximum value for each distribution.*

3.4 Comparison with Tadmor model

3.4.1 Tadmor Experiments

The aim of Tadmor experiment describes in [45] was to prove that the as-placed contact angle, θ_{AP}, of a sessile drop on a horizontal surface decreases with the increase of drop size due to the intensification of hydrostatic pressure. He used "Muscovite mica" as a substrate (rectangular sheets 1.5 cm × 3.5 cm- with a thickness in the range of 0.05 to 0.2 mm). Octadecyltrimethyl ammonium (OTA) monolayer using aqueous solutions of OTA-bromide was utilized to cover the mica. The surface was then cleaned with water to remove excess surfactant. It was used a hexadecane drop that reaches a quickly a stationary position after placed on the substrate, so the measurement were carried out after a minute since drop placement. The drops were placed carefully on the surface in order to not acquire a significant inertia. Contact angle was measured. A graphs in which contact angle value was put in y-coordinate and diameter in x-coordinate was plotted. As a results it was seen that θ_{AP} decreases as the drop diameter increases from ∼1.8 mm (drop volume V ∼ 0.5 µl) to ∼11 mm (V ∼ 70 µl). So Tadmor demonstrated that the drop contact angle decreases with increasing drop size (volume). This is true for hydrophilic surfaces, while on hydrophobic ones the behavior should be reversed, with contact angle increasing with the drop volume. So a series of tests were performed in this work to verify if the Tadmor results for wetting drops could be reproduced using the in-house setup, and if the supposed extension to nonwetting drops (not investigated by Tadmor) could be verified.

Aluminum, brass, normal and gel nail polish, ceramic polish and FEP membrane were investigated to verify the presence of a Tadmor trend. On each sample about 15 drops were placed with different volume size from the smallest one to the biggest. The volume raise was achieved adding a small quantity of water starting from a small drop as illustrated in Figure 3.6.

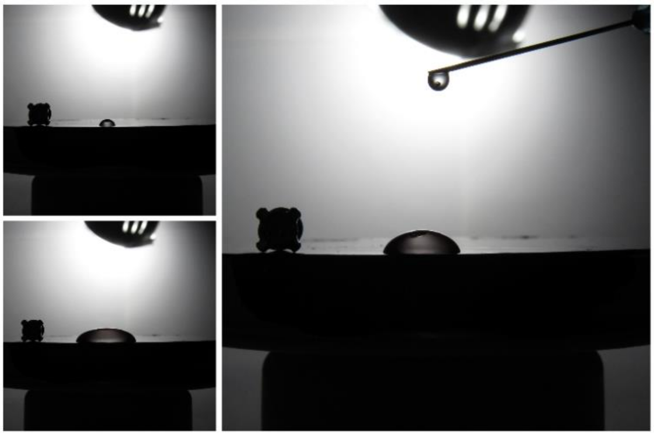

Figure 3.6 *- Procedure for the drop volume increase on the gel nail polish surface.*

3.4.2 Results

Drop volume was calculated making the conversion from pixel to mm^3 (equivalent to microliters that are a sort of standard unit for drop volumes).

A small object of known dimensions was included in the pictures – specifically an earring. Knowing the real dimension of the earring in mm and measuring the equivalent dimension in pixel from the picture it was found the conversion factor from pixel to mm. This, together with the measurement of the drop maximum diameter, made it possible to convert the volume first from the dimensionless world of the Laplace-Young integration into voxels, and then from voxels to cubic millimeters.

It was also estimated the height of the drop thanks to the implementation of a specific code in MATLAB. Thus the contact angles evaluated were plotted along the y-coordinate, with the volume or height along the x-coordinate.

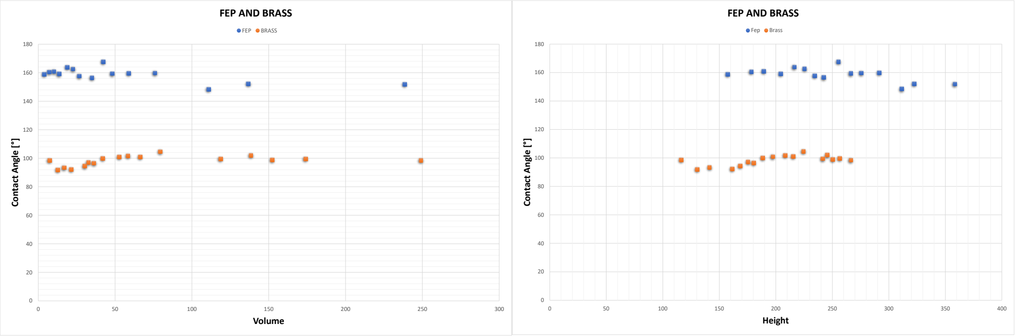

Figure 3.7 *- FEP and BRASS contact angle trend with respect to volume and height.*

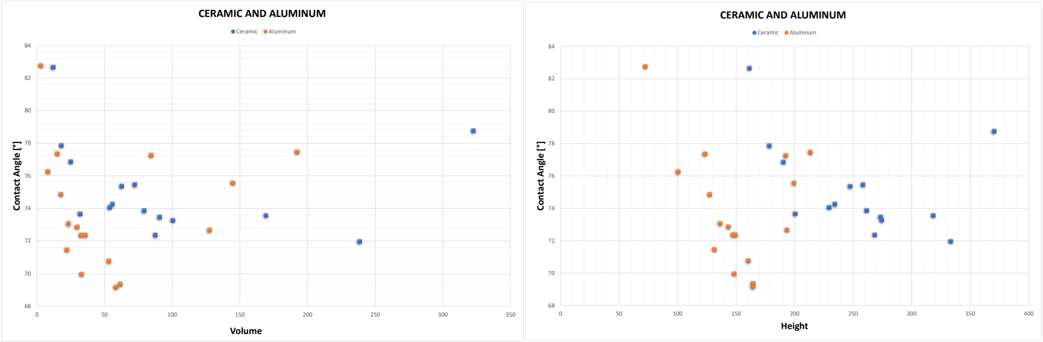

Figure 3.8 *- CERAMIC and ALUMINUM contact angle trend with respect to volume and height.*

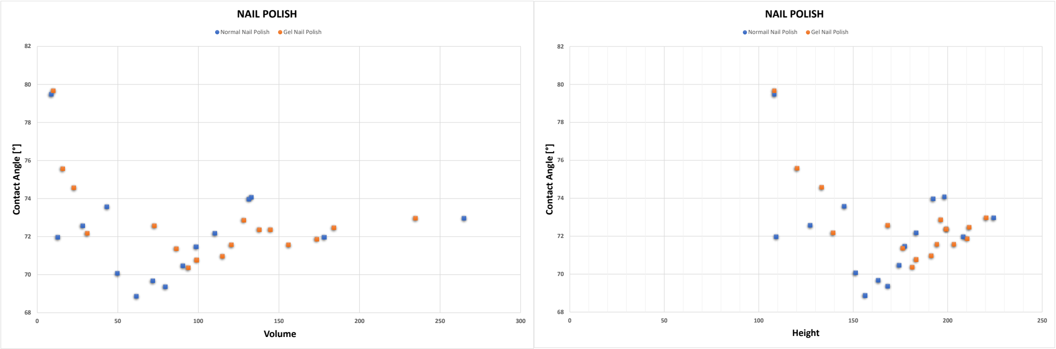

Figure 3.9 *- NORMAL and GEL nail polish contact angle trend with respect to volume and height.*

Figures evidences a non-clear Tadmor trend. For FEP, brass, gel nail polish and ceramic polish we can notice that in the graphs “Contact Angle-Volume” points respect Tadmor trend, even if there are some outliers. Concerning the “Contact Angle-Height” charts, instead, we can clearly affirm that there is no trend, only clouds of points.

Chapter 4

Results for the graphene oxide membranes

4.1 Graphene Oxide Membranes

The self-assembling sulfonated graphene oxide (SGO-X) membranes were obtained with a sulfonation procedure based on a temperature-aided reaction with sulfuric acid.

As already said, graphene oxide GO is the best candidate for the preparation of self-standing membranes for PEMFCs. Thanks to its exceptional self-assembling it can be easily processed into single or multilayer films, moreover, it presents good mechanical and electrically insulating properties.

Innovative approaches involve the modification of GO flakes with the scope of improving both ionic conductivity and structural cohesion. A particularly way to follow consists in the addiction of some acid moieties more firmly bound to the skeleton of GO, such as sulfonic acid ones (–SO3H) analogous to those of Nafion®.

Sulfonation of GO methodology followed was given by Cheng et al. [70] with some change to reach the formation of a self-standing membrane; sulfuric acid was used as functionalizing agent also by Gahlot et al. [140] in combination with chlorosulfonic acid, by Xu et al. [46] and Ayyaru et al. [141].

At the Department of Chemistry, Politecnico di Milano, the Mat4En2 group created GO pure membrane and different SGO membranes varying the sulfuric acid-to-GO molar ratios calculated by considering a rough estimate of the molecular weight of GO ($\approx$ 35.3 g mol$_{-1}$) , according to the procedure described in the following sub-section [142].

4.1.1 Materials and Methods for Membrane Manufacturing

The components used to produce the membranes are the following:

-A commercial water-based dispersion of GO (0.4 wt%).
-A durapore polyvinylidene fluoride (PVDF) filter disks (0.22 µm pore size, hydrophilic).
-Concentrated sulfuric acid (ACS reagent, 95.0–97.0%).
-Magnesium nitrate hexahydrate ($Mg(NO_3)_2 \cdot 6H_2O$, ACS reagent, 99.0%).
-Sodium chloride (NaCl, ACS reagent, $\geq$ 99.0%).
-Sodium hydroxide pellets (NaOH, ACS reagent, $\geq$ 97.0%).

The procedure was as follows:
A beaker containing 25 mL of the dispersion(with 100 mg of GO) was submitted to 1 h of an ultrasound bath to improve its homogeneity. To avoid an excessive increase of temperature, ice was added to the bath. Afterwards, the dispersion was filtered on a PVDF filter disk placed inside a Büchner funnel; after the filtration process the funnel, separated from the flask, was placed in oven at 40 °C for a few hours, in order to dry the deposit and created the self-assemble membrane.
In the case of sulfonated membranes, 25 mL of the GO dispersion was submitted 10 min of a slight ultrasound bath, also here ice was used to prevent overheating. The selected amount of sulfuric acid was incorporated dropwise, so the solution obtained was immersed into an oil bath, connected to a reflux condenser and submitted to 3 h of magnetic stirring (850 rpm) at 25 °C (± 2 °C) followed by 3 h at 100 °C (± 5 °C) in order to achieve an efficient mix between GO and sulfuric acid and to let the functionalization take place. Afterwards, mixture was filtrated and diluted, while filtering, with deionized water (300 mL) to increase its pH, preventing damages to the vacuum pump due to acid vapors, and to perform a soft washing of the product. At the end, the deposit was put in oven at 50 °C for some hours, until the SGO membrane has been properly assembled on the PVDF filter disk [142].

4.2 Graphene Oxide Results

Table 4.1 shows the values of the contact angles measured on the graphene oxide membranes. These manifest degradation with water as show in Figure 4.1 so it was possibly to acquire only 15 drop pictures to evaluate contact angles; furthermore it was not possible to depose consecutive drops on the same point because drops after the first are rapidly absorbed As it can be seen, all membranes show a hydrophilic behavior with contact angle values less of 90°, except the SGO-20 that shows hydrophobic contact angle values. With the exception of SGO-1, an increasing trend is evident in the contact angle with the increase of sulfuric acid-to-GO molar ratio.

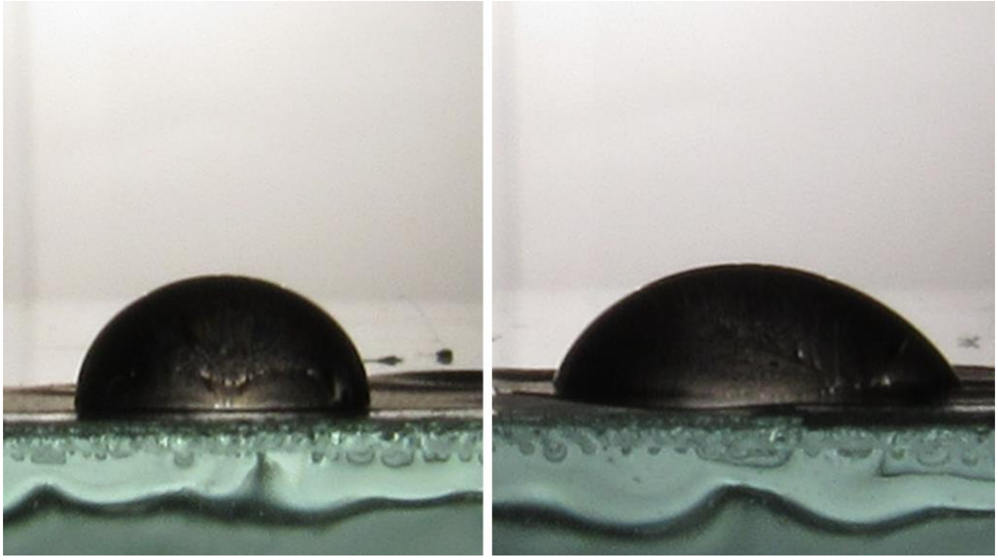

Figure 4.1*- example of membrane degradation. On the left: first drop deposed. On the right third drop deposed: lower contact angle and membrane inclination at the extremity are evident.*

GRAPHENE OXIDE MEMBRANES							
SAMPLE	**DROP/TEST**	**1.1**	**1.2**	**1.3**	**2**	**3**	**TOTAL MEAN**
GO	1	65.2 (0.7)	63.8 (0.5)	63.9 (1.2)	59.2 (0.6)	65.2 (2.5)	**61.8**
SGO-1	1	94.5 (3.1)	80.0 (2.9)	68.9 (1.3)	83.3 (2.1)	65.2 (5.3)	**76.6**
SGO-2.5	1	56.6 (1.5)	56.4 (0.8)	53.4 (0.5)	53.3 (2.1)	51.7 (0.8)	**53.5**
SGO-5	1	74.9 (0.5)	73.5 (1.0)	73.0 (1.5)	56.3 (0.6)	67.2 (0.2)	**65.7**
SGO-10	1	86.4 (1.9)	84.9 (88.6)	88.6 (7.0)	88.4 (0.8)	87.0 (1.0)	**87.3**
SGO-15	1	87.8 (0.6)	88.4 (0.9)	89.0 (2.5)	82.9 (2.0)	92.7 (1.3)	**88.0**
SGO-20	1	103.4 (1.5)	103.2 (1.4)	98.8 (5.6)	115.5 (0.2)	116.0 (4.9)	**111.1**

Table 4.1 *- Contact angle values (MAPE and standard deviation) on graphene oxide membranes.*

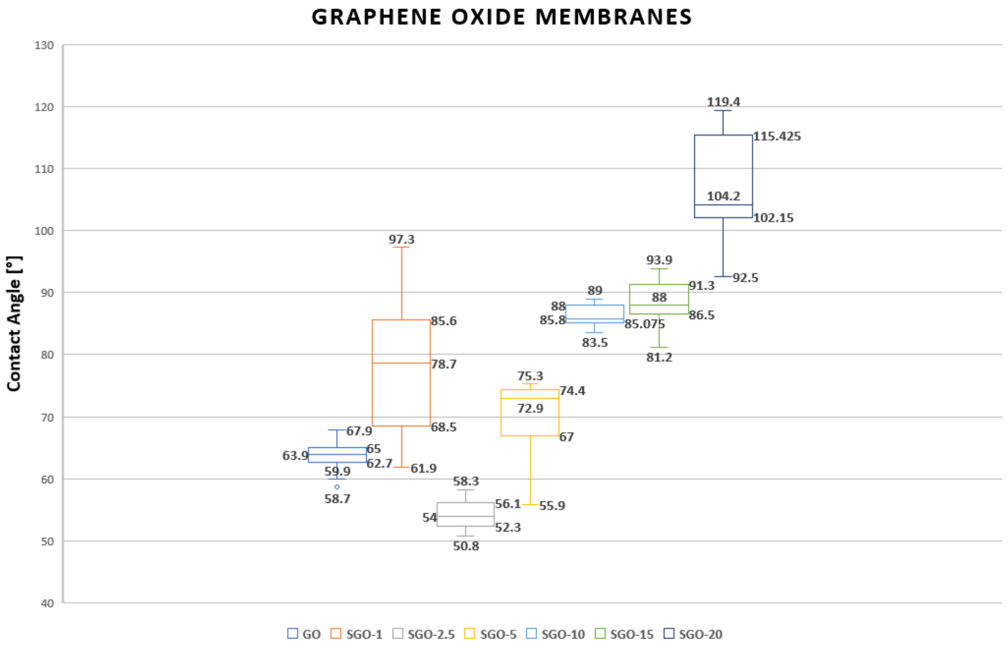

Figure 4.2 *- Box plot of the contact angle values on the graphene oxide membranes. In each box plot are respectively represented the minimum, first quartile, median, third quartile and maximum value for each distribution*

Generally in the fuel cell where Nafion is used the formation of moist domains supports the ions passege, so it needs to work in 100% humidity conditions. The introduction of graphene oxide membranes comes from the idea to reduce the humidity condition (ideally equal to 0%) in order to achieve a better design of the fuel cell and to better manage water that comes from reaction. The fuel cell functioning with these new membranes is not yet tested so making a conclusion is now a “risk”. What we can state up to know is that a hydrophilic behavior is requested, so GO, SGO-1, SGO-2.5 AND SGO-5 result to be promising future membranes. In general more tests should be performed to verify and further assess the results.

Conclusions

The original scope of this work was to carry out a wettability analysis on graphene oxide membranes used for fuel cells, performing the experimental tests in the Thermo-fluid Dynamics Laboratory of the Department of Energy. Due to the COVID19 pandemy, access to the laboratory was impossible and new, in-house, setup had to be developed to use it during the lockdown.

Wettability analyses were conducted measuring the static contact angle, that is a fundamental parameter for the characterization of surface, by means of the Axisymmetric Drop Shape Analysis technique. The latter includes some process parameters whose values must be selected by the operator and the results rely on such choices. So an extensive sensitive analysis was conducted on the technique to understand how the different parameters can affect measurement. It was showed that the variation of the number of iterations in the fitting process and the smoothing value for contour approximation lead to a really small variation in the contact angle measurement. What influenced significantly the measurement is the baseline value defined as the height at which the tracing of the drop profile is stopped and at which the contact angle is calculated. A non-correct evaluation of this, even in the order of ±1 pixel, can bring an incorrect contact angle valuation. Finally it was observed that with the increase of drop picture resolution errors decrease. So it is important to acquire high resolution images and to evaluate accurately the baseline value.

Concerning the in-house setup, it was built with everyday-use objects and tested first of all with a series of measurements on home-made samples (both clean and covered with limestone) and then with measurements for validation by re-testing fuel cell surfaces for which previous measurements in the Polimi laboratory had been done. Such tests evidenced that despite its obvious limitations, the in-house setup was able to grant an accuracy comparable with that of a common commercial contact angle meter.

From home-made samples we discovered that gel nail polish has an higher contact angle respect common nail polish, so it can better resist to water and degradation for women happiness. It was also surprising how limestone did not bring a hydrophobic behavior to samples, as often reported in the literature.

Returning to the final scope of the work, sulfonated graphene oxide (SGO-X) membranes produced by the Department of Chemistry, Materials and Chemical

Engineering “Giulio Natta” were caracterized. All membranes showed a hydrophilic behavior with contact angle values less of 90°, apart from the SGO-20 that reaches a contact angle of 110°. It was also observed an increasing trend of the angle with the increase of sulfuric acid-to-GO molar ratios. Generally membranes show a water uptake attitude.

These, according to other evaluated properties, making them an attractive candidate for future fuel cells with the possibility to work at reduced humidification.

Appendix A

Matlab process description

1. Preparation of the images

The procedure expects two imagines for each drop that must be analyzed, respectively one with the drop itself and one of its background, this is useful for a better fit of the drop especially for ones with not perfectly homogeneous background. In the folder must be present sequentially one drop imagine and its respective background, for all the drops to be analyzed. In case the background is sufficiently homogeneous this step can be skipped.

2. Crop of the imagines

This step is suggested to reduce the weight of calculation. Drop take only a part of the imagines and for this reason it is reasonable to consider only such part. We use the following function:

`M_imm_crop_rotate_scale_auto(car_noncar,car_iniz,car_iniz_new_name,x_sx,y_top,x_dx,y_bot,angle,scal e,type,quality)`

where:

- *Car_noncar* : stands for the possibility to process imagines that start or not with a character.

- *Car_iniz* : stands for the character of the imagines that must be processed; generally is 'D' for the photos taken with a reflex camera.

- *Car_iniz_new_name*: it is the character that the software puts before the imagine name when it saves the cropped image. Generally we use 'k';

- *x_sx, y_top, x_dx, y_bot* : are the four coordinates in pixel respectively of the upper left and lower right corners of the part of the imagine we want to keep, all parts out of these coordinate are cut off;

- *Angle, scale*: angle of rotation and rescaling factor of the images; generally we keep both at 0;

- *Type*: type of the imagine we want to save, generally we use 'png' format;

- *Quality:* quality of the imagine, this is useful only for JPG saving, it can be left at 100 for PNG.

3. Register the images and calculate the difference

The next step is to calculate the difference between the drop images and the corresponding background images, cropped. In the case of images that are not perfectly aligned, it is possible to register them first (i.e. realign them one to the other). We use the following function:

```
MA_imm_reg_diff_RGB_auto(car_noncar,car_iniz,reg,quota_reg,quota_cut,ordine)
```

where:

- *Car_noncar:* same of the previous step.
- *Car_iniz:* previously saved with the initial ‘k’;
- *Reg*: is the value that determinates if we want to register imagines; we put 0 to avoid this passage as it is not needed for our images, that are already well aligned.
- *Quota_reg:* indicates which part of the imagine we want to use for registration, if we put the previous value to 0 we can use any value; generally we put 1;
- *Quota_cut:* the quota below which the difference between the images is automatically set to zero. It is used because, despite the attentions, if the samples are "complex" there is no way to avoid non-zero differences between image with and without drop (even only because of the shadow of the drop or reflections). It is used also - especially for the case of fabrics, etc. - to avoid disturbances from fibers etc. that protrudes from the surface. The value is generally set above the minimum height at which the drop appears;
- *Ordine:* 1 if in the directory list the image with the background comes before the one with the drop, -1 if viceversa;

4. Extract the drop profile from the difference images

At this point we extract the drop profile from the difference images. We use the following function:

MB_estrai_contorno_bwtraceboundary_auto(car_noncar,car_iniz,quota_cut,thresh_val,col)

where:

- *Car_noncar*: 'car'.
- *Car_iniz*: generally 'd'.
- *Quota cut*: the same of the previous step.
- *Thresh_val:* it is the threshold value used to binarize the difference image by passing it from tones of gray to white / black. If the experimental images are very well contrasted - as often in the fast camera images - a value of 0.3 often works well.
- *Col:* the color we use to draw the drop profile superposed to the original images.

5. Fit the Laplace-Young equation to the experimental boundary and determine its angle of contact.

   Finally we can make the fitting of the theoretical Laplace- Young equation (2D version assuming the drop axisymmetric). All is made automatically using the following function:

   MC_DSA_contour_fit_Eo_auto(car_noncar,car_iniz,col_cont,col_cont_new_sx,col_cont_new_dx,smooth,smooth_x_err,num_iter,fi_max,Eot,modo,ystop_px)

   where:

   - *Car_noncar:* 'car'.
   - *Car_iniz*: generally 'c';
   - *Col_cont*: color used to design the drop profile. Same of the previous step.

- *Col_cont_new_sx, col_cont_new_dx* : the colors used to trace the left and right contours resulting from the L-Y fitting in the final image.

- *Smooth, smooth_x_err, num_iter, fi_max, Eot, modo*: input parameters for the fitting procedure and can be typically left respectively at the values of 0.05,0.05, 2500, pi, 0.5, 2.

- *Ystop_px*: height at which the tracing of the drop profile is stopped and at which the contact angle is calculated. It is the quota of the base segment, lateral projection of the triple line. It is necessary to pay attention in choosing this value because consistent errors can be make, especially for condition of high hydrophobicity and hydrophilicity a single pixel of difference can vary the contact angle measurement of various degree.

The latter file creates a ‘LY…’ imagine with graphical representation of result plus two file texts with the value of contact angle and other parameters.

List of Figure

List of Tables

Nomenclature

σ (or γ)	Surface tension
K	Interface curvature
R_I R_{II}	Principal curvature radii of the surface
λ	Capillary length
g	Acceleration gravity
ΔP	Pressure difference
σ_{LV}	Interfacial energy between liquid and vapor
σ_{SL}	Interfacial energy between solid and liquid
σ_{SV}	Interfacial energy between solid and vapor
Θ_Y	Young contact
W_{LS}	Work of adhesion
S	Spreading coefficient
h	Capillary height/ Capillary rise
ρ	Liquid density
r	Tube radius
θ	Contact angle of the liquid on the tube surface.
θ_{adv}	Advancing contact angle
θ_{rec}	Receding contact angle
H	Contact angle hysteresis
r	Roughness parameter ($r = A_T/A_N$)
θ^Y	Equilibrium contact angle
A_T	True surface area
A_N	Nominal area
θ^w	Apparent contact angle on the rough surface (Wenzel angle)
θ^C	Cassie angle
θ_1^Y , θ_2^Y	Young's contact angles respectively of the two components of heterogeneous surface
f	Fractional area of a component of the solid surface
f_1, f_2	Total areas of the solid–liquid interface and liquid–air interface
θ^{CB}	Cassie- Baxter contact angle
f_s	Fraction of the liquid base in contact with the solid surface
F	Total force exerted on the plate
p	Pressure
V	Volume of the displaced liquid
$\Delta\rho$	Density difference
r	Capillary radius

References

[1] T. Bayer et al. Journal of Power Sources 272 (2014) 239 e 247

[2] *Grove, W. R. 1843, Philosophical Transactions of the Royal Society of London, Vol. 133, p. 91-112.*

[3] *Q. Li, R. He, J.O. Jensen, N.J. Bjerrum, Chem. Mater. 15 (2003) 4896 e 4915.*

[4] *V. a. Sethuraman, J.W. Weidner, A.T. Haug, S. Motupally, L.V. Protsailo, J. Electrochem. Soc. 155 (2008) B50.*

[5] *S.C. Yeo, a. Eisenberg, J. Appl. Polym. Sci. 21 (1977) 875-898.*

[6] *N.H. Jalani, K. Dunn, R. Datta, Electrochim. Acta 51 (2005) 553 e 560.*

[7] *C. Francia, V.S. Ijeri, S. Specchia, P. Spinelli, J. Power Sources 196 (2011) 1833-1839.*

[8] *J. Ling, O. Savadogo, J. Electrochem. Soc. 151 (2004) A1604.*

[9] *J. Liu, D. Takeshi, K. Sasaki, S.M. Lyth, J. Electrochem. Soc. 161 (2014) F838 e F844.*

[10] *S.M. Lyth, Y. Nabae, N.M. Islam, T. Hayakawa, S. Kuroki, M. Kakimoto, e-J. Surf.Sci. Nanotech. 10 (2012) 29 e 32.*

[11] *M.J. Allen, V.C. Tung, R.B. Kaner, Chem. Rev. 110 (2010) 132e145.*

[12] *C.N.R. Rao, A.K. Sood, K.S. Subrahmanyam, A. Govindaraj, Angew. Chem. Int. Ed. 48 (2009) 7752 e 7777.*

[13] *Y. Zhu, S. Murali, W. Cai, X. Li, J.W. Suk, J.R. Potts, R.S. Ruoff, Adv. Mater 22 (2010) 3906 e 3924.*

[14] *K.I. Bolotin, K.J. Sikes, Z. Jiang, M. Klima, G. Fudenberg, J. Hone, P. Kim, H.L. Stormer, Solid State Commun. 146 (2008) 351 e 355.*

[15] *M.D. Stoller, S. Park, Y. Zhu, J. An, R.S. Ruoff, Nano Lett. 8 (2008) 3498 e 3502.*

[16] *C. Lee, X. Wei, J.W. Kysar, J. Hone, Science 321 (2008) 385 e 388.*

[17] *A.A. Balandin, S. Ghosh, W. Bao, I. Calizo, D. Teweldebrhan, F. Miao, C.N. Lau, Nano Lett. 8 (2008) 902 e 907.*

[18] *R.R. Nair, P. Blake, A.N. Grigorenko, K.S. Novoselov, T.J. Booth, T. Stauber,N.M.R. Peres, A.K. Geim, Science 320 (2008), 1308 e 1308.*

[19] *Y. Zhu, S. Murali, W. Cai, X. Li, J.W. Suk, J.R. Potts, R.S. Ruoff, Adv. Mater. 22 (2010) 3906 e 3924.*

[20] *H.P. Boehm, A. Clauss, G.O. Fischer, U. Hofmann, Z. Anorg. Allg. Chem. 316 (1962) 119 e 127.*

[21] *D.R. Dreyer, S. Park, C.W. Bielawski, R.S. Ruoff, Chem. Soc. Rev. 39 (2010) 228 e 240.*

[22] *K.P. Loh, Q. Bao, G. Eda, M. Chhowalla, Nat. Chem. 2 (2010) 1015 e 1024.*

[23] *H. He, J. Klinowski, M. Forster, A. Lerf, Chem. Phys. Lett. 287 (1998) 53 e 56.*

[24] *A. Lerf, H. He, M. Forster, J. Klinowski, J. Phys. Chem. B 102 (1998) 4477 e 4482.*

[25] *R.R. Nair, H.A. Wu, P.N. Jayaram, I.V. Grigorieva, A.K. Geim, Science 335 (2012) 442 e 444.*

[26] *R. Kumar, C. Xu, K. Scott, RSC Adv. 2 (2012) 8777.*

[27] *Z. Jiang, X. Zhao, Y. Fu, A. Manthiram, J. Mater. Chem. 22 (2012) 24862.*

[28] *C. Xu, Y. Cao, R. Kumar, X. Wu, X. Wang, K. Scott, J. Mater. Chem. 21 (2011) 11359 e 11364.*

[29] *H. Tateishi, K. Hatakeyama, C. Ogata, K. Gezuhara, J. Kuroda, a. Funatsu, M. Koinuma, T. Taniguchi, S. Hayami, Y. Matsumoto, J. Electrochem. Soc. 160 (2013) F1175 e F1178.*

[30] *K. Scott, Ravikumar, Chem. Commun. 48 (2012) 5584.*

[31] *Lopez VH, Kennedy AR. J Colloid Interface Sci 2006;298–1:356–62.*

[32] *Vianco PT, Frear DR. JOM July 1993:14–9.*

[33] *Frear DR, Jones WB, Kinsman KR.* A TMS Publication; 1991. p. 1–104.

[34] Schwartz MM, Aircraft S. Metals hand book, 10th edition, vol. 6. Metals Park, OH: ASM; 1991. p. 126–9.

[35] *G. Kumar, K.N. Prabhu / Advances in Colloid and Interface Science 133 (2007) 61–89.*

[36] *Schwartz AM, Tejada SB. J Colloid Interface Sci 1972;38–2:359–75.*

[37] *H. Rathgen, "Superhydrophobic Surfaces : from Fluid Mechanics to Optics," University Of Twente, 2008.*

[38] *Y. Yuan and T.R. Lee;2013.* Springer Series in Surface Sciences 51, DOI 10.1007/978-3-642-34243-1_1,

[39] *M.Guilizzoni, S. De Antonellis; IOP Conf. Series: Journal of Physics: Conf. Series 1249 (2019) 012005.*

[40] *Young T 1805 An essay on the cohesion of fluids Philos Trans R Soc Lond 95 65–87.*

[41] *M. Guilizzoni, slides of the course "Heat Transfer and Thermal Analysis", Politecnico di Milano, A.Y. 2019-20".*

[42] *B. Bhushan, Y.C. Jung / Progress in Materials Science 56 (2011) 1–108*

[43] *L.A. Lobo, A.D. Nikolov, A.S. Dimitrov, P.A. Kralchevsky, D.T. Wasan.* Langmuir 6 (1990) 995.

[44] *Drelich JW, Boinovich L, Chibowski E et al. (2020), Contact angles: history of over 200 years of open questions.Surface Innovations 8(1–2): 3–27.*

[45] Rafael Tadmor ∗, Preeti S. Yadav Journal of Colloid and Interface Science 317 (2008) 241–246.

[46] A.W. Adamson, A.P. Gast, Physical Chemistry of Surfaces, Wiley, New York, 1997

[47] Long J, Hyder MN, Huang RYM, Chen P. Adv Colloid Interface Sci 2005;118:173–6.

[48] *Kamusewitz H, Possart W, Paul D. Colloids Surf A 1999;156:271–9.*

[49] *Quere D. Physica A 2002;313:32–46.*

[50] Davis JT, Rideal EK. Interfacial phenomena. 2nd Edition. NY: Academic Press; 1966. p. 1–52.

[51] *B. Krasovitski, A. Marmur, Langmuir 21 (2005) 3881.*

[52] A. Amirfazli, D.Y. Kwok, J. Gaydos, A.W. Neumann, J. Colloid Interface Sci. 205 (1998) 1.

[53] *M. Yekta-Fard, A.B. Ponter, J. Colloid Interface Sci. 126 (1988) 134.*

[54] *W.J. Herzberg, J.E. Marian, J. Colloid Interface Sci. 33 (1970) 161.*

[55] *R.J. Good, M.N. Koo, J. Colloid Interface Sci. 71 (1979) 283.*

[56] *G. Wolansky, A. Marmur, Langmuir 14 (1998) 5292.*

[57] *Nosonovsky M, Bhushan B. Microsyst Technol 2005;11:535–49.*

[58] *Jung YC, Bhushan B. Nanotechnology 2006;17:4970–80.*

[59] *Mackie AC. Circuits Assembly March 2003:26–35.*

[60] *Theriault M, Blostein P. SMT; June 2000.*

[61] *Sattiraju SV, Dang B, Johnson RW, Li Y, Smith JS, Bozack MJ. IEEE Trans Electron Packag Manuf July 2002;25–3:168–84.*

[62] *Bernardin JD, Mudawar I, Walsh CB, Franses I. Int J Heat Mass Transfer 1997;40–5:1017–33.*

[63] *Lopez VH, Kennedy AR. J Colloid Interface Sci 2006;298–1:356–62.*

[64] *Manko HH. Solders and soldering. 3rd Edition. NY: McGraw-Hill Inc.*

[65] *Frear DR, Jones WB, Kinsman KR. Solder mechanics—a state of the art assessment. A TMS Publication; 1991. p. 1–104.*

[66] *Claesson E, Choquenet L, Nilson M, Brasage — 97.*

[77] *Mortensen A, Drevet B, Eustathopoulos N. Scripta Mater 1997;36–6: 645–51.*

[78] *Chen K, Lin KL. International Symposium on Electronic Materials and Packaging; 2002. p. 49–54.*

[79] *Wang H, Wang F, Gao F, Ma X, Qian Y. J Alloys Compd 2007;433–1 (2):302–5.*

[80] *Bigelow W, Pickett D, Zisman W. Oleophobic monolayers: I. Films adsorbed from solution in non-polar liquids. J Colloid Sci 1946;1:513e38.*

[81] *R.W. Smithwich, J. Colloid Interface Sci. 123, 482 (1988).*

[82] *D.Y. Kwok, R. Lin, M. Mui, A.W. Neumann, Colloids Surf. A 116, 63 (1996).*

[83] *S. Brandon, N. Haimovich, E. Yeger, A. Marmur, J. Colloid Interface Sci. 263, 237 (2003).*

[84] *P. Letellier, A. Mayaffre, M. Turmine, J. Colloid Interface Sci. 314, 604 (2007).*

[85] *A.W. Neumann, R.J. Good, in Surface and Colloid Science: Experimental Methods, vol. 11.*

[86] *R.J. Hunter, Foundations of Colloid Science, 2nd edn. (Clarendon Press, Oxford, 2001.*

[87] *G. MacDougall, C. Ockrent, Proc. R. Soc. 180A, 151 (1942).*

[88] *C.W. Extrand, Y. Kumagai, J. Colloid Interface Sci. 184, 191 (1996).*

[89] *C.W. Extrand, Y. Kumagai, J. Colloid Interface Sci. 191, 378 (1997).*

[90] *W.A. Zisman, Adv. Chem. Ser. 87, 1 (1968).*

[91] *M.C. Phillips, A.C. Riddiford, J. Colloid Interface Sci. 41, 77 (1972).*

[92] *D.E. McIntyre.The Institute of Paper Chemistry, Appleton, WI, 1969.*

[93] *A.F. Taggart, T.C. Taylor, C.R. Ince, Trans. Am. Inst. Min. Metall. Pet. Eng. 87, 285 (1930).*

[94] *Roma´nszki L, Mohos M, Telegdi J, Keresztes Z, Nyikos L. Period Polytech Chem Eng 2014;58:53..*

[95] *J.C. Cain, D.W. Francis, R.D. Venter, A.W. Neumann, J. Colloid Interface Sci. 94, 123 (1983).*

[96] *C.J. Budziak, E.I. Vargha-Butler, A.W. Neumann, J. Appl. Polym. Sci. 42, 1959 (1991).*

[97] *Y. Rotenberg, L. Boruvka, A.W. Neumann, J. Colloid Interface Sci. 93, 169 (1983).*

[98] *P. Cheng, D. Li, L. Boruvka, Y. Rotenberg, A.W. Neumann, Colloids Surf. 43, 151 (1990).*

[99] *R.O. Duda, P.E. Hart, Pattern Classification and Scene Analysis (Wiley, New York, 1973).*

[100] *O.I. del Río, A.W. Neumann, J. Colloid Interface Sci. 196, 136 (1997).*

[101] *F.K. Skinner, Y. Rotenberg, A.W. Neumann, J. Colloid Interface Sci. 130, 25 (1989).*

[102] *E. Moy, P. Cheng, Z. Policova, S. Treppo, D. Kwok, D.R. Mack, P.M. Sherman, A.W. Neumann,Colloids Surf. 58, 215 (1991).*

[103] *Burton Z, Bhushan B. Ultramicroscopy 2006;106:709–19.*

[104] *Bhushan B, Jung YC. Nanotechnology 2006;17:2758–72.*

[105] *Barthlott W, Neinhuis C. Planta 1997;202:1–8.*

[106] *Bhushan B, Jung YC, Koch K. Phil Trans R Soc A 2009;367:1631–72.*

[107] *Koch K, Bhushan B, Jung YC, Barthlott W. Soft Matter 2009;5:1386–93.*

[108] *Neinhuis C, Barthlott W. Ann Bot 1997;79:667–77.*

[109] *Zhang JL, Li JA, Han YC. Superhydrophobic PTFE surfaces by extension. Macromol Rapid Commun 2004;25:1105–8.*

[110] *Shiu J-Y, Kuo C-W, Chen P. The International Society for Optical Engineering, vol. 5648; 2005. p. 325–32.*

[111] *Singh A, Steely L, Allcock HR. Langmuir 2005;21:11604–7.*

[112] *Yabu H, Shimomura M. Chem Mater 2005;17:5231–4.*

[113] *Xu L, Chen W, Mulchandani A, Yan Y. Angew Chem Int Ed 2005;44:6009–12. .*

[114] *Khorasani MT, Mirzadeh H, Kermani Z. Appl Surf Sci 2005;242:339–45.*

[115] *Jin MH, Feng XJ, Xi JM, Zhai J, Cho KW, Feng L, et al..Macromol Rapid Commun 2005;26:1805–9.*

[116] *Sun MH, Luo CX, Xu LP, Ji H, Qi OY, Yu DP, et a. Langmuir 2005;21:8978–81.*

[117] *Ma M, Hill RM, Lowery JL, Fridrikh SV, RutledgeGC. Langmuir2005;21:5549–54.*

[118] *Lu XY, Zhang CC, Han YC.Macromol Rapid Commun2004;25:1606–10.*

[119] *Jiang L, Zhao Y, Zhai J. AngewChemInt Ed 2004;43:4338–41.*

[120] *Zhang J, Lu X, Huang W, Han Y. Macromol Rapid Commun 2005;26:477–80.*

[121] *Zhao N, Xu J, Xie QD,Weng LH, Guo XL, Zhang XL, et al. Macromol Rapid Commun 2005;26:1075–80.*

[122] *Mohammadi R,Wassink J, Amirfazli A. Langmuir 2004;20:9657–62.*

[123] *Yan H, Kurogi K, Mayama H, Tsujii K. Angew Chem Int Ed 2005;44:3453–6..*

[124] *Feng XJ, Feng L, Jin MH, Zhai J, Jiang L, Zhu DB. J Am Chem Soc 2004;126:62–3.*

[125] *Yang YH, Li ZY, Wang B, Wang CX, Chen DH, Yang GW. J Phys, Condens Matter 2005;17:5441–6.*

[126] *Furstner R, Barthlott W, Neinhuis C, Walzel P. Langmuir 2005;21:956–61.*

[127] *Callies M, Chen Y, Marty F, Pepin A, Quere D. Microelectron Eng 2005;78–79:100–5.*

[128] *Abdelsalam ME, Bartlett PN, Kelf T, Baumberg J. Langmuir 2005;21:1753–7.*

[129] *Martines E, Seunarine K, Morgan H, Gadegaard N, Wilkinson CDW Riehle MO. Nano Lett 2005;5:2097–103.*

[130] *Feng XJ, Zhai J, Jiang L. Angew Chem Int Ed 2005;44:5115–8.*

[131] *Shirtcliffe NJ, McHale G, Newton MI, Perry CC, Roach P. Chem Commun 2005:3135–7.*

[132] *Hikita M, Tanaka K, Nakamura T, Kajiyama T, Takahara A. Langmuir 2005;21:7299–302.*

[133] *Wu X, Zheng L, Wu D. Langmuir 2005;21:2665–7.*

[134] *Shang HM, Wang Y, Limmer SJ, Chou TP, Takahashi K, Cao GZ. Thin Solid Films 2005;472:37–43.*

[135] *Shang HM, Wang Y, Limmer SJ, Chou TP, Takahashi K, Cao GZ. Thin Solid Films 2005;472:37–43.*

[136] *Zhai L, Cebeci FC, Cohen RE, Rubner MF. Nano Lett 2004;4:1349–53.*

[137] *https://it.mathworks.com/.*

[138] *Otsu, N., "A Threshold Selection Method from Gray-Level Histograms." IEEE Transactions on Systems, Man, and Cybernetics. Vol. 9, No. 1, 1979, pp. 62–66.].*

[139] *Schneeweiss S. Pharmacoepidemiol Drug Saf 2006, 15(5):291–303..*

[140] *Saltelli, A. (2002). "Sensitivity Analysis for Importance Assessment". Risk Analysis. 22 (3): 1–12. CiteSeerX 10.1.1.194.7359. doi:10.1111/0272-4332.00040. PMID 12088235.*

[141] *Saltelli, A.; Ratto, M.; Andres, T.; Campolongo, F.; Cariboni, J.; Gatelli, D.; Saisana, M.; Tarantola, S. (2008). Global Sensitivity Analysis: The Primer. John Wiley & Sons.*

[142] *A.B. Peressut, S. Latorrata, P.G. Stampino, G. Dotelli, Development of self-assembling sulfonated graphene oxide membranes as a potential proton conductor, Materials Chemistry and Physics (2020), doi: https://doi.org/10.1016/j.matchemphys.2020.123768.*